Durham E-Theses

Radiochemical studies of Nuclear reactions

James, Robin Harold

"RADIOCHEMICAL STUDIES OF NUCLEAR REACTIONS"

THESIS

presented in candidature

for the degree of

DOCTOR OF PHILOSOPHY

in the

University of Durham

by

ROBIN HAROLD JAMES, B.Sc. (London), A.R.I.C.

The work described in this Thesis was carried
out in the Londonderry Laboratory for Radiochemistry,
University of Durham, between April 1955, and September
1958, under the supervision of Mr. G.R. Martin, B.Sc.,
A.R.C.S., F.R.I.C., Reader in Radiochemistry. (now
Professor of Chemistry in the University of Kent at
Canterbury).

SUMMARY

The Mass/Yield curve for the fission of natural uranium by 14.7 MeV neutrons has been established by the radiochemical separation and counting of a number of fission product isotopes. The familiar double peaked curve is obtained with a peak to trough ratio of 10, peaks at 99 and 136 mass units and yields at the peaks of 6.5%. The number of prompt neutrons emitted per fission, which gives the best fit for "mirror - points", is 4.

A modification of the associated particle method has been used to determine the cross - section of the Al^{27} $(n, \alpha)Na^{24}$ reaction for 13.5 MeV neutrons. A cross - section value of 113.7 $\pm$ 10.1 mb has been obtained; this compares favourably with values from other sources.

CONTENTS

PREFACE

With the ready availability of tritium in this country, fast neutron sources based on the (D+T) reaction offered a means of research to assist in the interpretation of nuclear theories. The major advantages of this source were the high energy of neutrons produced at comparatively low bombarding energies ($\sim$ 100 KeV) and the very small angular variation in energy, giving a source of virtually monoenergetic neutrons. One obvious channel of investigation was nuclear fission.

When this work started much information was available on the fission of uranium by thermal neutrons (essentially fission of U^{235}) and the results have been summarised by Steinberg and Glendenin (1). Very little had been reported, however, on fission by neutrons of higher energies (2,3) and the work was mainly concerned with fission spectrum neutrons. The study of the fission of natural uranium by 14 MeV neutrons was therefore carried out to add further information to assist in the interpretation of the theory of nuclear fission, to add to the fund of experimental data being accumulated and to obtain information of potential practical importance to the design of nuclear reactors and processing plants.

The mass/yield curve for thermal neutron fission of U^{235} follows the now familiar shape of two peaks at mass numbers 95 and 140 with a deep trough at mass number 118 (the peak to trough ratio is approximately 600). Irregularities are found in the form of fine structure in the region of the peaks which has been explained (4) by the preferential formation of nuclei with closed shells of 50 or 82 neutrons. At very high energies, however, the trough disappears and the yield curve consists of a single peak; an example of this is the fission of Bi^{209} with 190 MeV deuterons (5). At intermediate energies (e.g. fission spectrum neutrons) a curve similar to that for thermal neutron fission is found but with a reduced peak to trough ratio (₁00-200). It was, therefore, expected that the mass/yield curve for fission by 14 MeV neutrons would exhibit dual peaks with a comparatively small peak to trough ratio.

Information on the mass distribution of the fission fragments has been obtained mainly in two ways (i) the ionization chamber technique, which measures the frequency of various kinetic energy releases, from which data a mass/yield curve can be deduced and (ii) radiochemical identification of the fission fragments. The latter method,

-4-

which led to the discovery of nuclear fission (6) is more
sensitive and it is this procedure which has been adopted
for this investigation.

The two main fragments produced in fission have
approximately the same neutron to proton ratio as the
original nucleus. This ratio is too high for stability
of the nuclei produced, even after the emission of the
prompt fission neutrons and the nuclei attain stability
by a series of β -decay processes. Isolation and
estimation of one of the isobars in the decay chain enables
its fission yield to be calculated. A proportion of any
given isobar may have been produced directly from the
fission process and the proportion of such fissions to the
total number of fissions is the independent yield. The
independent yields of the later members of the decay chains
are small in comparison with the total chain yields and in
general there is little loss of accuracy in ignoring them.
Ternary fission occurs rarely relative to binary fission
and for the purpose of establishing the mass/yield curve
may be ignored.

Part 1 of this thesis describes the irradiation of
natural uranium with 14.7 MeV neutrons, the subsequent
radiochemical separations and counting techniques involved
in constructing the mass/yield curve. The effect of the

U^{235} present in the natural uranium in the proportion
1 in 140 may be ignored since the fission cross-sections
of U^{235} and U^{238} are similar (7) and hence the mass/yield
curve is essentially that for the fission of U^{238}.

The difficulties of measurement of the neutron flux
in all fast neutron irradiations are discussed more fully
in the introduction to Part II, which describes a method
for the accurate determination of the 14 MeV neutron
cross section for the reaction Al^{27} $(n,\alpha)Na^{24}$. The
establishment of one accurate cross-section value offers
a ready means of neutron flux monitoring and for determining
other cross-section values by comparative methods.

THE ESTABLISHMENT OF THE MASS/YIELD CURVE FOR THE FISSION OF NATURAL URANIUM WITH 14.7 MeV NEUTRONS

1. INTRODUCTION

The net rate of production of a radioactive isotope by fission of a heavy atom follows an exponential law. A saturation activity is approached at a rate dependent on the half-life of the isotope, when the rate of production from the fission process equals the rate of radioactive decay. The value of this saturation activity depends on the fission yield of the isotope, the neutron flux, the fission cross-section and the mass of the target.

Due to inaccuracies in determining the fission rate, it is convenient to calculate fission yields relative to one isotope as unity and hence construct a relative mass/yield curve, which can then be normalised to a total fission yield of 200. It is often both uneconomical and impracticable to irradiate samples for such a time as to produce saturation activities for all isotopes under consideration and it is more convenient therefore to calculate the saturation activity from the length of the irradiation and the activity at the end of the irradiation (A_0). A_0 is determined by extrapolating the decay curve back to the time at the end of the irradiation $(t = 0)$.

The neutron flux from the generator used for these irradiations is never constant and decreases over the length of the irradiation; corrections to the saturation activity calculation are therefore necessary.

Activity produced is proportional to $Ie^{-\lambda t}$. I is the number of neutrons emitted per unit time at time (t) and λ is the decay constant of the isotope produced.

The activity at the end of the irradiation is therefore proportional to $\int_0^t Ie^{-\lambda t}\, dt$, but it is more convenient to use a summation (Σ):_

$$\Sigma = I_1 e^{-\lambda t_1} + I_2 e^{-\lambda t_2} + \ldots \ldots I_n e^{-\lambda t_n}$$

(t_1, t_2 etc are calculated backwards from the end of the irradiation).

During each irradiation, the comparative neutron count is recorded at suitable intervals of time and the summation (Σ) is carried out for each isotope separated and counted. The fission yield of a particular isotope is therefore proportional to $\dfrac{A_0 \times t_{\frac{1}{2}}}{\Sigma}$ and the proportionality constant is the same for all isotopes separated from one irradiation.

$$\therefore \quad \frac{\text{Fission Yield (A)}}{\text{Fission Yield (B)}} = \frac{A_{0A} \times t_{\frac{1}{2}A} \times \Sigma_B}{A_{0B} \times t_{\frac{1}{2}B} \times \Sigma_A}$$

On account of the large number of isotopes of various

half-lives requiring separation and counting, it is necessary to carry out a number of irradiations varying in length from 20 minutes up to a maximum of $4\frac{1}{2}$ hours. The individual irradiations are compared by calculating the fission yields relative to Ba^{139} as unity. (This isotope was selected because of its high fission yield, unambiguous chemical behaviour, ease of separation, and convenient half-life).

2. NEUTRON GENERATOR

The generator consists of a Cockcroft - Walton type voltage quadrupling circuit capable of producing up to 300 KV. D.C. potential, an ion source giving up to $500 \mu a$ of deuterons and an accelerating tube in which the high voltage is used to impart a high energy to the ions. The deuteron beam strikes a tritium target and neutrons are emitted.

$$D_1^2 + T_1^3 \longrightarrow He_2^4 + n_0^1 + 17.6 \text{ MeV.}$$

2.1 Cockcroft - Walton Circuit and Measurement of Voltage

Power from the mains is applied to a Variac which supplies a Ferranti transformer connected to give up to 100 KV peak output voltage.

The quadrupling circuit (Fig I) consists of a string of four metal rectifiers and four $0.03 \mu F$ condensers, two of which (C_3 and C_4) serve to smooth the output voltage.

A_1 = Primary amps

V_1 = Primary volts

A_2 = D.C. amps

V_2 = Output volts
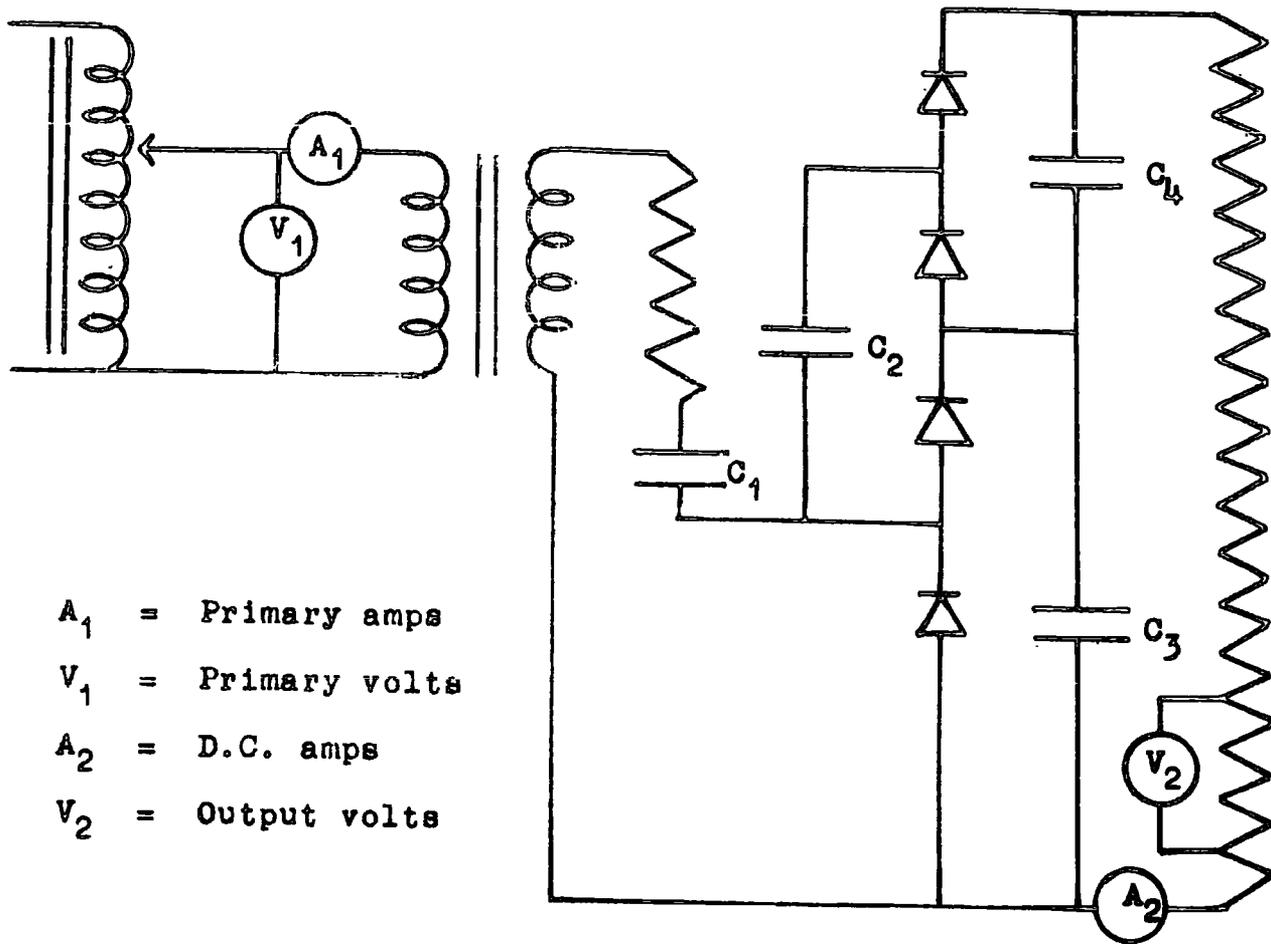
VOLTAGE QUADRUPLICATING CIRCUIT

FIG. I

2.1 Contd.

The high voltage is measured by means of an oil - cooled measuring resistance, across a fraction of which ($\frac{1}{200}$) a voltmeter (V_2) is connected.

2.2 Ion Source (Fig. 2)

The function of the ion source is to produce a stream of D^+ ions for acceleration by high voltage.

Deuterium gas is supplied through a heated palladium thimble from a heavy water electrolyser and fed into the ion source at a pressure of about 10^{-2} mms of mercury. Ionisation is produced by means of a high frequency electrodeless discharge, which is maintained by means of an R.F. oscillator giving approximately 100 watts at about 20 - 30 megacycles. Power is fed by means of a coupling loop of copper which encircles the ion source near its base and is cooled by an air blower. The ion source is also surrounded by a coil of copper tube which together with a variable air condenser, forms a circuit which is tuned to resonate with the oscillator.

Ions are extracted from the discharge through a narrow aluminium canal by applying a voltage of a few KV between the canal and the tungsten probe at the top of the ion source.

Tungsten
probe

Palladium leak

ION SOURCE

FIG. 2

Aluminium
canal
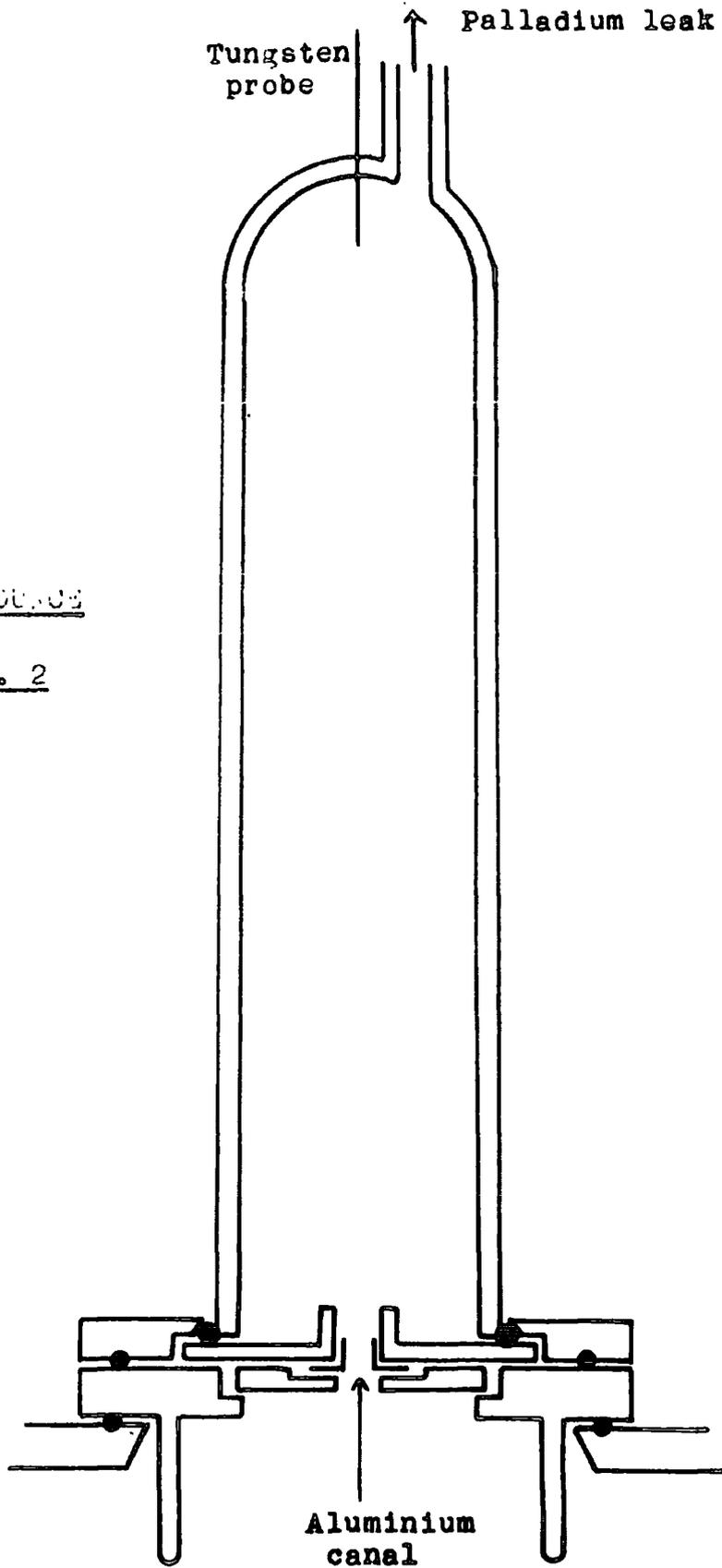
2.3 Accelerating Tube (Fig. 3)

The accelerating tube is composed of a series of three accelerating gaps. The first of these is a focussing gap to which is applied a variable voltage of about 40 KV and the voltage from the quadrupling circuit is split equally between the remaining two gaps. The system is enclosed in 12" Pyrex chemical pipe - line and is continuously pumped by a 9" Edwards Diffusion Pump, backed by an Edwards Rotary Pump; a Penning gauge records the pressure in the system ($\sim 10^{-5}$ mms of mercury pressure). The beam current reaching the target chamber (unresolved) and the current reaching the target block (resolved) are recorded.

2.4 Target Chamber (Fig. 4)

The target block is water - cooled and is attached to a 2" pipe at the bottom of the target chamber. The 2" pipe is capable of isolation from the main vacuum system for changing the target by means of a plate held in position by Sylphon bellows. The target consists of tritium absorbed into zirconium metal deposited onto a copper backing, which is secured to the target block by soldering with Wood's metal.

2.5 Estimation of Neutron Emission

Since relative neutron emissions only are required

Focussing
gap

First gap

ACCELERATING TUBE

FIG. 3

Second gap

Penning
gauge

Pumps

Target

Water - cooling
pipes

Tritium
Target
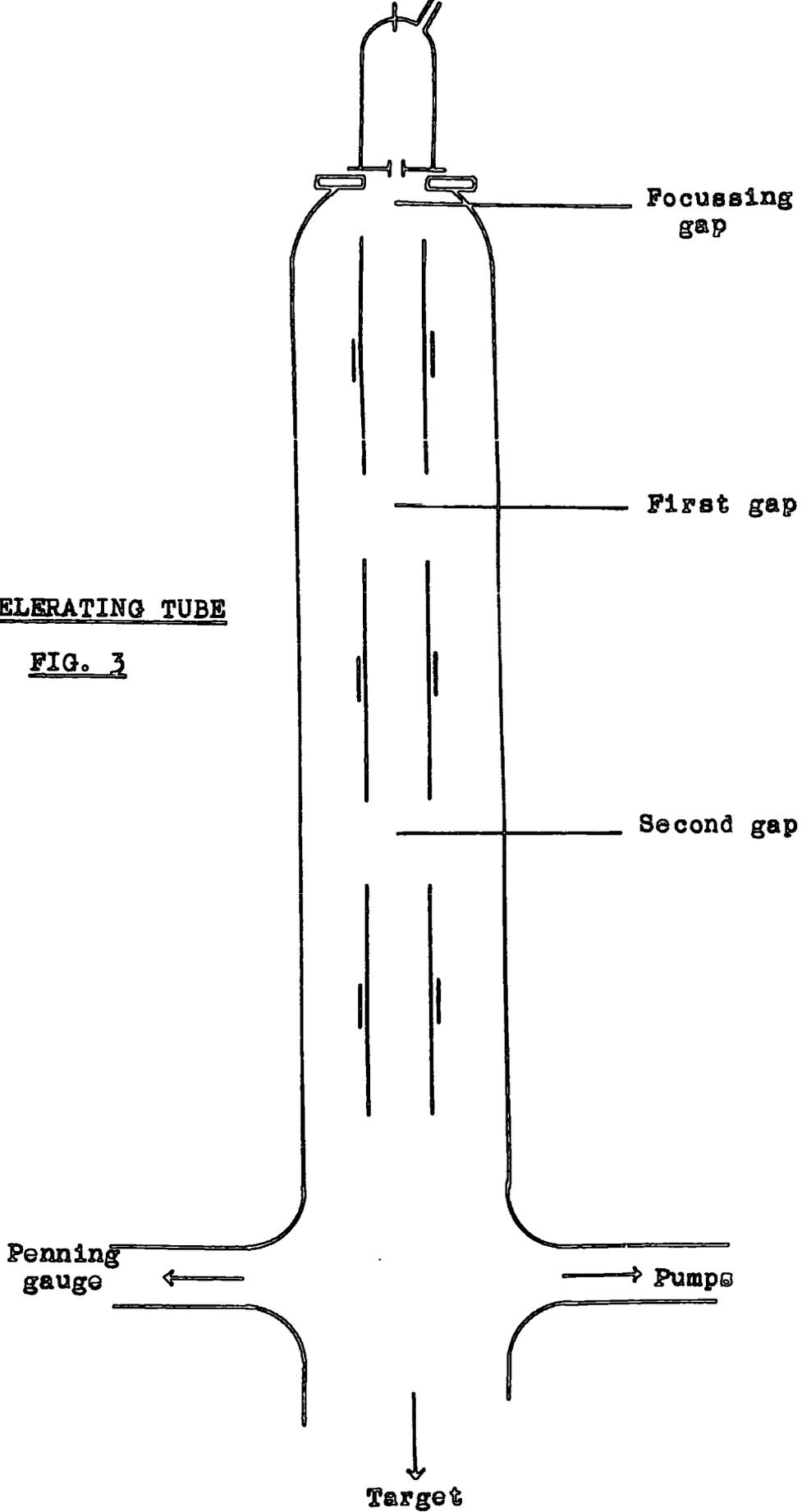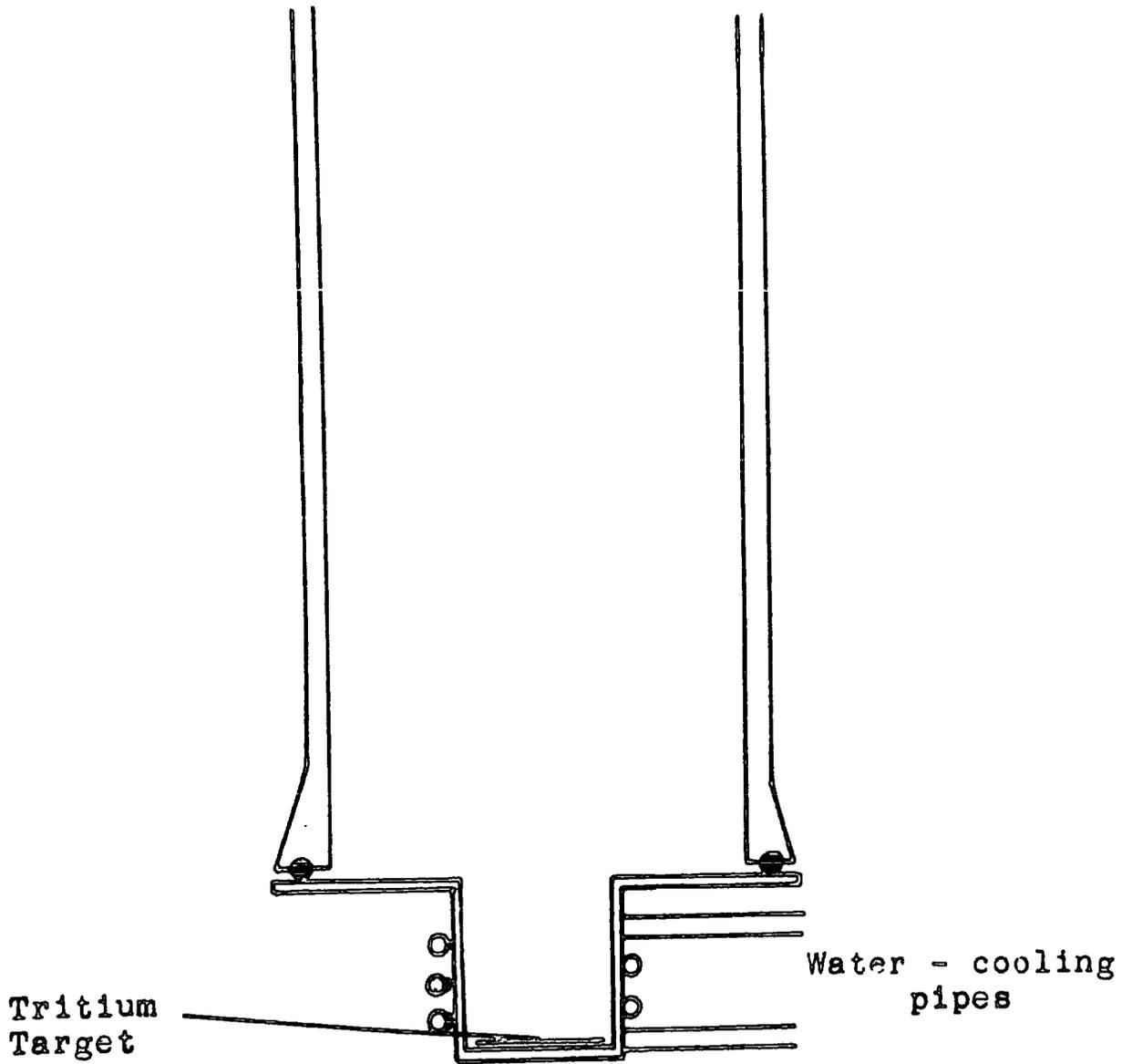
TARGET CHAMBER

FIG. 4

2.5 Contd.

for calculation of the fission yields, it is sufficient to fix a neutron detector in the vicinity of the target chamber. An organic phosphor is used to monitor the emission; proton recoils are counted, through a photo-multiplier, amplifier and scaler, biased to reject recoils from neutrons of lower energies (i.e. scattered from the walls of the target chamber or from the D + D reaction). Calibration of this neutron detector may be carried out by irradiation of a weighed copper disc which is then counted under standard conditions.

Some spread of neutron energies arises from energy loss of the deuterons in the target thickness and from the rather large angle subtended by the uranium sample at the target; the mean effective neutron energy is estimated at 14.7 MeV with limits of 14.9 MeV and 14.5 MeV.

2.6 Reasons for Reduction in Neutron Emission

The neutron emission was usually $10^9 - 10^{10}$ neutrons/second and any reduction could be attributed to one or more of the following conditions:-

1. Removal of tritium from the target by over-heating or replacement by deuterium from the beam.

2. Deposition of pump - oil vapour onto the target surface.

3. Movement of the deuteron beam away from the target.

2.6 Contd.

The life - time of a target was seldom more than 4 hours and throughout this time the neutron emission decreased considerably. A record of the neutron emission throughout a typical irradiation is given in Fig. 5.

3. RADIOCHEMICAL SEPARATIONS

The decay chains for the fission products expected to be produced from the 14.7 MeV neutron fission of natural uranium (see Appendix 1) were examined.

From this list, selection was made of elements for chemical separation followed by a counting procedure. The criteria for this selection were concerned with providing a source from which absolute disintegration rates could be assessed with confidence. The principal considerations were:-

1. The element should be capable of easy and rapid separation from all other elements.

2. The isotope should belong to a mass chain having a reasonably high expected fission yield (i.e. greater than 0.6%, mass will lie between 83 and 153).

3. The isotope should have a half - life in the range 20 mins to 3 days.

4. The isotope should not be produced from a pre-cursor of long half - life.

FIG. 5

VARIATION OF NEUTRON EMISSION DURING AN IRRADIATION

Position of the beam altered with respect to the target

neutrons per second

Time

3. Contd.

  5. The decay of the isotope should follow a simple β-emission to an isotope of very long half - life or to a stable isotope.

  6. There should be no other isotopes of similar half - life (or at least not more than two) due to the difficulty of resolving decay curves.

On the basis of the above criteria the following isotopes were selected:-

Br^{84} (31.8min.) $\longrightarrow Kr^{84}(s)$

Sr^{91} (9.7hr.) $\longrightarrow Y^{91m}(50.3min.)$
$\hspace{5cm} \downarrow$
$\hspace{4cm} Y^{91}$ (57d) $\longrightarrow Zr^{91}(s)$

Y^{93} (10.0hr.) $\longrightarrow Zr^{93}(1.1 \times 10^{6}yr.) \longrightarrow Nb^{93}(s)$

Mo^{99} (67.0hr.) $\longrightarrow Tc^{99m}(6.0hr.) \longrightarrow Tc^{99}(2 \times 10^{5}yr.)$
$\hspace{10cm} \downarrow$
$\hspace{9.5cm} Ru^{99}(s)$

Ru^{105} (4.5hr.) $\longrightarrow Rh^{105m}(45secs.) \longrightarrow Rh^{105}(36.5hr.)$
$\hspace{11cm} \downarrow$
$\hspace{10.5cm} Pd^{105}(s)$

Ag^{115} (21.1min.) $\longrightarrow Cd^{115m}(43d) \longrightarrow In^{115m}(4.5hr.)$
$\hspace{13.5cm} \searrow$
$\hspace{14cm} Sn^{115}(s)$
$\hspace{4.5cm} \searrow Cd^{115}$ (53hr.) $\rightarrow In^{115}(6 \times 10^{14}yr.)$

Ba^{139} (85min.) $\longrightarrow La^{139}(s)$

Ba^{141} (18min.) $\longrightarrow La^{141}(3.9hr.) \longrightarrow Ce^{141}(32.5d)$
$\hspace{10.5cm} \downarrow$
$\hspace{10cm} Pr^{141}(s)$

Ce^{143} (33hr.) $\longrightarrow Pr^{143}(13.8d) \longrightarrow Nd$ (s)

-14-

3. Contd.

Br^{84}, Sr^{91}, Y^{93}, Mo^{99}, Ru^{105}, Ag^{115}, Ba^{139}, Ba^{141} (or La^{141}) and Ce^{143} had quite straightforward decay chains with the β -emitting daughters of sufficiently long half lives to give negligible contribution to the β -particle counting. The radiochemical separations of Ba^{139} were delayed $1\frac{1}{2}$ hours to allow its precursor (half - life 9.5 mins) to decay. Similarly Sr^{92} (half - life 2.7 hr) and La^{143} (half - life 14 mins) were allowed to decay before commencing the separations of strontium and cerium respectively.

Further points, however, were required to complete an accurate mass/yield curve and relaxation of the restrictions permitted the inclusion of the following isotopes:-

$$\underline{Zr^{97}}(17.0hr.) \longrightarrow Nb^{97m}(60sec.) \longrightarrow Nb^{97}(72min)$$
$$\downarrow$$
$$Mo^{97} \ (s)$$
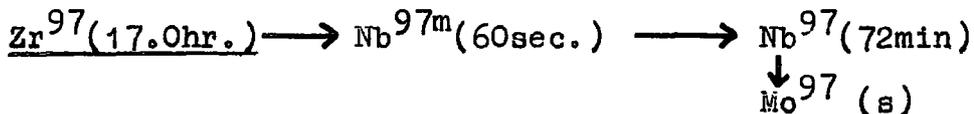
Corrections were applied for the presence of Nb^{97m} and Nb^{97}.

$$\underline{Pd^{109}}(13.5hr.) \longrightarrow Ag^{109m}(44.3sec.) \longrightarrow Ag^{109} \ (s)$$

$$\underline{Pd^{112}}(21hr.) \longrightarrow Ag^{112}(3.4hr.) \longrightarrow Cd \ (s)$$
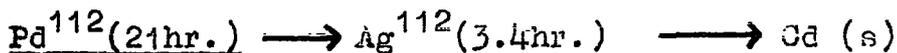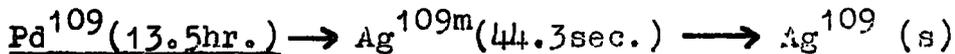
The decay was followed for a sufficient time to exclude the effect of Pd^{111} (half - life 5.5 hr.) and then

3. Contd.

the decay curve resolved into the Pd^{109} and $Pd^{112} - Ag^{112}$ components; the latter was further corrected for the presence of Ag^{112}.

$$Sb^{129}(4.6hr.) \xrightarrow[36\%]{64\%} \begin{array}{l} Te^{129}(72min) \longrightarrow I^{129}(1.6 \times 10^7 yr.) \\ Te^{129}(33d) \qquad\qquad Xe^{129} (s) \end{array}$$
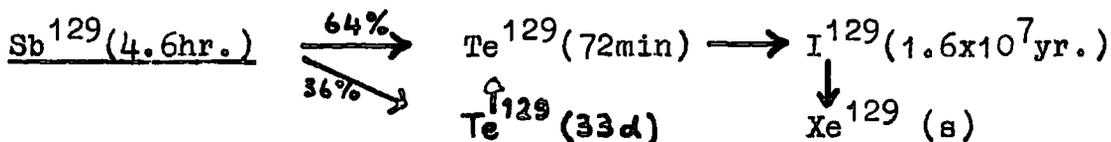
The count rate was corrected for the presence of Te^{129}. Ag^{111} (7.5 days), I^{131} (8.1 days) and Ba^{140} (12.8 days) were considered possible isotopes for separation and counting, providing sufficiently high count rates were obtained. Ag^{113} (5.3 hrs.) was also included, though a correction for the decay of Ag^{113m} (1.2min) direct to Cd^{113} would have to be applied.

The procedure adopted for the determination of the absolute disintegration rates of the isotopes was the counting of solid sources separated from the irradiated uranyl nitrate by chemical methods after the addition of inactive carriers. The separation methods were chosen for speed and effective decontamination from other elements rather than a quantitative yield and were mainly such that only one separation was carried out on each aliquot. Hence it was necessary at the commencement of the separations to know the exact quantity of inactive carrier added and to ensure that the inactive carrier and the

3. Contd.

radioactive isotope were present as the same ionic species. The final stage in the separation was the precipitation of the element in such a form that it could be filtered readily and the exact weight of the element present could be calculated from the weight of the precipitate. Hence the chemical yield (the ratio of the weight of the element in the final precipitate to that originally present) was determined.

Rapid and effective chemical separations were therefore required for silver, barium, strontium, molybdenum, ruthenium, yttrium, palladium, iodine, bromine, antimony, cerium and zirconium.

Due to the rapid decay of many of the radioactive species involved, it was seldom possible for one person to make measurements on more than a few elements at a time. To make the best use of the irradiated material Dr. D.J. Silvester (Research Student at this Laboratory) carried out the barium, yttrium, iodine, bromine, antimony and zirconium separations. For completeness, a brief outline of all the separations is given below and more detailed descriptions of the author's separations are given in Appendix II.

3.1 Silver (8)

Silver chloride is precipitated from the solution of irradiated uranyl nitrate with hydrochloric acid (the supernate is retained for barium and strontium separations). Purification is effected by alternate ferric hydroxide scavenges, to reduce the level of general contamination and silver sulphide precipitations to remove the halogen contamination. The silver is finally precipitated as silver chloride for weighing and counting.

3.2 Barium (9)

The supernate from the silver separation is evaporated to small bulk and three barium chloride precipitations are carried out with ice - cold hydrochloric acid - ether mixtures (the supernate from the first precipitation is retained for strontium separation). The final barium chloride precipitate is filtered and weighed, ready for counting.

3.3 Strontium (10)

Strontium nitrate is precipitated with fuming nitric acid from the supernate from the barium separation. Two ferric hydroxide scavenges are carried out, followed by a further strontium nitrate precipitation. The strontium is finally precipitated as the oxalate for weighing and counting.

3.4 Molybdenum (11)

Molybdenum is precipitated from acid solution containing oxalic acid (to complex the niobium) with an alcoholic solution of α-benzoinoxime. The precipitate is dissolved in a perchloric acid - nitric acid mixture and two ferric hydroxide scavenges are carried out. The α-benzoinoxime precipitation is repeated and the molybdenum is finally precipitated as the oxime (12) from an acetate buffered solution for weighing and counting.

3.5 Ruthenium (13)

Ruthenium tetroxide is distilled into sodium hydroxide solution from the irradiated uranyl nitrate solution containing perchloric acid, sodium bismuthate (to oxidise halogens to their highest oxidation state) and phosphoric acid (to reduce the volatilization of molybdenum). The ruthenium is precipitated by reduction of the ruthenate to lower oxides (Ru_2O_3 and RuO_2) with ethanol (leaving technetium in solution). The ruthenium oxide is dissolved in hydrochloric acid and finally precipitated as the metal for weighing and counting, by reduction with aluminium powder. The metal contains a small, but constant amount of oxide and the weight is 6% greater than the weight obtained by ignition in hydrogen (13).

-19-

3.6 Yttrium (14, 15)

The solution of irradiated uranyl nitrate containing yttrium, lanthanum, cerium[III] and zirconium carrier solutions is treated with tri - butyl phosphate to remove the uranium. Hydrofluoric acid is added to precipitate the yttrium and the rare earth elements, leaving the zirconium and any residual uranium in the supernate. The fluorides are dissolved in boric acid - nitric acid solution, reprecipitated and redissolved. The hydroxides are precipitated leaving any barium and strontium con- tamination in solution. The hydroxides are dissolved, the cerium oxidised with potassium bromate to the tetravalent state and extracted into tri - butyl phosphate (21). The hydroxide precipitation and cerium extraction are repeated. The rare - earths are removed by two precipitations of potassium lanthanum carbonate and the yttrium is finally precipitated as oxalate for weighing and counting.

3.7 Palladium (16)

Palladium is precipitated from dilute acid solution with dimethyl glyoxime. Purification from possible contaminants (selenium, silver and zirconium) is effected by ferric hydroxide and silver iodide scavenges. The palladium is finally reprecipitated as the dimethyl glyoxime for weighing and counting.

3.8 Iodine (17)

Interchange of tracer and carrier iodine and bromine is effected by oxidation to periodate and bromate respectively with sodium hypochlorite solution. The periodate is reduced by hydroxylamine hydrochloride solution to iodine which is extracted into carbon tetrachloride, while the bromine as bromide remains in the aqueous layer, which is retained for the bromine separation. The iodine is back - extracted as iodide into sodium bisulphite solution. The extraction cycle is repeated using nitric acid - sodium nitrite mixture for the oxidation and sodium bisulphite for the reduction. The iodine is finally precipitated as silver iodide for weighing and counting.

3.9 Bromine (18)

The bromine from the aqueous layer in the iodine separation is oxidised with potassium permanganate solution extracted into carbon tetrachloride and back - extracted into hydroxylamine hydrochloride solution. The extraction cycles are repeated twice, back - extracting into sodium bisulphite solution. The bromine is finally precipitated as silver bromide for weighing and counting.

3.10 Antimony (19)

Antimony[IV], produced by oxidation by potassium permanganate solution, is extracted into ethyl acetate as the oxalate - citrate complex. The ethyl acetate is removed by evaporation, the residue dissolved in concentrated hydrochloric acid and antimony sulphide precipitated. The sulphide is dissolved in concentrated hydrochloric acid. The antimony is reduced to the trivalent state with sulphurous acid and finally precipitated as the pyrogallate[20] in the presence of tartrate ions for weighing and counting.

3.11 Cerium (21)

The cerium is oxidised to the tetravalent state with sodium bismuthate, extracted into tri - butyl phosphate and back - extracted into hydroxylamine hydrochloride solution. Cerium oxalate is finally precipitated for weighing and counting.

3.12 Zirconium (22)

Zirconium is extracted into chloroform as the cupferron complex from dilute sulphuric acid solution. The chloroform is evaporated and the residue dissolved in a sulphuric acid - nitric acid mixture. The hydroxide is precipitated, dissolved in concentrated hydrochloric acid and the zirconium is finally precipitated as the

tetramandelate (23) for weighing and counting.   Table I
shows the chemical form of the carrier solution and of
the final precipitate and the usual quantity of carrier
added.

TABLE (1)

Element	Chemical Form in carrier solution	Weight of carrier (mg of element)	Chemical form of final precipitate
Br	$NaBrO_3$	9.98	Ag Br
Sr	$Sr(NO_3)_2$	9.55	Sr oxalate
Y	$Y_2(NO_3)_3$	10.0	Y oxalate
Zr	$Zr(NO_3)_4$	4.75	Zr tetramandelate
Mo	$Mo\ O_3$	24.3	Mo 8-hydroxy-quinolate
Ru	$RuCl_3$	10.0	Ru metal
Pd	$PdCl_2$	8.08	Pd dimethyl-glyoxime
Ag	$AgNO_3$	9.65	Ag Cl
Sb	$SbCl_3$	8.15	Sb pyrogallate
I	KI	9.60	Ag I
Ba	$Ba(NO_3)_2$	9.60	$BaCl_2 \cdot H_2O$
Ce	$Ce_2(NO_3)_3$	4.92	Ce oxalate

4. COUNTING PROCEDURE

4.1 The β-Energies of the Isotopes

The β-energies of the isotopes examined are as follows (24):-

Br^{83}	0.94MeV
Br^{84}	4.7MeV(40%), 3.56MeV(9%), 2.53MeV(16%) 1.72MeV(35%)
Sr^{91}	2.67MeV(26%), 2.03MeV(4%), 1.36MeV(29%) 1.09MeV(33%), 0.62MeV(8%)
Y^{93}	2.88MeV
Zr^{97}	1.91MeV
Nb^{97}	1.27MeV
Mo^{99}	1.18MeV(83%), 0.80MeV(3%), 0.41MeV(14%)
Ru^{105}	1.15MeV
Pd^{109}	1.02MeV
Ag^{111}	1.04MeV(91%), 0.80MeV(1%), 0.70MeV(8%)
Pd^{112}	0.28MeV
Ag^{112}	4.1MeV(25%), 3.5MeV(40%), 2.7MeV(20%) 1.0MeV(15%)
Ag^{113}	2.0MeV
Ag^{115}	2.9MeV
Sb^{129}	1.87MeV
Te^{129}	1.46MeV(80%), 1.01MeV(20%)
I^{131}	0.815MeV(1%), 0.61MeV(86%), 0.335MeV(10%), 0.25MeV(3%)

4.1   <u>Contd.</u>

Ba^{139}	2.38MeV(15%), 2.23MeV(66%), 0.82MeV(19%)
Ba^{140}	1.0MeV(75%), 0.4MeV(25%)
La^{140}	2.20MeV(10%), 1.62MeV(14%), 1.36MeV(30%), 1.15MeV(20%), 0.86MeV(12%), 0.42MeV(14%)
Ba^{141}	2.8MeV
La^{141}	2.43MeV(95%), 0.9MeV(5%)
Ce^{143}	1.40MeV(37%), 1.13MeV(40%), 0.74MeV(5%), 0.50MeV(12%), 0.20MeV(6%).

4.2   <u>Counting Equipment</u>

In the selection of the type of counter for use in determining the β-activity of the isotopes separated radiochemically, attention must be given to the following points:-

(i)   High geometry.

(ii)   Long - term stability (due to the fact that counting from one run may last over a number of days).

(iii) Low background.

(iv)   Ease of operation.

It was decided from these conditions to use a Harwell $2\pi\beta$-proportional counter type 1222A (Fig. 6) in conjunction with an H.F. head amplifier (type 1008), a main amplifier (type 1008) and a scaler (type 1009A). The potential to the anode was supplied from a power unit

-25-

COUNTING GAS CONNECTIONS

LOOP ANODE 5-7 MM DIA

O RING SEAL

3"

1·25

2"

3½"

FIXING BOLTS

1"/16   3"/16

SAMPLE SLIDE

RECESSES TO TAKE
SAMPLE TRAYS
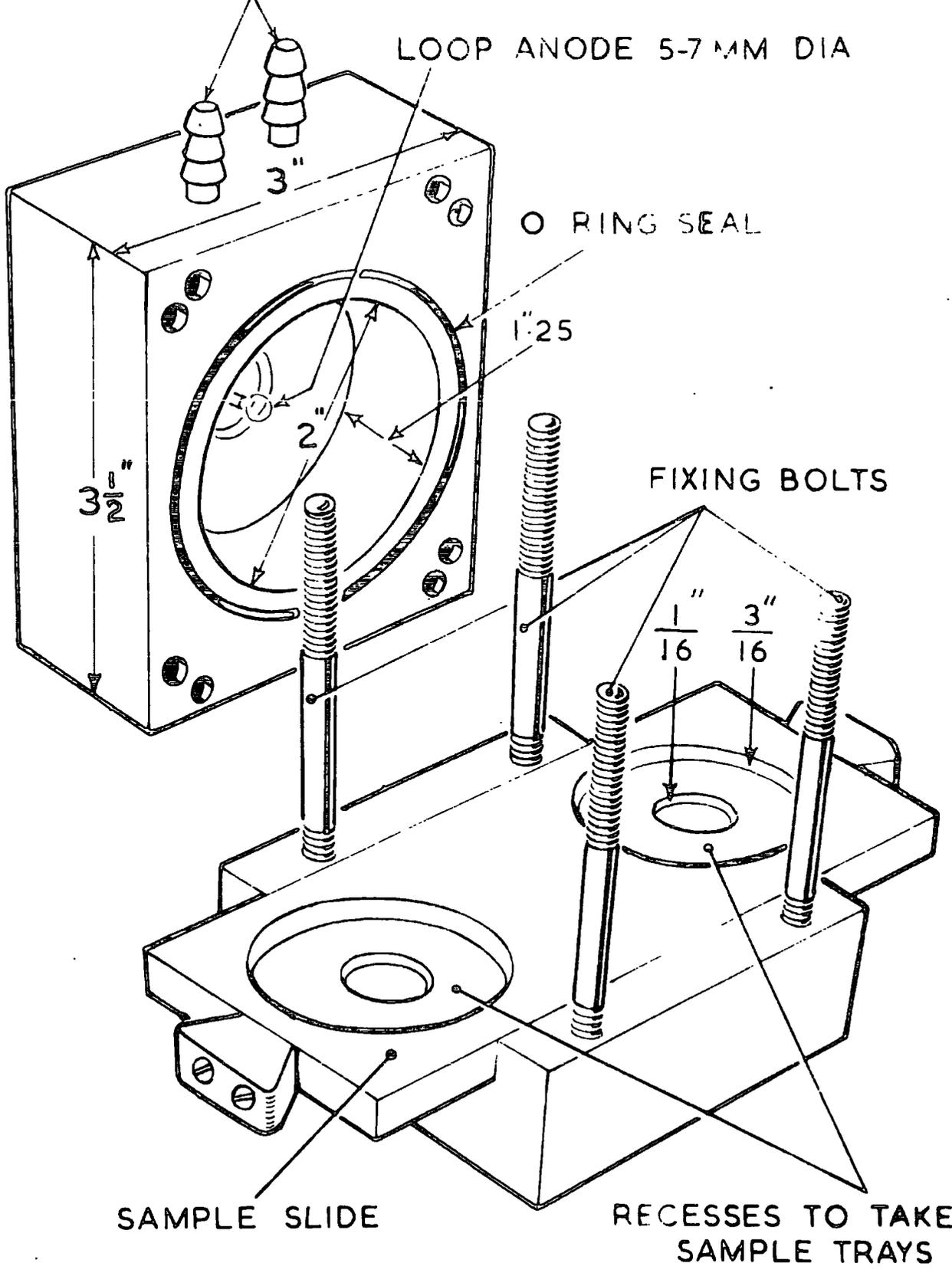
FIG. 6. PROPORTIONAL COUNTER

4.2 <u>Contd.</u>

(type 200) and the pulses could be monitored on a cathode
ray oscilloscope (type 1000). To eliminate spurious
pulses, a 3-stage decoupling circuit was included in the
E.H.T. supply.

The counting gas used was industrial methane purified
by passing over a heated platinum gauze ($500^{o}C$) and then
through an Anhydrone drier. Changes in the gas flow rate
made little difference to the counting efficiency and a
constant rate of about 35 ccs per minute was used. To
reduce the background count, the counter was surrounded by
a lead shield (1.25 inches thick).

4.3 <u>Stability</u>

The counter was found to exhibit good plateau
characteristics, the length of the plateau being about
300v. Typical values of counts/min. of a source against
anode potential are given in Table 2.

TABLE (2)

Anode Potential kV	Counts/min
2.60	6116
2.70	7866
2.80	9321
2.84	9790
2.88	9829
2.92	10011
2.96	10112
3.00	9956
3.04	10046
3.08	10207
3.12	10147
3.20	10606
3.30	11375

Typical values of counts/min. of a phosphorus – 32 source (E max. = 2.3 MeV) against discriminator bias voltage are given in Table 3.

TABLE (3.)

D.B.V.	Counts/min.
5.0	4050
7.5	3716
10.0	3514
12.5	3347
15.0	3365
20.0	3264
25.0	3298
30.0	3207
40.0	3159
50.0	3144

The β-energy of phosphorus - 32 is about the mean of the energies of the isotopes examined and so a discriminator bias voltage of 15.0v. and a counting voltage of 2.96 KV would be selected from the above two tables.

A number of 1 minute counts were recorded from a source. The mean count rate was 8384 counts/min. with a standard deviation of ± 92 counts/min. which compared very well with the theoretical standard deviation of ± 91 counts/min. This indicated that the counter was operating

4.3 Contd.

satisfactorily and that no spurious counts were being recorded.

To test the long - term stability of the counter, five one minute counts were recorded once a day for five days. The daily mean values were 10116, 10024, 9970, 10070, 9979 counts/min. The maximum spread was just over 1%, there was no obvious trend and the calculated standard deviation ($\pm$ 110 counts/min.) was very close to the theoretical standard deviation ($\pm$ 100 counts/min.).

It was, therefore, considered that the long - term stability of the counter was satisfactory.

4.4 Counter Flushing

One disadvantage of this type of counter was that as the source was situated within the counting volume, air was admitted to the counter on replacement of a source and had to be flushed out with methane. To reduce the volume of air admitted on changing sources, a cylindrical block of aluminium (3/16" thick) was inserted into the spare tray in the counter. A standard procedure was adopted for rapid source changing. This involved changing the source ($\frac{1}{2}$ minute), flushing at about 250 ccs per minute (1 minute), followed by normal flow ($3\frac{1}{2}$ minutes); by this time, the counter had settled down to a steady count rate. This procedure enabled the large number of

sources produced after an irradiation to be counted at such intervals as to enable satisfactory decay curves to be constructed.

4.5 Counting Corrections

The absolute disintegration rate of a source is given by the expression:-

Disintegration rate = Count rate x E x A x B x S

E is the counter factor.

A is the absorption factor.

B is the back - scatter factor.

S is the self - absorption factor.

The counter factor is constant ($\sim$2) but the other factors are dependent on the β -energies of the isotopes examined.

4.5.1. Back - Scatter and Self - Absorption Factors

Experimental data are available (25, 26) on the back - scatter and self - absorption factors for a number of isotopes examined under similar conditions of 2π counting and the factors for the remainder were deduced from the same data.

4.5.2. Absorption Factor

To protect the sources during handling and counting, they were covered with a layer of Sellotape (one roll was reserved solely for this purpose). It was not possible to determine the absorption factor for all isotopes examined by counting the sources

-30-

4.5.2. Contd.

before and after covering with Sellotape, since a
number of sources did not decay with a unique half -
life on account of the presence of shorter or longer
lived isotopes or a disequilibrium between parent and
daughter activities. It was decided, therefore, to
determine the absorption coefficient of the Sellotape
and to apply a theoretical calculation to determine
the absorption factor to be applied for each isotope.
This factor would be checked for those isotopes for
which a practical value could be obtained.

The relative count rates of an iodine - 131
source covered by various thicknesses of aluminium foil
and a varying number of layers of Sellotape were
determined. It is seen from the results (Fig. 7)
that the equivalent thickness of one layer of
Sellotape is 10.26 mg. aluminium/cm^2.

The absorption of β -radiation may be approxi-
mately represented by:-

$$I = I_o \, e^{-\mu d}$$

I = transmitted radiation.

I_o = incident radiation.

μ = absorption coefficient (cm^2/mg)

d = absorber thickness (mg/cm^2).

FIG. 7

RELATIVE ABSORPTION CURVE FOR SELLOTAPE AND ALUMINIUM
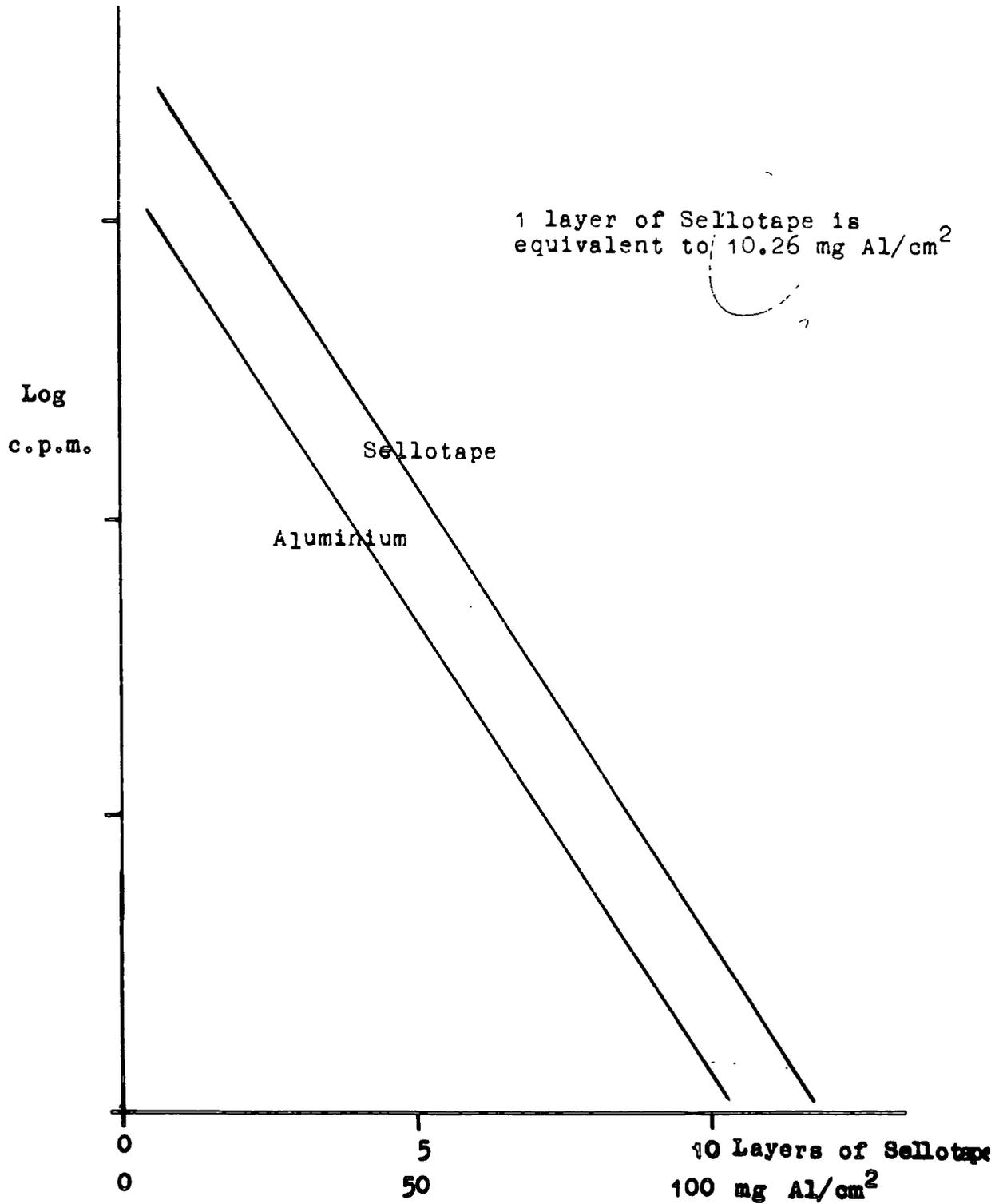
4.5.2. Contd.

If $D_{\frac{1}{2}}$ is the absorption half - thickness, this may be rewritten

$$\frac{I_o}{I} = e^{\frac{0.693 \mu}{D_{\frac{1}{2}}}}$$

Curie et al (27) have suggested an empirical relationship between half - thickness and β -energy of the form:-

$$D_{\frac{1}{2}} = 40 \; E^{1.14}$$

(E = E max. in MeV; $D_{\frac{1}{2}}$ in mg/cm^2)

Since this equation is applicable to incident radiation passing almost normally through the absorber, a correction must be applied for the β -particles entering the Sellotape through a solid angle of 2π.

If θ is the angle of incidence, the fraction of particles emerging (F) is given by

$$F = \frac{\int_o^{\frac{\pi}{2}} \sin\theta \; e^{-\mu d \; \sec\theta} \; d\theta}{\int_o^{\frac{\pi}{2}} \sin\theta \; d\theta}$$

Values of this integral have been tabulated (28) and are shown graphically in Fig. 8.

Values of absorption factors for varying E max values were calculated and are shown in Table 4 and Fig. 9.

FIG. 8

FRACTIONAL TRANSMISSION F v μ d
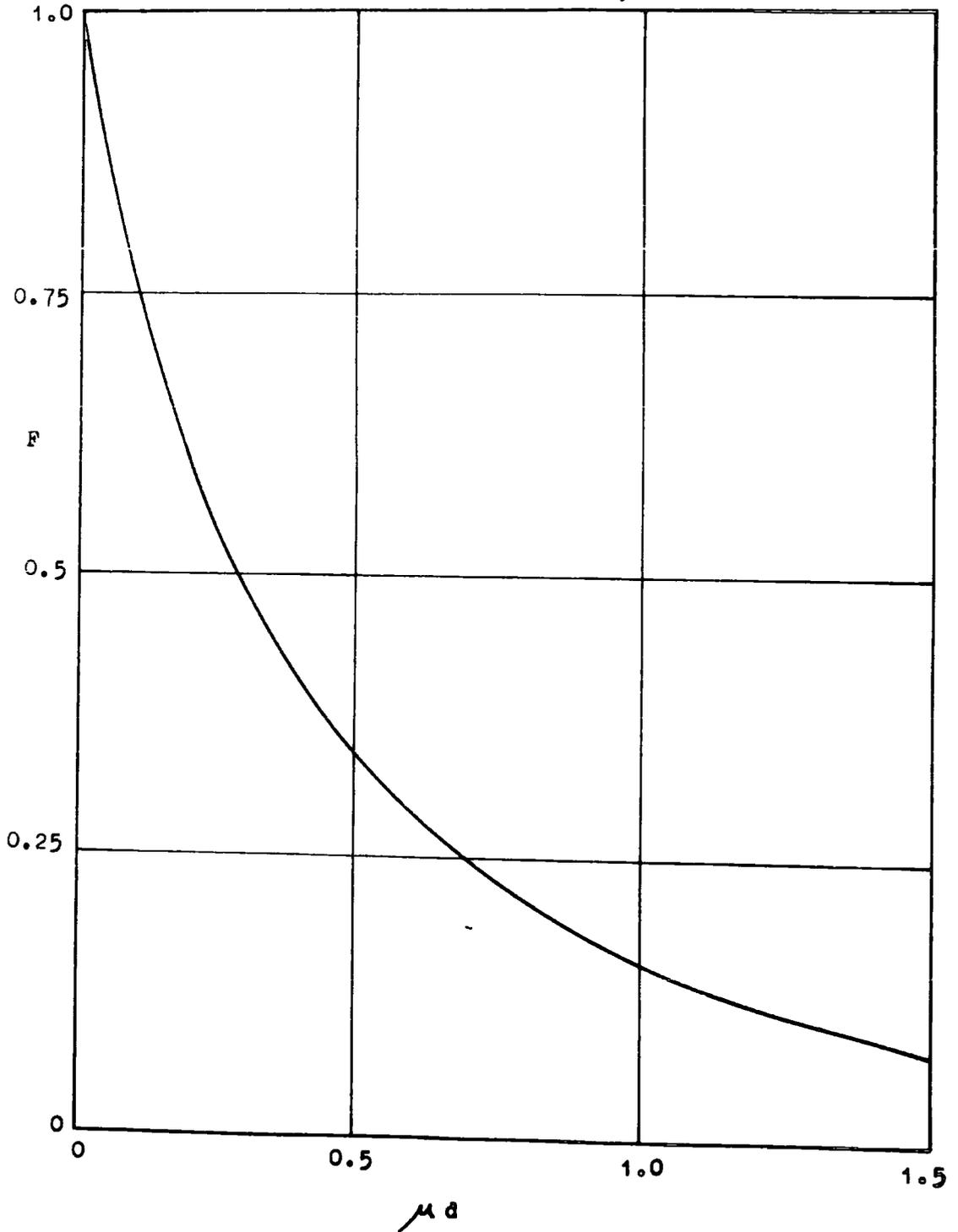
TABLE (4)

E max MeV	E max$^{1.14}$	$D_{\frac{1}{2}}$ mg/cm^2	$\frac{\mu d\ (0.693 \times 10.26)}{D_{\frac{1}{2}}}$	F (28)	Absorption Factor (A)
0.2	0.160	6.40	1.110	0.1265	7.91
0.25	0.196	7.84	0.907	0.1706	5.86
0.3	0.254	10.16	0.700	0.235	4.26
0.4	0.352	14.08	0.505	0.324	3.09
0.5	0.454	18.16	0.392	0.395	2.53
0.75	0.722	28.88	0.246	0.522	1.92
1.0	1.00	40.0	0.178	0.602	1.66
1.5	1.61	64.4	0.110	0.705	1.42
2.0	2.21	88.4	0.080	0.761	1.31
3.0	3.50	140.0	0.051	0.825	1.21
4.0	4.85	194.0	0.037	0.862	1.16
5.0	6.27	251.0	0.028	0.888	1.13

From Fig. 9, the absorption factors are calculated for
I^{131}, Mo^{99}, Sr^{91} and Ba^{139} for which practical values had been obtained (Table 5).

FIG. 9

FRACTIONAL TRANSMISSION F v. E_{max}
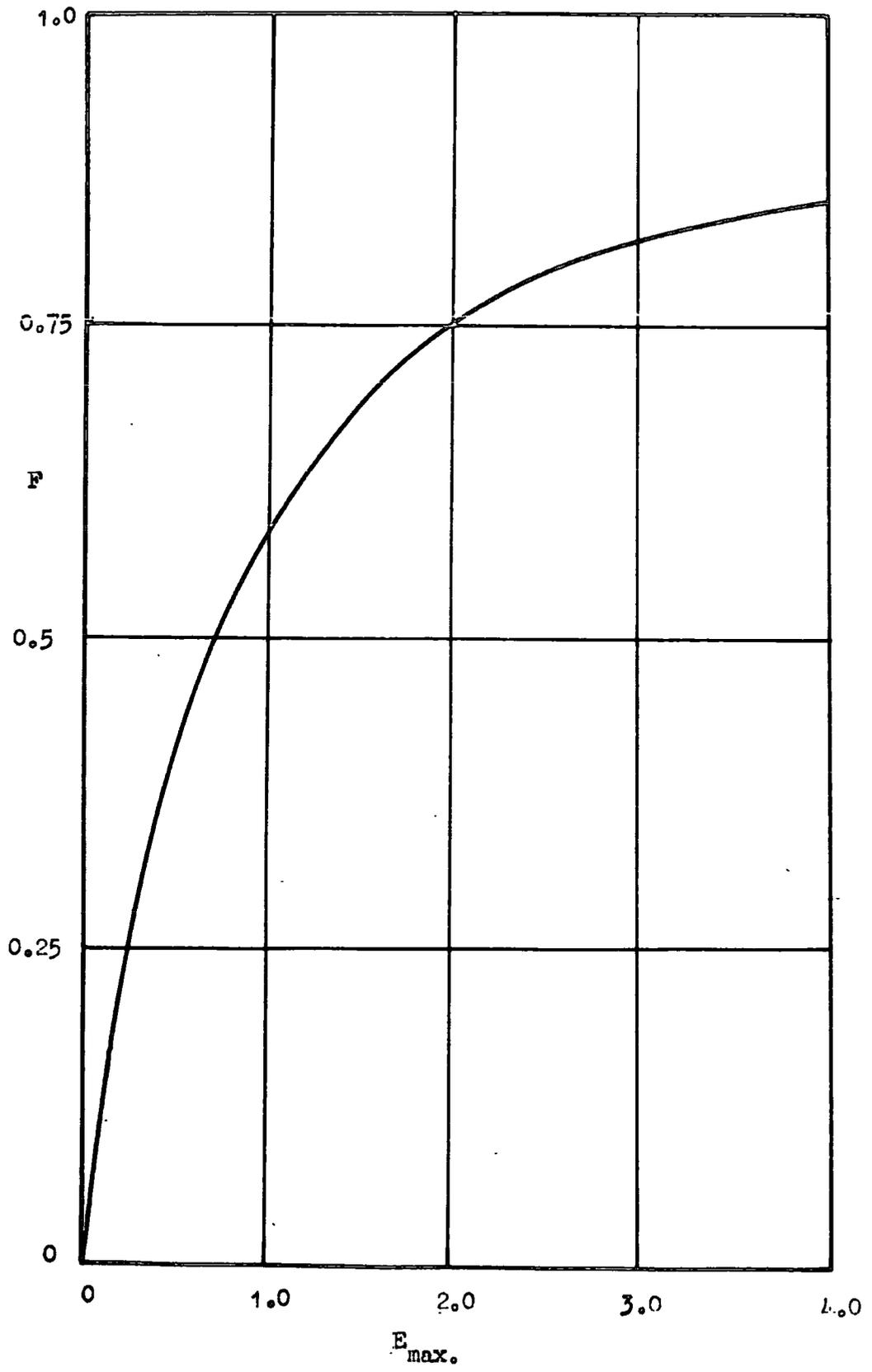
TABLE (5)

Isotope	E max	Proportion (a)	F	F x a	Weighted F	Absorption Factor
I^{131}	0.815 0.610 0.335 0.250	0.01 0.86 0.10 0.03	0.550 0.465 0.265 0.171	0.006 0.400 0.027 0.005	0.438	2.28
Mo^{99}	1.18 0.80 0.41	0.83 0.03 0.14	0.650 0.540 0.350	0.539 0.016 0.049	0.604	1.66
Sr^{91}	2.67 2.03 1.36 1.09 0.62	0.26 0.04 0.29 0.33 0.08	0.810 0.765 0.680 0.630 0.455	0.211 0.031 0.197 0.208 0.036	0.683	1.46
Ba^{139}	2.38 2.23 0.82	0.15 0.66 0.19	0.790 0.780 0.550	0.119 0.504 0.105	0.728	1.37

The experimental values for the fractional transmission (F) are compared with the calculated values in Table 6.

TABLE (6)

Isotope	Experimental F	Calculated F	Calculated / Experimental
I^{131}	0.634	0.438	0.690
Mo^{99}	0.752	0.604	0.802
Sr^{91}	0.823	0.683	0.830
Ba^{139}	0.840	0.728	0.865

4.5.2. <u>Contd.</u>

It is seen in Table 6 that calculation of the absorption factor does not agree with the experimental factor and that the lower the energy the larger is the discrepancy. This may be due to the fact that absorption of β -particles is not strictly exponential and that the softest particles are less readily absorbed than theory would suggest. A plot of the calculated values against the experimental values gives a smooth curve (one of the points being a hypothetical β -emitter with an absorption factor of unity both calculated and experimental). From this curve (Fig. 10), it is possible to correct all the calculated absorption factors to a more accurate value. The absorption factors for all the isotopes examined have been calculated and are listed in Table 7.

FIG. 10

CALCULATED F v EXPERIMENTAL F
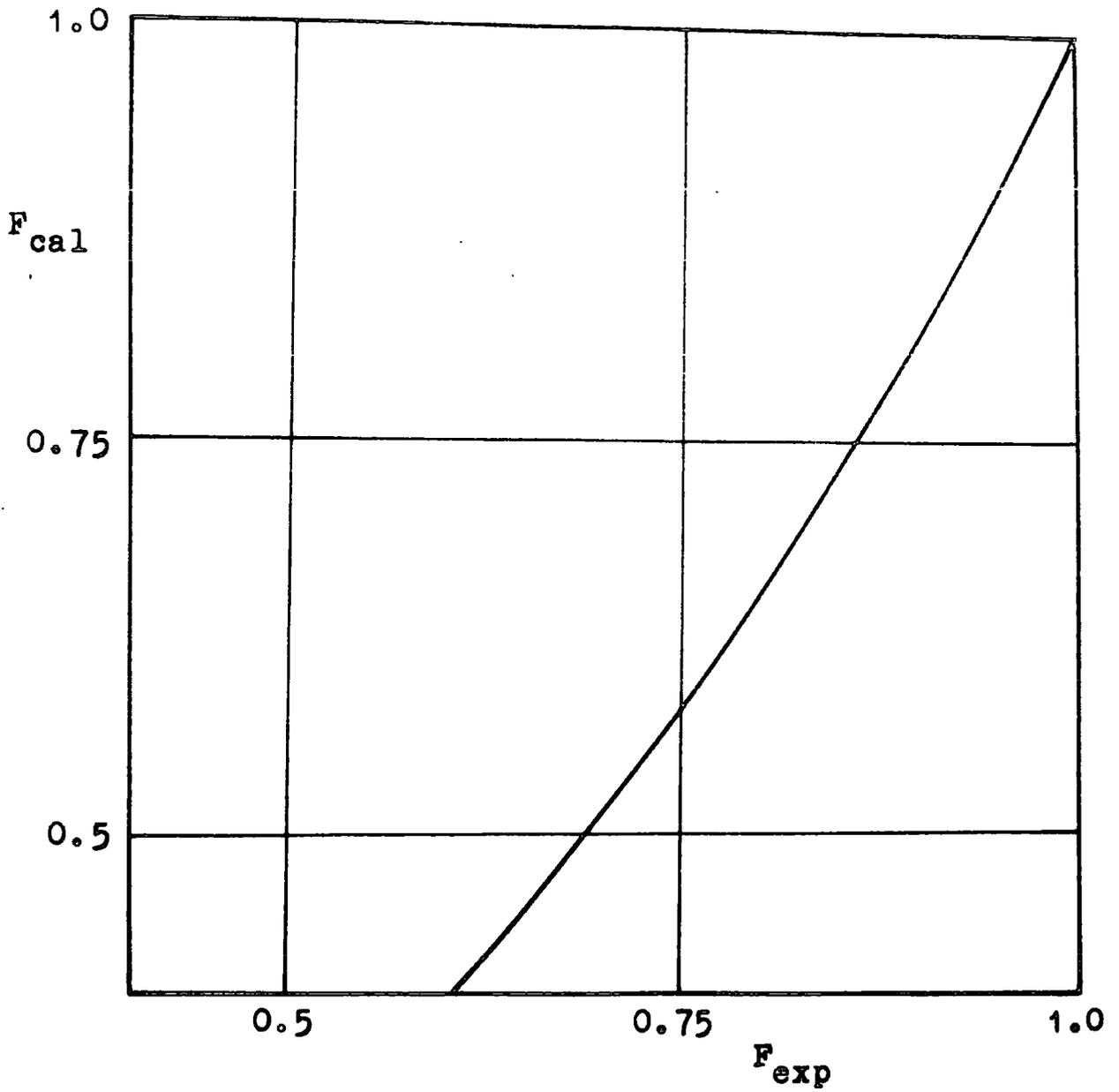
TABLE (7)

Isotope	E max	Proportion (a)	F	F x a	Weighted F	Corrected F	Absorption Factor
Br^{83}	0.94				0.590	0.750	1.33
Br^{84}	4.70 3.56 2.53 1.72	0.40 0.09 0.16 0.35	0.880 0.850 0.800 0.735	0.352 0.076 0.128 0.250	0.806	0.880	1.14
Sr^{91}					0.820	0.823	1.21
Y^{93}	2.88					0.900	1.11
Zr^{97}	1.91				0.755	0.860	1.16
Nb^{97}	1.27				0.665	0.800	1.25
Mo^{99}						0.752	1.33
Ru^{105}	1.15				0.640	0.785	1.27
Pd^{109}	1.02				0.610	0.765	1.31
Pd^{111}	3.5				0.850	0.915	1.09
Ag^{111}	1.04 0.80 0.70	0.91 0.01 0.08	0.615 0.540 0.500	0.559 0.005 0.040	0.604	0.760	1.32
Pd^{112}	0.28				0.160*		

* Since the value of F for Pd^{112} is too low for accurate correction from Fig. 10, correction is postponed until after the next section in order that it can be combined with Ag^{112}.

-36-

TABLE (7) Contd.

Isotope	E max	Proportion (a)	F	F x a	Weighted F	Corrected F	Absorption Factor
Ag^{112}	4.1 3.5 2.7 1.0	0.25 0.40 0.20 0.15	0.865 0.850 0.810 0.602	0.216 0.340 0.162 0.090	0.808	0.890	1.12
Ag^{113}	2.0				0.761	0.860	1.16
Ag^{115}	2.9				0.820	0.900	1.11
Sb^{129}	1.87				0.750	0.855	1.17
Te^{129}	1.46 1.01	0.80 0.20	0.700 0.605	0.560 0.121	0.681	0.810	1.23
I^{131}						0.634	1.58
Ba^{139}						0.840	1.19
Ba^{140}	1.0 0.4	0.75 0.25	0.602 0.324	0.451 0.081	0.532	0.705	1.42
La^{140}	2.20 1.62 1.36 1.15 0.86 0.42	0.10 0.14 0.30 0.20 0.12 0.14	0.780 0.725 0.685 0.640 0.565 0.340	0.078 0.101 0.206 0.128 0.068 0.054	0.635	0.780	1.28

TABLE (7) Cont'd.

Isotope	E max	Proportion (a)	F	F x a	Weighted F	Corrected F	Absorption Factor
Ce^{143}	1.40	0.37	0.690	0.255	0.592	0.750	1.33
	1.13	0.40	0.640	0.256			
	0.74	0.05	0.520	0.026			
	0.50	0.12	0.395	0.047			
	0.20	0.06	0.1265	0.008			

4.6 Equilibrium Corrections

Corrections for transient and secular equilibrium conditions (section 3) must be applied as follows:-

In the decay chain $A \xrightarrow{\lambda_A} B \xrightarrow{\lambda_B} C$, the number of atoms of B present at time t is given by

$$N_B = \frac{\lambda_A (N_A)_0}{\lambda_B - \lambda_A} \left(e^{-\lambda_A t} - e^{-\lambda_B t} \right)$$

The relative contributions to the disintegration rate by parent and daughter are thus given by

$$\frac{\text{Relative contribution of parent (A)}}{\text{Relative contribution of daughter (B)}} = \frac{N_A \lambda_A}{N_B \lambda_B}$$

for $t \gg {}^1/\lambda_B$ this equals $\dfrac{\lambda_B - \lambda_A}{\lambda_B}$

The corrections must be applied to the following decay chains:-

$$Zr^{97}(17.0\text{hr.}) \longrightarrow Nb^{97}(72\text{min.})$$
$$Pd^{112}(21\text{hr.}) \longrightarrow Ag^{112}(3.4\text{hr.})$$
$$Sb^{129}(4.6\text{hr.}) \longrightarrow Te^{129}(72\text{min.})$$
$$Ba^{140}(12.8\text{day}) \longrightarrow La^{140}(40\text{hr.})$$
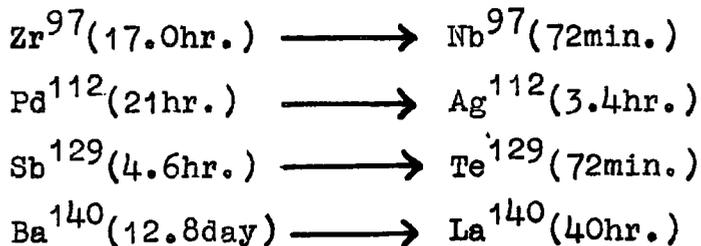
Table 8 shows the relative contributions to count rate.

TABLE (8)

Chain A – B	λ_A hr^{-1}	λ_B hr^{-1}	$\dfrac{\lambda_B - \lambda_A}{\lambda_B}$	% from A	% from B
$Zr^{97} - Nb^{97}$	0.0407	0.578	0.928	48.1	51.9
$Pd^{112} - Ag^{112}$	0.0330	0.204	0.837	45.5	54.5
$Sb^{129} - Te^{129}$	0.165	0.578	0.715*	52.3	47.7
$Ba^{140} - La^{140}$	0.00226	0.0172	0.866	46.4	53.6

* Only 64% of the Sb^{129} decays to Te^{129}, hence 0.715

becomes $\dfrac{0.715}{0.64}$ i.e. 1.115

Since a number of conversion electrons are emitted in the case of $Ba^{140} - La^{140}$, it is not possible to use the above calculation. Silvester (29) has determined experimentally the growth curve of $Ba^{140} - La^{140}$ and found a factor of 2.60 between the extrapolated activity and the initial Ba^{140} activity. This factor will be used in the calculation of the absolute Ba^{140} activity.

In the case of Ba^{139}, a correction is necessary due to the significant half - life of its precursor Cs^{139} (9.5 min.). The correction factor is $\dfrac{85 - 9.5}{85}$ i.e. 0.888. A similar correction is applied to Br^{84}.

The weighted correction F (Table 7) for $Pd^{112} - Ag^{112}$ is 0.455 x 0.160 + 0.545 x 0.808 i.e. 0.513, giving an absorption factor of 1.44.

-40-

5. EXPERIMENTAL DETAILS AND RESULTS

5.1 Procedure

Uranyl nitrate hexahydrate crystals were ground up in a pestle and mortar, wrapped in an envelope of filter – paper and sealed with Sellotape. The exact weight of uranium to be irradiated was not required to be known, but the quantity depended on the number of isotopes to be separated and it was usual to allow about 5g. uranyl nitrate hexahydrate for each separation. The envelope was attached to the bottom of the target chamber (Fig. 4) with Sellotape; the neutron generator was prepared for irradiation and the irradiation was commenced. The neutron count was recorded every 5 or 10 minutes according to the length of the irradiation.

At the end of the irradiation, the sample of uranyl nitrate was allowed to "cool" for 1-5 minutes, removed from the target chamber and dissolved in 0.1M nitric acid with appropriate carrier solutions to give a solution containing approximately 250 mg U/ml.

Portions of the solution were removed for radiochemical separations (Section 3). The final precipitates were collected in a perspex filter stick (Fig. 11) onto weighed filter paper discs, which had been washed and dried under the same conditions as in the separation procedure. The weighing of the filter paper discs was always carried out in a glass weighing bottle to avoid pick – up of moisture.

Filter
paper
disc

Perforated
Perspex
disc

FILTER STICK

FIG. 11
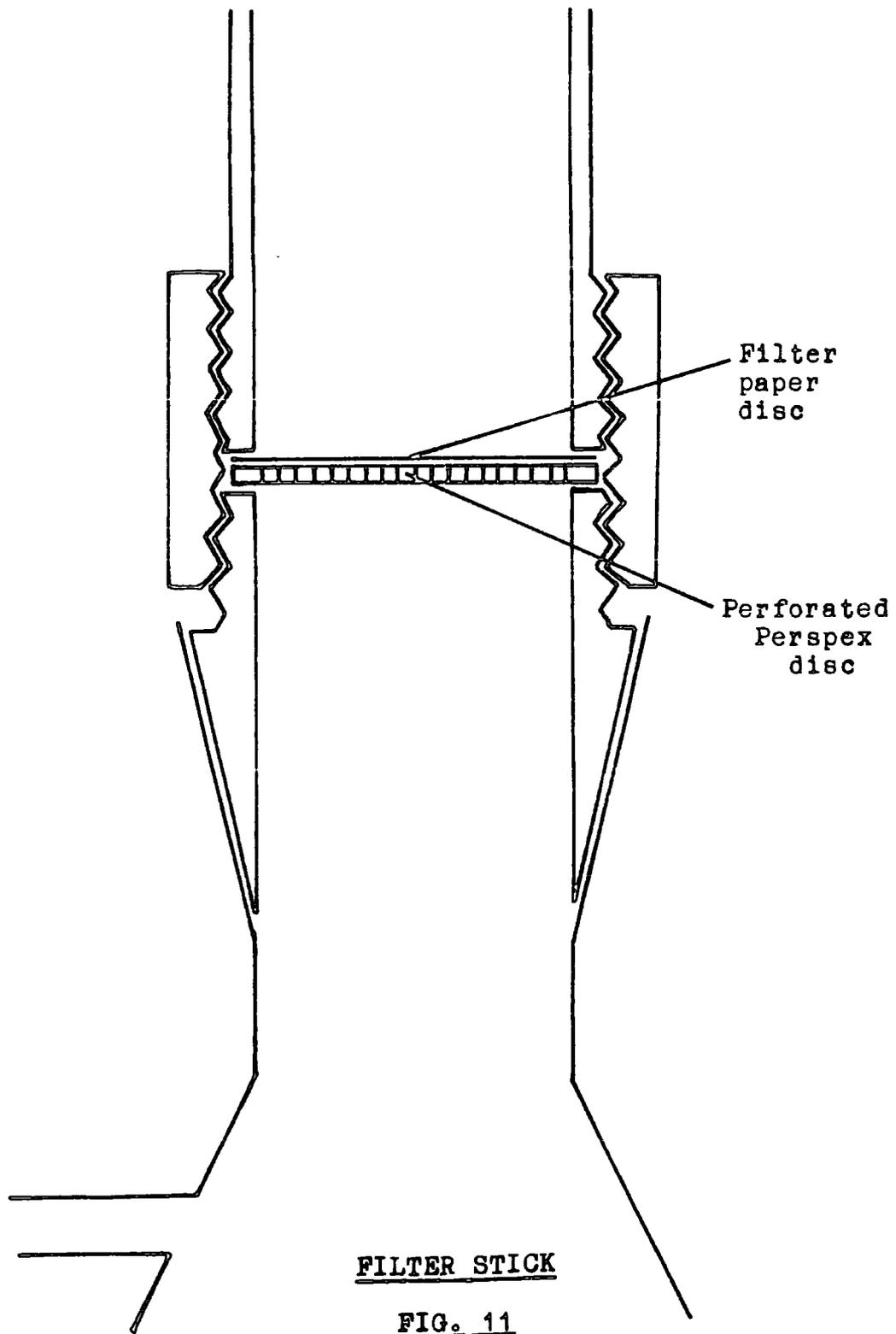
5.1 Contd.

The filter paper discs containing the final precipitates were covered on both sides with Sellotape for ease of handling and to avoid loss of precipitate. The sources were counted under standard conditions (Section 4), until a sufficient number of points on the decay curve had been obtained to determine the activity of the particular isotope at the end of irradiation (A_o). The decay curves were good straight lines or could be resolved into good straight lines with the half - lives agreeing with published values (24), with the exception of $Pd^{109} - Pd^{112}$. This curve (a typical plot is shown in Fig. 12) could not be resolved in the normal way due to the similarity of the two half - lives (13.5 hrs and 21 hrs).

$$A_t = A_1 e^{-\lambda_1 t} + A_2 e^{-\lambda_2 t}$$

Where A_t = Total activity at time t.

$A_1 A_2$ = Activity of species 1, 2 at time t = 0.

$\lambda_1 \lambda_2$ = Decay constants of species 1, 2.

This equation may be rewritten:-

$$A_t e^{\lambda_1 t} = A_1 + A_2 e^{-(\lambda_2 - \lambda_1)t}$$

A graph of $A_t e^{\lambda_1 t}$ against $e^{-(\lambda_2 - \lambda_1)t}$ will give an intercept of A_1 and a gradient of A_2. Resolution of $Pd^{109} - Pd^{112}$ decay curve in this way is shown in Fig. 13.

FIG. 12

Pd DECAY CURVE

Time in minutes
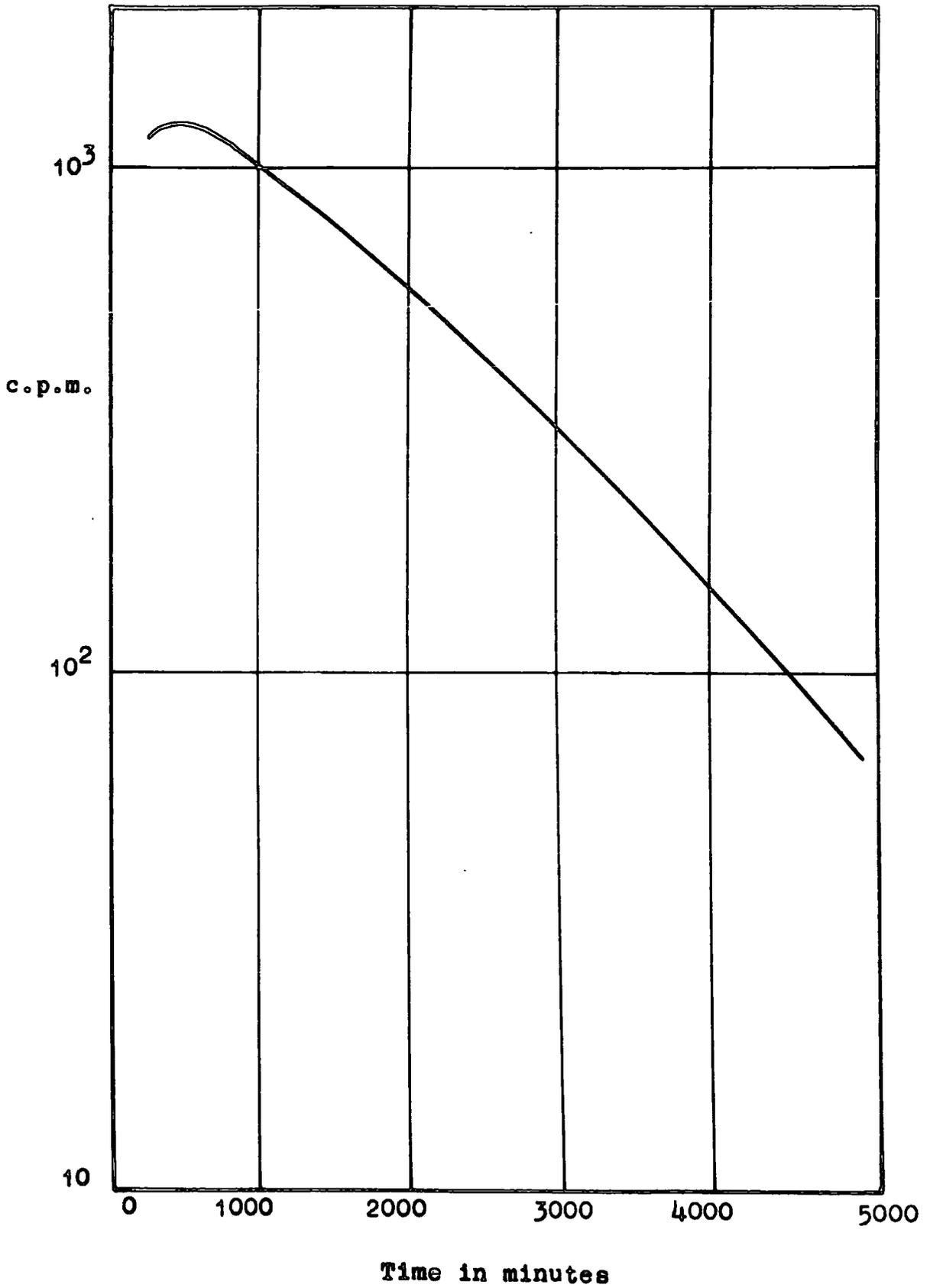
FIG. 13

$Pd^{109} - Pd^{112}$ RESOLUTION CURVE

$A_1 = 1.06 \times 10^3$

$A_2 = 1.13 \times 10^3$
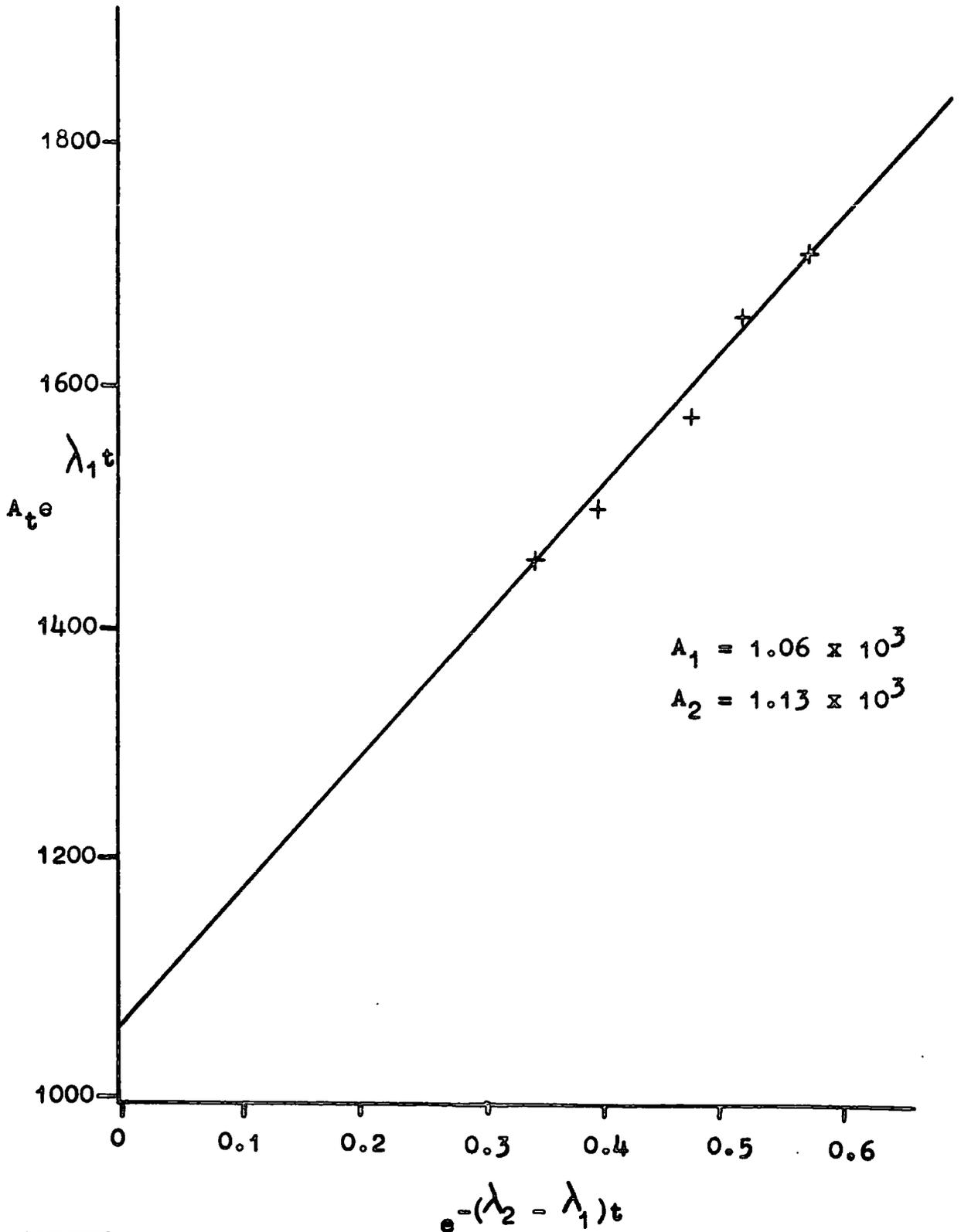
5.2 Results

A number of preliminary irradiations were carried out to assess the count rates to be expected from various isotopes, the efficiency of the radiochemical separations, the counting procedures and the approximate fission yields. These preliminary runs will not, therefore, be discussed, nor will those which for a variety of reasons were not successful.

The details of the successful irradiations are given in Table 9.

TABLE 9

Run Number	Isotope	A_0 from Curve c.p.m.	Chemical Yield	Σ	Counting Correction Factor	A_0 Corrected c.p.m.	Relative Fission Yield
A	Ba^{139}	3.30×10^3	28.4	2937	1.65	1.92×10^4	1.00
	Br^{84}	7.20×10^3	62.8	2080	1.47	1.68×10^4	0.231[1]
	Ru^{105}	8.50×10^2	75.5	3430	2.40	2.70×10^3	0.382
	Br^{83}	8.20×10^2	62.8	3218	2.18	2.35×10^3	0.110[1]
B	Ba^{139}	7.25×10^3	65.4	1915	1.80	2.00×10^4	1.00
	Br^{84}	3.70×10^3	48.4	1619	1.45	1.11×10^4	0.245
	Ag^{113}	2.07×10^3	85.6	2078	2.01	4.86×10^3	0.838(0.184)[2]
	Ag^{115}	2.10×10^4	85.6	1378	1.52	3.73×10^4	0.644(0.141)[2]
C	Ba^{139}	8.70×10^3	52.4	2695	1.73	2.87×10^4	1.00
	Zr^{97}	6.50×10^2	13.4	4697	0.844	4.09×10^3	0.981
	Ru^{105}	1.30×10^3	61.3	4148	2.18	4.62×10^3	0.332
	Ag^{113}	5.70×10^2	73.7	4289	2.00	1.45×10^3	0.127

(1) Twice volume of uranium solution used for Br.
(2) Ag^{115} yield calculated from Ag^{113} yield (assumed 0.181).

-44-

TABLE 9 (Contd.)

Run Number	Isotope	A_0 from Curve c.p.m.	Chemical Yield	$\sum$	Counting Correction Factor	A_0 Corrected c.p.m.	Relative Fission Yield
D	Ba139	3.90×10^4	85.0	3252	1.82	8.35×10^4	1.00
	Br84	1.20×10^4	42.9	2630	1.51	4.23×10^4	0.234
	Pd111	1.30×10^4	27.6	2282	1.43	6.74×10^4	0.298
	Br83	1.30×10^4	42.9	3433	2.29	6.94×10^4	0.128
E	Ba139	6.10×10^3	31.6	1481	1.60	3.09×10^4	1.00
	Y93	9.80×10^2	27.5	2772	1.52	5.42×10^3	0.992(1)
	Zr97	1.70×10^3	23.2	2902	0.832	6.10×10^3	1.21
	Ru105	1.20×10^3	62.3	2423	2.35	4.53×10^3	0.427(1)
F	Ba139	2.20×10^3	42.1	2947	1.63	8.52×10^3	1.00
	Br84	1.93×10^3	64.3	2548	1.47	4.40×10^3	0.223
	Pd111	1.80×10^3	44.3	2271	1.45	5.89×10^3	0.232

(1) 10 mls of uranium solution for Y and Ru, 15 mls for Ba.

TABLE 9 (Contd.)

Run Number	Isotope	A_o from Curve c.p.m.	Chemical Yield	$\sum$	Counting Correction Factor	A_o Corrected c.p.m.	Relative Fission Yield
G	Ba^{139}	1.70×10^4	40.9	1325	1.63	6.78×10^4	1.00
	Sr^{91}	3.05×10^3	27.3	3281	1.84	2.06×10^4	0.840
	Y^{93}	1.60×10^3	22.5	3298	1.50	1.065×10^4	0.890[1]
	Zr^{97}	5.00×10^3	28.5	3534	0.844	1.48×10^4	0.982
	Ru^{105}	4.10×10^3	49.8	2676	2.18	1.79×10^4	0.415
	Ag^{113}	2.60×10^3	69.0	2850	1.98	7.46×10^3	0.191
	I^{131}	1.40×10^2	82.9	3878	3.86	6.52×10^2	0.902[1]
	Ba^{140}	3.10×10^2	40.9	3890	1.03	7.81×10^2	0.851

(1) 10 mls of uranium solution for Y and I, 20 mls for Ba.

TABLE 9 (Contd.)

Run Number	Isotope	A_o from Curve c.p.m.	Chemical Yield	$\sum$	Counting Correction Factor	A_o Corrected c.p.m.	Relative Fission Yield
H	Ba^{139}	1.40×10^4	30.4	2564	1.60	7.37×10^4	1.00
	Sr^{91}	4.60×10^3	31.2	5172	1.86	2.74×10^4	1.26
	Zr^{97}	3.50×10^3	14.5	5483	0.810	1.96×10^4	1.48
	Pd^{109}	1.10×10^3	66.4	5362	2.42	4.01×10^3	0.248
	Pd^{112}	1.10×10^3	66.4	5579	1.44	2.39×10^3	0.221
	Ag^{113}	2.50×10^3	62.0	4619	1.97	7.94×10^3	0.224
	I^{131}	3.00×10^2	71.4	5920	3.76	1.58×10^3	1.27
	Ba^{140}	2.10×10^2	30.4	5936	1.01	6.98×10^2	0.887
	Ce^{143}	6.60×10^2	47.4	5714	2.35	3.56×10^3	0.504

TABLE 9 (Contd.)

Run Number	Isotope	A_0 from Curve c.p.m.	Chemical Yield	$\sum$	Counting Correction Factor	λ_0 Corrected c.p.m.	Relative Fission Yield
J	Ba^{139}	2.50×10^4	63.3	2280	1.65	6.51×10^4	1.00
	Sr^{91}	3.30×10^3	28.9	5610	1.86	2.12×10^4	0.905
	Zr^{97}	7.70×10^3	41.4	6029	0.832	1.55×10^4	1.08
	Pd^{109}	6.30×10^2	23.8	5878	2.23	5.90×10^3	0.334
	Pd^{112}	3.60×10^2	23.8	6185	1.31	1.98×10^3	0.166
	Ag^{113}	2.70×10^3	73.8	4846	2.00	7.32×10^3	0.198
	Ce^{143}	1.80×10^3	56.7	6379	2.69	8.27×10^3	1.06
	Mo^{99}	5.90×10^2	26.8	6561	2.51	5.53×10^3	1.395
	Ba^{140}	5.30×10^2	63.3	6707	1.05	3.79×10^2	0.994
K	Ba^{139}	7.60×10^3	23.7	3720	1.60	5.13×10^4	1.00
	Ag^{113}	1.80×10^3	94.8	4060	2.03	3.85×10^3	0.257
	Ag^{115}	1.70×10^4	94.8	2663	1.54	2.76×10^4	0.187

TABLE 9 (Contd.)

Run Number	Isotope	A_0 from Curve c.p.m.	Chemical Yield	Σ	Counting Correction Factor	A_0 Corrected c.p.m.	Relative Fission Yield
L	Ba^{139}	1.50×10^4	32.5	5161	1.60	7.38×10^4	1.00
	Y^{93}	3.80×10^3	27.2	11499	1.52	2.12×10^4	0.910
	Zr^{97}	1.60×10^4	84.6	11789	0.867	1.64×10^4	1.165
	Mo^{99}	4.90×10^2	21.5	12656	2.42	5.52×10^3	1.44
	Ru^{105}	3.50×10^3	37.4	9277	2.22	2.08×10^4	0.498
	Pd^{109}	6.00×10^2	42.5	11502	2.29	3.23×10^3	0.187
	Ag^{111}	1.10×10^2	76.7	12760	2.44	3.50×10^2	0.244
	Pd^{112}	5.70×10^2	42.5	12021	1.36	1.825×10^3	0.157
	Ag^{113}	2.80×10^3	76.7	9742	2.00	7.30×10^3	0.196
	I^{131}	2.60×10^2	68.7	12769	3.76	1.42×10^3	1.065
	Ce^{143}	1.20×10^3	66.7	12348	2.69	4.69×10^3	0.618
	Ba^{140}	2.20×10^2	32.5	12840	1.01	6.84×10^2	0.808

TABLE 9 (Contd.)

Run Number	Isotope	A from Curve c.p.m.	Chemical Yield	$\sum$	Counting Correction Factor	A_0 Corrected c.p.m.	Relative Fission Yield
M	Ba^{139}	2.50×10^4	47.7	1877	1.63	8.54×10^4	1.00
	Sr^{91}	3.80×10^3	31.4	4616	1.86	2.25×10^4	0.733
	Y^{93}	2.80×10^3	15.8	4639	1.50	2.66×10^4	0.889
	Zr^{97}	1.40×10^4	57.3	4964	0.856	2.09×10^4	1.11
	Mo^{99}	7.30×10^3	30.3	5342	2.55	6.14×10^4	1.195
	Pd^{109}	1.96×10^3	69.9	4822	1.85(1)	5.19×10^3	0.225
	Ag^{111}	0.80×10^2	54.1	5463	2.36	3.49×10^2	0.178
	Pd^{112}	1.50×10^3	69.9	5056	1.03(1)	2.21×10^3	0.142
	Ag^{113}	1.90×10^3	54.1	4021	1.96	6.88×10^3	0.141
	Sb^{129}	7.40×10^3	54.6	3841	0.967	1.31×10^4	0.243
	I^{131}	1.00×10^2	21.2	5466	3.29	1.55×10^3	0.855
	Ba^{140}	4.40×10^2	47.7	5482	1.04	9.59×10^2	0.834

(1) No Sellotape on source.

-50-

TABLE 9 (Contd.)

Run Number	Isotope	A_0 from Curve c.p.m.	Chemical Yield	$\sum$	Counting Correction Factor	A_0 Corrected c.p.m.	Relative Fission Yield
N	Ba^{139}	2.30×10^4	49.0	1335	1.63	7.63×10^4	1.00
	Ag^{113}	2.50×10^3	75.5	2847	2.09	6.92×10^3	0.159
	Sb^{129}	4.50×10^3	37.7	2723	0.950	1.135×10^4	0.237
	I^{131}	1.00×10^2	45.1	3810	3.51	7.78×10^2	0.980[1]
	Ba^{140}	3.80×10^2	49.0	3820	1.04	8.07×10^2	0.801
P	Ba^{139}	4.80×10^4	69.7	1793	1.68	1.155×10^5	1.00
	Br^{83}	6.20×10^3	64.5	2039	2.18	$2.?0 \times 10^4$	0.130[2]
	Br^{84}	4.40×10^4	64.5	1121	1.47	1.00×10^5	0.258[2]
	Ag^{113}	1.06×10^4	86.2	2263	2.11	2.59×10^4	0.664[3](0.181)
	Ag^{115}	4.76×10^4	86.2	721	1.57	8.67×10^4	0.463[3](0.126)

(1) 10 mls of uranium solution for I, 20 mls for Ba.
(2) 20 mls of uranium solution for Br, 10 mls for Ba.
(3) Ag^{115} yield calculated from Ag^{113} yield (assumed 0.181).

-51-

TABLE 9 (Contd.)

Run Number	Isotope	A_0 from Curve c.p.m.	Chemical Yield	Σ	Counting Correction Factor	A_0 Corrected c.p.m.	Relative Fission Yield
Q	Ba^{139}	3.20×10^4	55.3	1379	1.65	9.55×10^4	1.00
	Ag^{113}	1.80×10^3	86.8	1467	2.11	4.38×10^3	0.161
R	Ba^{139}	4.20×10^4	32.9	3167	1.61	2.06×10^5	1.00
	Br^{83}	2.90×10^3	42.5	3538	2.07	1.41×10^4	0.099
	Br^{84}	2.30×10^4	42.5	2040	1.45	7.84×10^4	0.221
	Ag^{113}	4.40×10^3	97.1	3872	2.15	9.74×10^3	0.145
	Ag^{115}	2.40×10^4	97.1	1548	1.59	3.93×10^4	0.097
S	Ba^{139}	7.60×10^4	57.0	7272	1.65	2.20×10^5	1.00
	Zr^{97}	6.00×10^3	26.6	12980	0.844	1.90×10^4	1.45[1]
	Ag^{113}	6.60×10^3	72.7	11270	2.08	1.89×10^4	0.207

(1) 10 mls of uranium solution for Zr, 25 mls for Ba.

6. DISCUSSION

The mean relative fission yields (Table 10) were plotted against mass number and the curve normalised to 100% in each peak. In drawing this curve, complementary ("mirror - image") points were plotted using a value for the mean number of secondary neutrons per fission ($\overline{\nu}$) or 4 (c.f. Cuningname (30), Flerov and Tamanov (31), Flerov and Talysin (32) and Billand (33)). A value of 3 or 5 would certainly give a poorer fit especially in the steeper parts of the curve which, although they contribute relatively little to the total yield, are very sensitive to the value chosen for $\overline{\nu}$. A normalising factor of 4.80 was obtained and the results for the normalised fission yields are seen in Table 10 and Fig. 14. The sources of error in fission yield measurements and their significance are discussed in Appendix III.

Two further points (133 and 135) were obtained by Silvester (29) by gas - counting the xenon members of the decay chain and these are included.

TABLE (10)
Fission Yield Results

Mass Number	Fission Yield Relative to Ba^{139}	Normalised Fission Yield %
83	0.117 ± 0.007	0.56 ± 0.03
84	0.235 ± 0.006	1.13 ± 0.03
91	0.94 ± 0.11	4.49 ± 0.53
93	0.92 ± 0.024	4.42 ± 0.12
97	1.18 ± 0.07	5.66 ± 0.34
99	1.34 ± 0.07	6.43 ± 0.34
105	0.411 ± 0.027	1.97 ± 0.13
109	0.248 ± 0.031	1.19 ± 0.15
111	0.238 ± 0.024	1.14 ± 0.12
112	0.172 ± 0.024	0.82 ± 0.12
113(*)	0.182 ± 0.013	0.87 ± 0.06
115	0.138 ± 0.021	0.66 ± 0.10
129	0.240 ± 0.003	1.15 ± 0.01
131	1.01 ± 0.056	4.85 ± 0.27
139	1.00	4.80
140	0.863 ± 0.029	4.15 ± 0.14
143	0.727 ± 0.150	3.49 ± 0.74
133	*1.061 ± 0.016	6.95 ± 0.51
135	*0.877 ± 0.004	5.74 ± 0.42

* Yields relative to Mo^{99}

(*) Since the branching ratio of Ag^{113m} was not determined and no information was available in the literature this fission yield represents a minimum value.

-54-

MASS/YIELD CURVE

FIG. 14

Experimental Points ——— X

Mirror points ——— ⊙

Cuninghame's points ——— ⊛

FISSION YIELD

MASS NUMBER
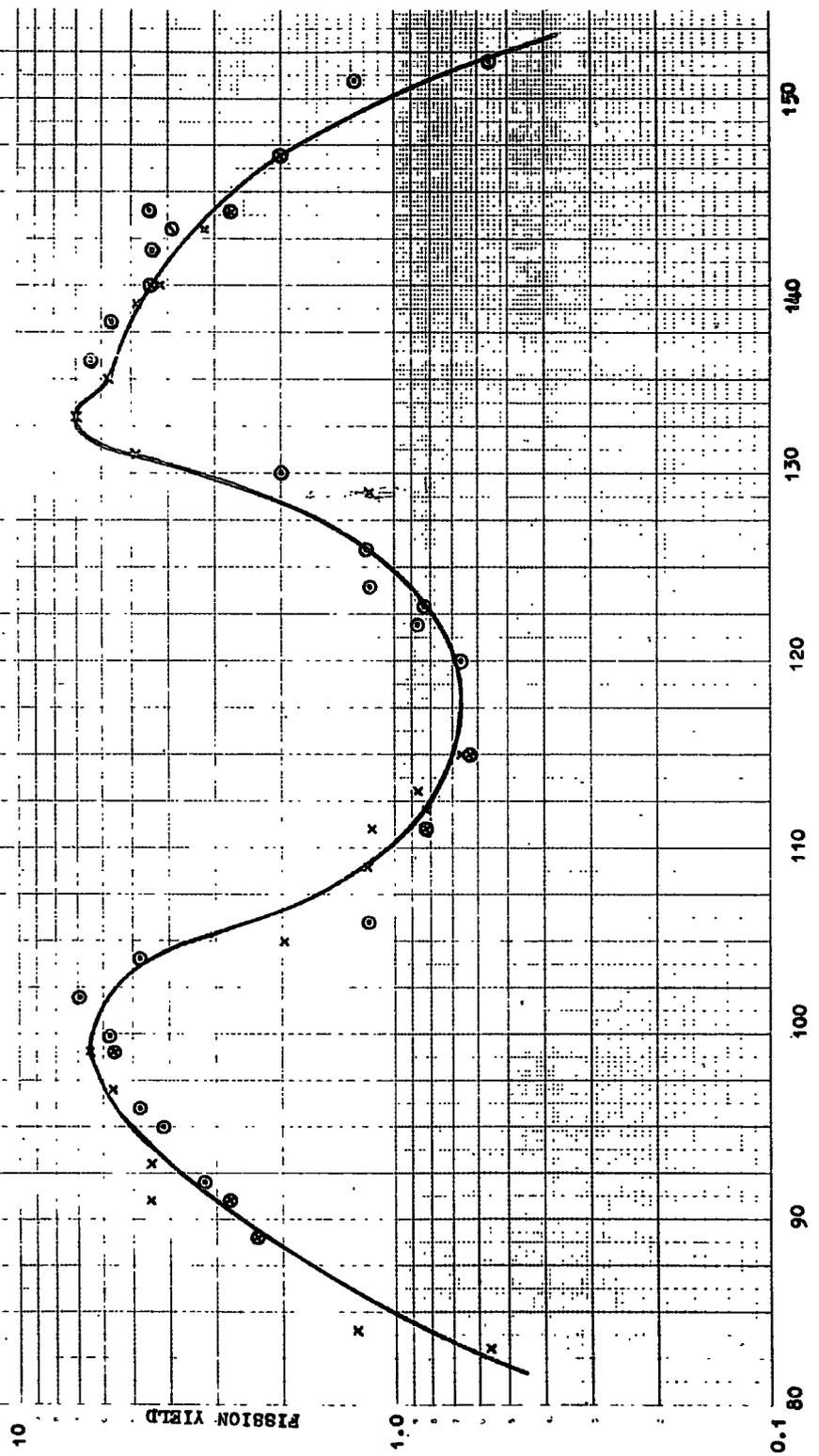
Also included in Fig. 14 are the results of
Cuninghame (30) which are in close agreement except for
Mo^{99} (5.58 ± 0.28), which was the only point in the peak
regions (95 - 105 and 130 - 140). Much of Cuninghame's
results are in the region 140 to 156 and so may be con-
sidered to a large extent as complementary to this work.

The following parameters are deduced from the mass -
yield curve:-

Peak to trough ratio   10

Position of peaks   99 and 136 mass units

Yield at peak   6.5%

The peak to trough ratio is rather higher than that
deduced by Cuninghame (9.1) though this difference depends
almost entirely on the values obtained from Mo^{99}.

It is possible that the fission yield values obtained
by Silvester (29) for the two masses 133 and 135 may be
less reliable, but the relative yields depend solely on
the analysis of the decay curve for the xenon sample. It
is reasonable to assume that in a gas - counting system
the efficiencies for the two β -emitting nuclides would
be identical and that the relative values are correct;
this constitutes some evidence for fine structure in the
yield curve at this point.

There is ample evidence for similar fine structure in this region in fission at lower energies (34). At 14 MeV, Wahl (35) has reported yields of iodine isotopes from U^{235} fission, but when corrected by adding a contribution from the direct formation of chain members below iodine, the total yields do not appear to show any fine structure in this region. Richter and Coryell (36), on the other hand, found evidence for a subsidiary peak, at mass 133 in the photofission of U^{238}, induced by x-rays of 9-14 MeV. It is certain that this is a point which will bear further investigation and it may be observed that measurements of the xenon members of the chain, although in some respects more difficult, have the advantage that the correction needed on account of direct formation of lower members is much smaller than in the case of iodine. This correction is especially hazardous in the immediate neighbourhood of closed shells, as in this case.

It is thought possible that in high energy fission there is a lessening of the influence of the closed shells on the actual mode of fission and that this results in a greater chance of symmetrical fission. If this is the case, it is possible that the observed fine structure is due to the emission of delayed neutrons from certain heavy

fragments after the actual fission event has taken place.
Since no experimental points lie in the region between
mass 99 and 105, it is not possible to confirm whether or
not fine structure is also present in the light peak. It
is suggested, however, that examination of the fission
yields in this region could prove fruitful.

It can be concluded that this work shows that the
mass - yield curve for the fission of U^{238} with 14.7 MeV
neutrons follows the general pattern of such curves.

A NEW METHOD FOR THE DETERMINATION OF THE CROSS SECTION FOR THE REACTION Al^{27} (n, α) FOR 14 MeV NEUTRONS

1. INTRODUCTION

Activation methods for the measurement of nuclear reaction cross - sections require a knowledge of the absolute flux of bombarding particles. In the case of fast neutron induced reactions, the "good geometry" condition implicit in most methods of absolute flux measurement is frequently incompatible with the production of a neutron intensity adequate for the measurement of the smaller cross - section values. In these circumstances, it is convenient to make measurements by comparison with activities induced in some reference substance for which the reaction cross - section is already known.

Reactions frequently chosen for this purpose are Al^{27} (n, α)Na^{24} and Fe^{56} (n,p)Mn^{56}. The criteria governing the selection of an element suitable for monitoring 14 MeV neutron irradiations are:-

(a) induced activity has convenient half - life and radiation characteristics (Na^{24}, half - life 15.0 hrs, β - energy 1.39 MeV; Mn^{56}, half - life 2.58 hrs, β - energies 2.86 MeV (60%), 1.04 MeV (25%), 0.75 MeV (15%).

(b) cross – section values large enough for easy
    measurement of induced activity.

(c) effectively only one induced activity (all others
    must be either very short or very long lived).

(d) easy availability of target material in adequate state
    of purity.

An essential part of this procedure is the establishment
of an absolutely known cross – section and this work describes
the determination of the Al^{27} $(n,\alpha)Na^{24}$ cross – section by a
variation of the associated particle method.

One of the main difficulties of this technique, as normally
used with the $H^3(d,n)He^4$ reaction is the large discrepancy
between the neutron flux needed to induce readily measurable
activities and the α-particle flux convenient for measurement
by proportional counting or other conventional methods. This
is usually resolved by accepting α-particles from only a very
small solid angle, but the overall result is, of course, very
sensitive to the exact basis of measurement of this parameter.
In this work, samples of aluminium are exposed to neutrons from
the D + T reaction and the α-particles, collected simultaneousl;
from the target over the identical solid angle, are measured
in terms of the volume of helium found on dissolving the
"catcher" foil in which they have been brought to rest.

Neutrons, α-particles and He^3 - particles (from the D + D reaction which inevitably follows the build - up of deuterium in the target) are intercepted from the solid target by a stack of three thin foils. The front foil is very thin (1.5 mg/cm^2) and its function is to stop the less energetic He^3 particles. The more energetic α-particles from the D + T reaction are brought to rest in the second foil (~ 7 mg/cm^2) and the third foil is subsequently dissolved for the absolute measurement of the Na^{24} induced activity in a liquid counter previously calibrated against 4π counting.

Neutrons and α-particles entering the same solid angle cannot be "associated", but at the low bombarding energies used in this work (Ed ~ 120 keV), the differential yield of the D + T reaction as a function of angle is well known and the calculation presents little difficulty. Against this slight disadvantage must be set the fact that the solid angles subtended by the foils at the target are virtually the same and the result is thus rather insensitive to errors in measuring distances and to movement of the deuteron beam during the course of the irradiation. Furthermore, since both neutrons and α-particles are intercepted on the same side of the target, errors due to lack of precise knowledge of the effective deuteron energy tend to cancel rather than reinforce.

2. IRRADIATION EQUIPMENT

The same neutron generator was used for the irradiations as that described in Part I, but with a modified target section (Fig. 15). It consisted of an accurately made support for the three aluminium foils fixed in position above a raised target. A shutter, operated by means of magnet, enabled the beam to be focussed fairly accurately before commencement of an irradiation. The exact dimensions of the foils relative to the target were measured. The mean neutron energy was estimated at 13.5 MeV.

3. SEPARATION AND MEASUREMENT OF HELIUM

3.1 The Helium Measuring Apparatus

The separation of helium from other gases and its subsequent measurement have been the subject of a number of papers (37, 38, 39, 40). The present helium apparatus owes much to the work of Gluckauf in the early 1940's who in his paper (39) describes the theory, selection of optimum conditions and design of apparatus for the micro-analysis of the helium and neon contents of air. Modifications and refinements have obviously been carried out over the last 20 years and the apparatus used in these experiments resulted from a design by Chackett (40) with later modifications by Hall (41).
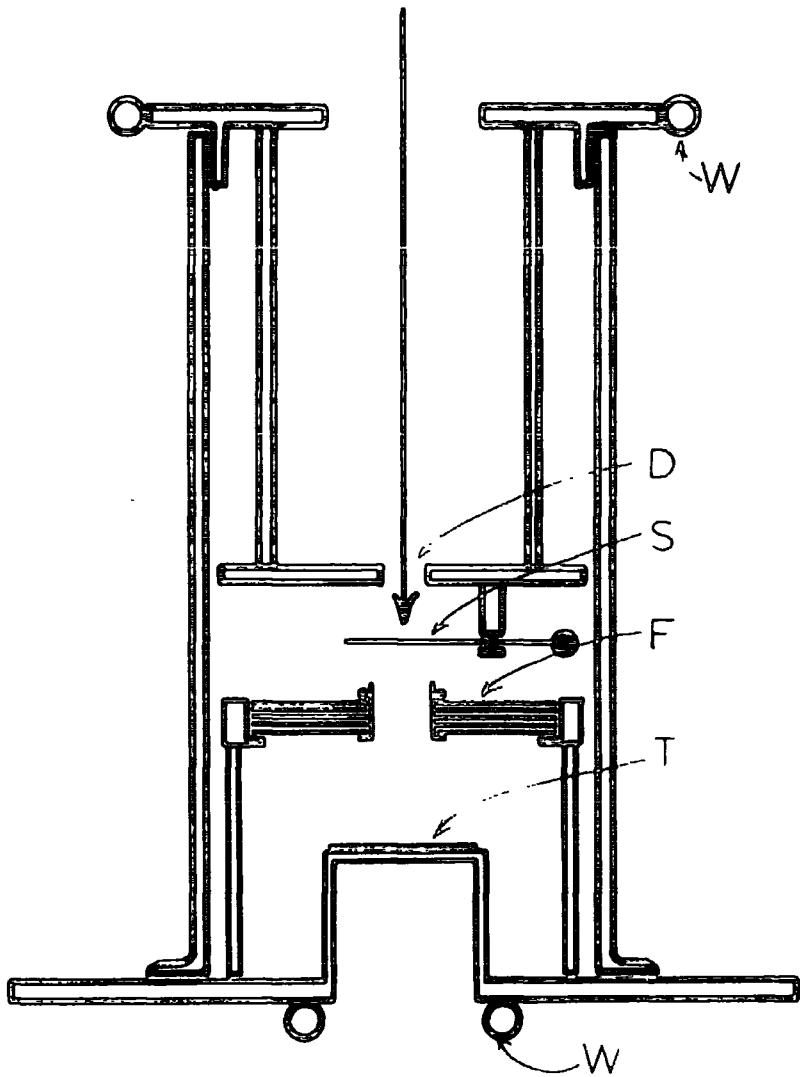
MODIFIED TARGET SECTION

Fig. 15

D = Deuteron beam
W = Water cooling
S = Shutter
F = Foil stack
T = Tritium target

3.1 Contd.

The measuring apparatus was constructed from soda glass since this is less permeable to atmospheric helium than Pyrex, the only exceptions being the Pirani gauges and the vacuum jacket of the palladium furnace used to remove traces of hydrogen. Care was taken to ensure that all tap keys were also made from soda glass, since it is usual for some manufacturers to construct the tap barrel in soda glass and the key in Pyrex.

The measuring apparatus (Fig. 16) may be divided into three sections:-

(a) Circulating system.

(b) Fractionation column.

(c) Measuring system.

The circulation system (Fig. 17) is required to remove hydrogen from the gas mixtures (this with helium and neon are the only gases not completely absorbed onto charcoal at $-195.8^{o}C$). The gases for separation, with oxygen carrier gas, are pumped slowly round a closed circuit over a heated palladium wire to convent hydrogen to water, which is subsequently removed in the liquid nitrogen trap. The gases are finally absorbed onto the charcoal trap cooled in liquid nitrogen.

FIG. 16

HELIUM MEASURING APPARATUS

From Dissolver → Circulating System → Fractionating Column → Transfer Bulb → Measuring System

Calibration System → Transfer Bulb

Gas sample entry

Dissolver

Charcoal
trap

Circulating
pump

Separation
column

Palladium
heater

Cold
trap

Toepler
pump
T
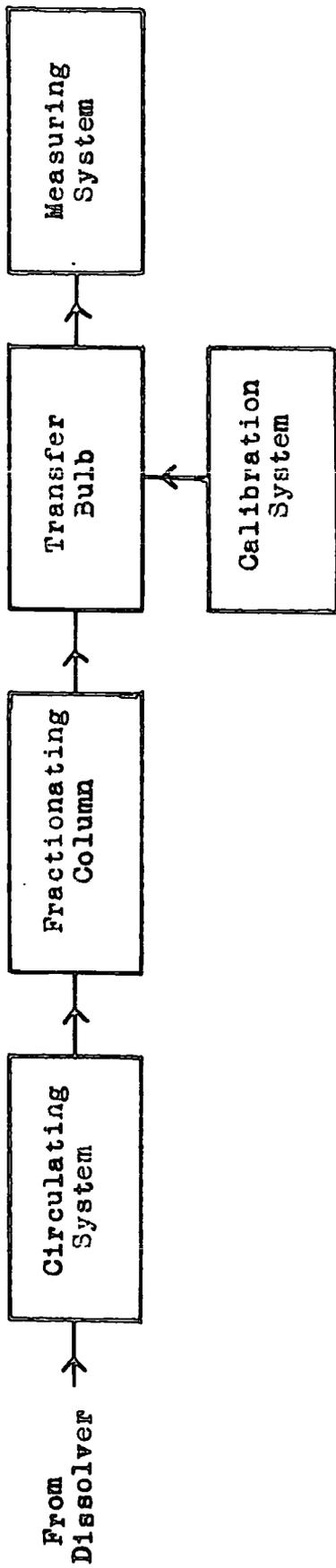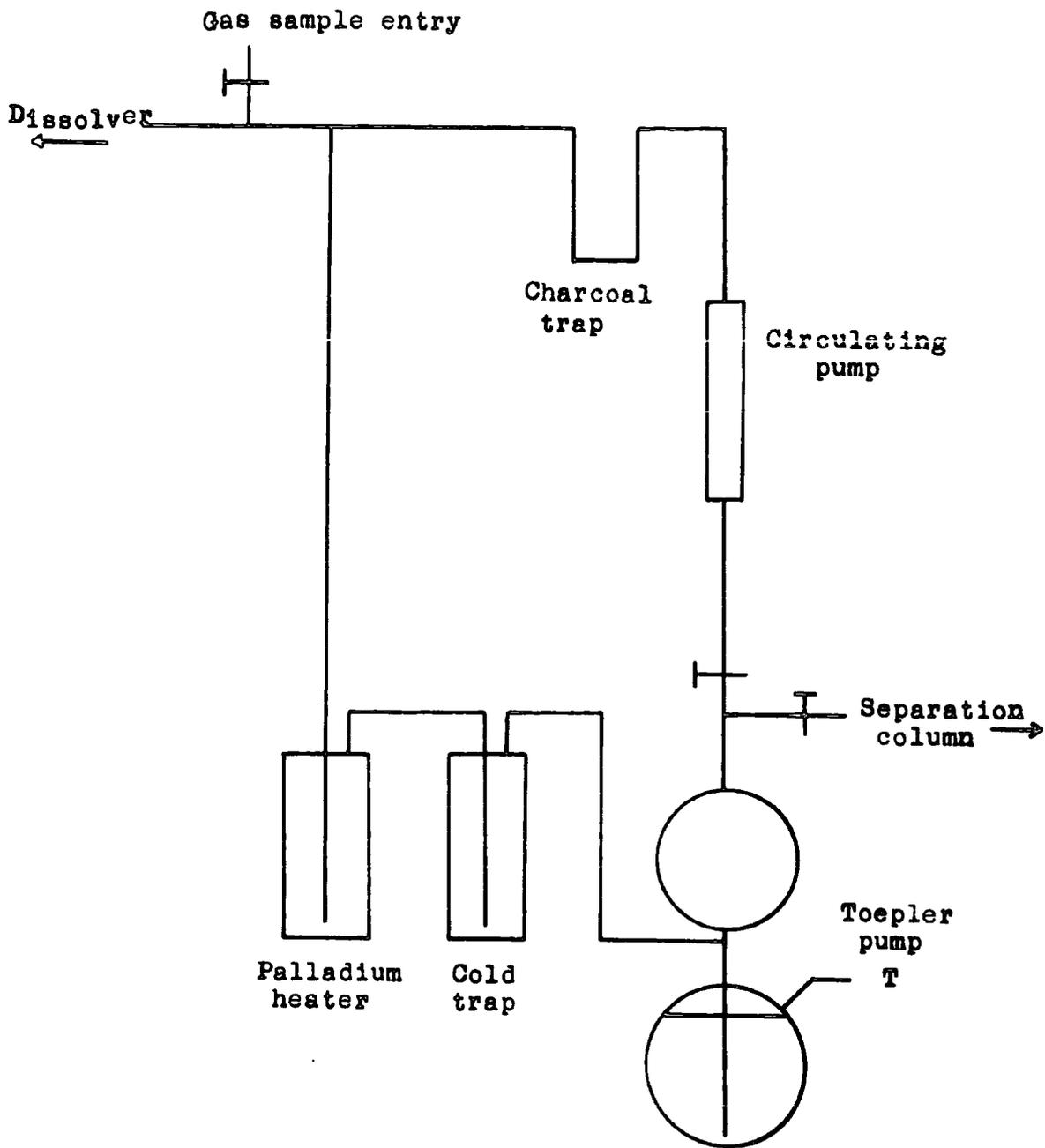
CIRCULATING SYSTEM

FIG. 17

3.1 Contd.

The fractionation column (Fig. 18) is composed of a series of fifteen adsorption units each consisting of a bulb containing a quantity of solid adsorbent (charcoal) connected to a glass bulb of known volume.

If S is the quantity of adsorbent, V is the volume in contact with the adsorbent and α and β are the respective adsorption coefficients of the two gases (i.e. helium and neon) in the adsorbent, then the distribution factors of the two gases may be written

$$a = \frac{1}{1 + \alpha(S/V)} \quad , \quad b = \frac{1}{1 + \beta(S/V)}$$

α and β depend only on the temperature, hence having selected the adsorbent and the lowest convenient temperature, the efficiency of separation of the two gases depends solely on the choice of the ratio S/V. For the best separation (i.e. when a maximum proportion of one of the substances would have to be transferred to the other phase in order to produce equal ratios of the two gases in both phases), $a - b$ should be a maximum, thus

$$\frac{d(a - b)}{d(S/V)} = 0 , \quad \text{the solution of which is}$$

$$V/S = \sqrt{\alpha\beta} \quad \text{or} \quad a + b = 1.$$

HELIUM SEPARATION COLUMN

FIG. 18
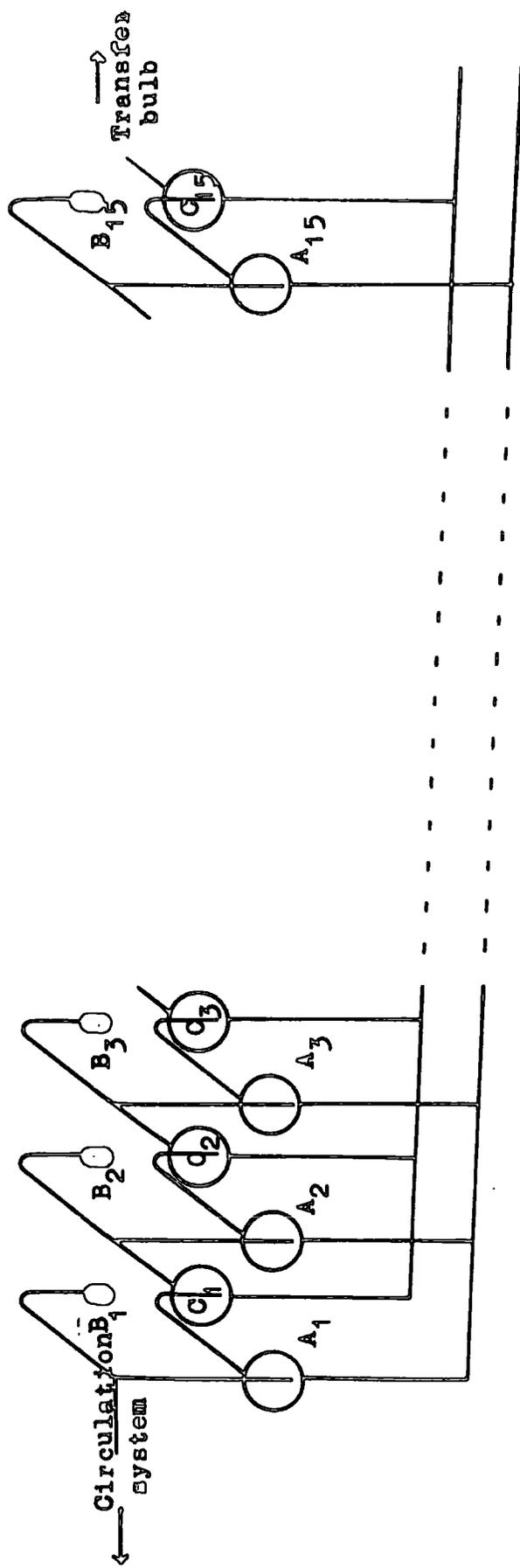
3.1 Contd.

Estimation of the adsorption coefficients can therefore give the optimum value of $^S/V$. 1 g. of hard nut charcoal cooled in liquid nitrogen will take up 10.6c.c. of helium (αS) and 117 c.c. of neon (βS) as measured at 760 mm Hg pressure and 20°C (39)

$$\therefore \quad V = \sqrt{(\alpha S \beta S)} \quad = \sqrt{10.6 \times 117} = 35.2 \text{ c.c.}$$

The gas spaces in the apparatus are smaller than this (approximately 30 c.c.) and the distribution factors had average values of a = 0.74 and b = 0.20. The theory offers formulae for the calculation of the optimum number of adsorption units and the number of fractionations (operations) required for the best separation of helium and neon, but it is better to use these values as a guide and having selected the number of adsorption units, the number of operations may be determined experimentally (see section 3.3).

Before starting a separation, the whole column is thoroughly degassed by pumping with the charcoal bulbs held at 250°C. The mercury is raised in the front and back portions of the column (Fig. 18) to fill the bulbs

3.1 Contd.

$(A_1 - A_{15})$ and $(C_1 - C_{15})$. Gas from the circulating system is transferred onto the charcoal in the first adsorption bulb (B_1) by means of the Toepler pump (T, Fig. 17). The mercury in the front row of bulbs is lowered to bring the gas adsorbed on the charcoal in contact with the first gas bulb (A1). The mercury in the front row of bulbs is raised, isolating the gas in bulb (A_1). The mercury in the back row of bulbs is lowered and the gas from bulb (A_1) expands into bulb (C_1) and into contact with the charcoal in the next bulb (B_2). Raising the mercury in the back row of bulbs and subsequent lowering of the mercury in the front row brings the gas adsorbed on the charcoal in bulb (B_2) into contact with bulb (A_2). At the same time, the gas adsorbed on the charcoal in bulb (B_1), but not desorbed at the first operation now comes into equilibrium with bulb (A_1). Thus, during successive adsorption and desorption, a separation is effected. Raising and lowering of the mercury is carried out automatically by means of a timing unit and electro-magnetically operated valves. An Edwards vacuum pump evacuates the mercury reservoir to cause the mercury in the column to be lowered and a carbon dioxide reservoir supplies gas at atmospheric pressure to raise the mercury.

3.1 Contd.

Carbon dioxide and not air was chosen since this will contain very little helium, in the event of gas being entrained in the mercury and entering the column.

The first fifteen operations of the column result only in the first fraction of helium reaching the last adsorption bulb, hence no gas should be evolved from the column during this period. In practice, however, a small amount of gas is collected which is referred to as the "fifteen operations blank" and is discussed later (section 3.2.1.). The helium fractions are collected in the next twenty one operations (i.e. after 36 operations total see Section 3.3.), when the column is stopped for helium measurement.

The measuring system (Fig 19) consists of two Pirani gauges immersed in liquid nitrogen and a large glass bulb (volume $\sim$1 litre) in which the gas from the separation column collects. The gas in this bulb is transferred to one of the Pirani gauges (Fig. 20) by filling the bulb with mercury from the reservoir below it. Another similar gauge continuously pumped forms the fourth arm of a Wheatstone Bridge network (Fig. 21) and helps to reduce the dependence of the balance point on casual fluctuations in operating conditions. Even so 3 - 6 hours

Separation column

Calibration system

Gas transfer system

Main vac line

Transfer bulb
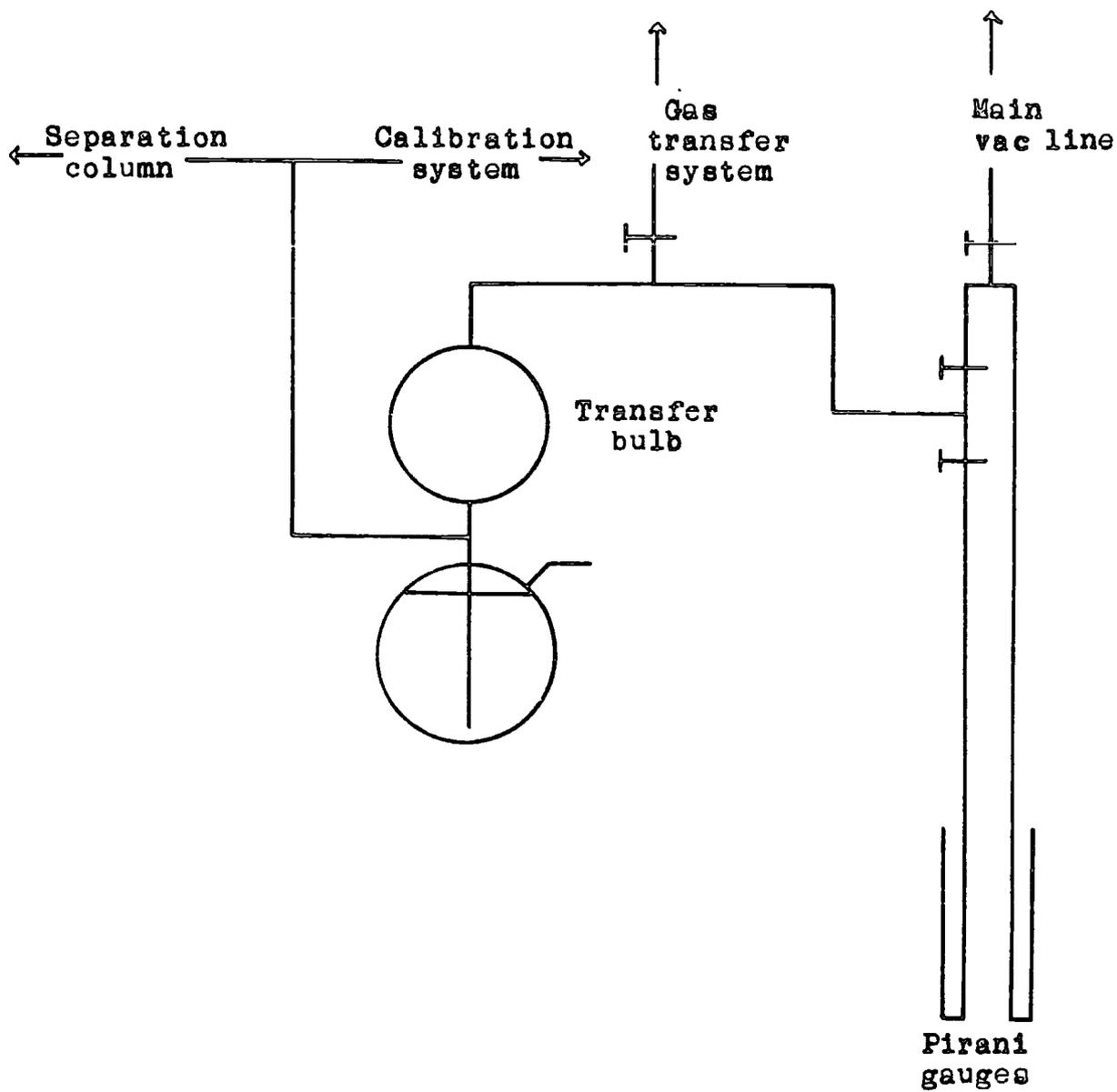
Pirani gauges

MEASURING SYSTEM

FIG. 19
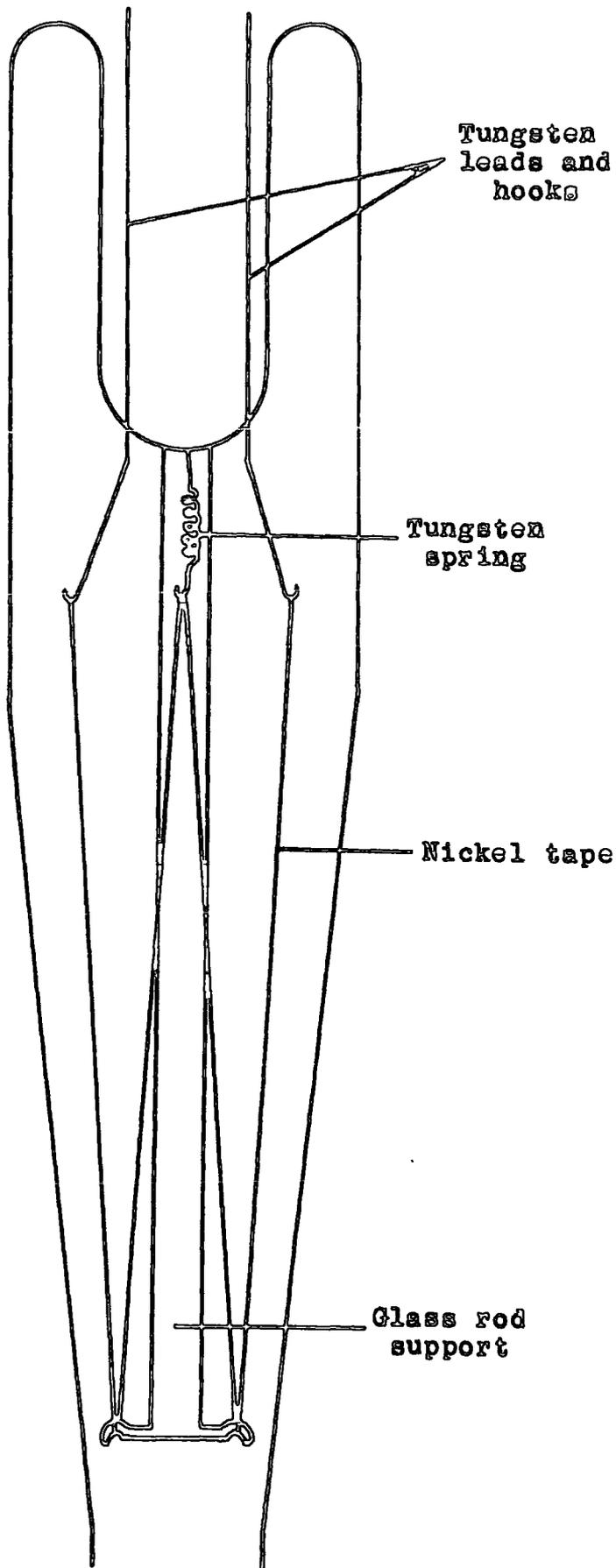
Tungsten
leads and
hooks

Tungsten
spring

Nickel tape

Glass rod
support

PIRANI GAUGE

FIG. 20
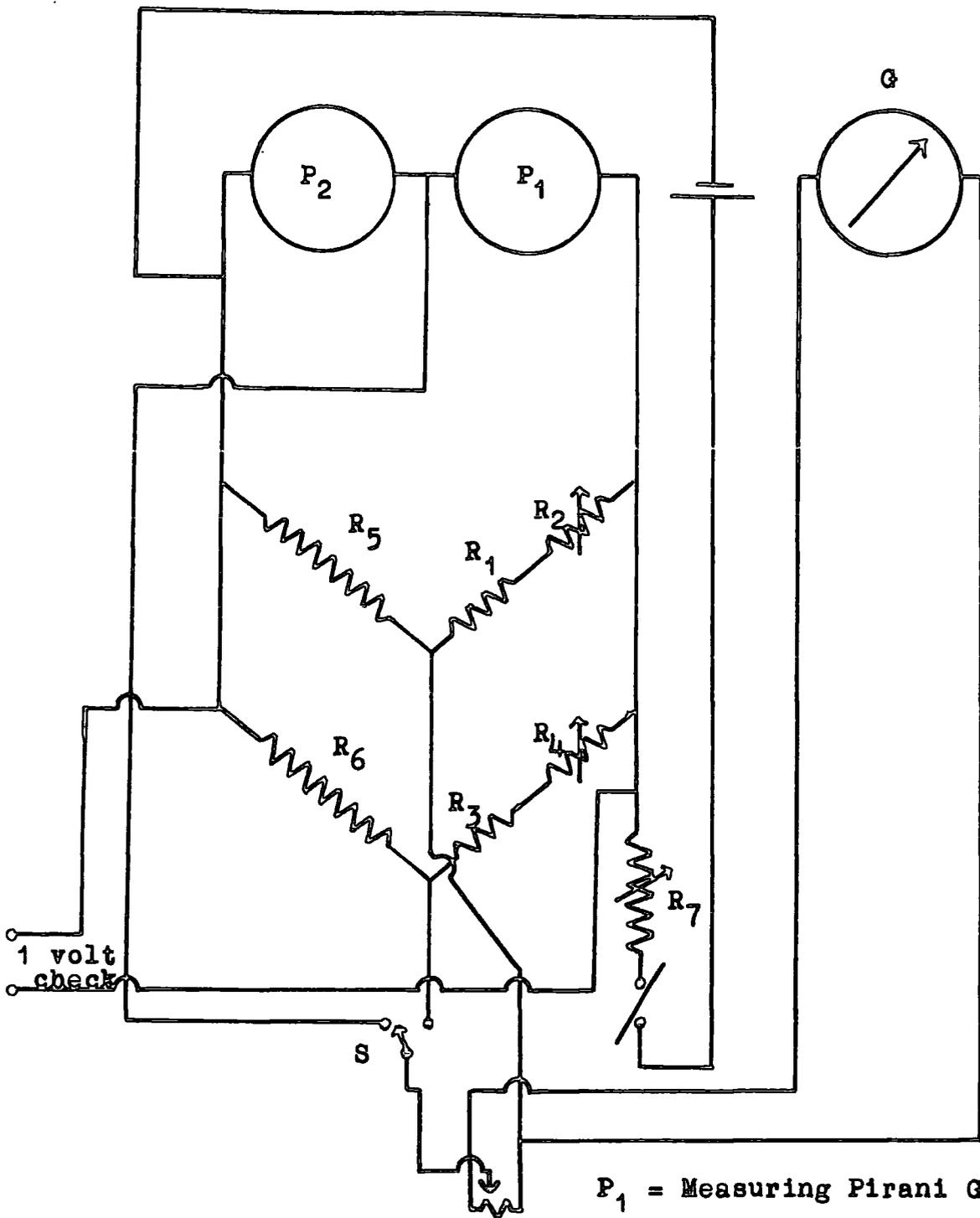
P_1 = Measuring Pirani Gauge.

P_2 = Compensating Pirani Gauge

R_1, R_3, R_5, R_6 = Fixed Resistances.

R_2, R_4, R_7, R_8 = Variable Resistances.

S = Selector Switch

G = Galvanometer

PIRANI BRIDGE CIRCUIT

FIG. 21

3.1 Contd.

under liquid nitrogen is required to attain a stable
operating condition.

The Pirani gauges (Fig. 20) are used for measuring
the pressure of the separated helium and neon and consist
of a Pyrex glass tube enclosing a length of nickel tape
(0.003 mm thick x 0.05 mm wide) supported in the shape
of a W on a glass and tungsten frame (41). The nickel
tape is soldered under a 10 g. tension onto the tungsten
hooks, which are previously copper plated. A piece of
gold foil is placed in the Pirani gauge connection tube
to absorb any mercury vapour and so prevent its attacking
the soldered connections. Charcoal is also included to
adsorb gases released into the system from tap grease.

The Pirani bridge circuit (P_1, P_2, R_1, R_2 and R_5)
for measuring the quantity of helium is shown in Figure 21.
R_2 is a variable resistance which is adjusted to give a
suitable reading on the galvanometer. R_7 is varied to
maintain a 1 volt potential difference across the Pirani
gauge tape, the value of which can be checked via the
"1 volt check" terminals. R_8 is a variable resistance
in order that the sensitivity of the bridge can be ad-
justed to varying amounts of helium. The secondary bridge

3.1 Contd.

circuit $(R_1, R_2, R_3, R_4, R_5$ and $R_6)$ is included to
check for drifting in the circuit (by throwing switch S)
without having to disconnect the Pirani gauges from the
circuit.

On introducing gas to the gauge, heat from the
tape is removed and conducted to the glass walls (main-
tained at $-195.8^{\circ}C$). The temperature and therefore the
resistance of the tape is hereby reduced. The change in
resistance produces an out of balance condition in the
bridge circuit, observed by a deflection on the galvano-
meter. At low pressures, when the mean free path of the
gas molecules is greater than the physical dimensions of
the gauge, the thermal conductivity is proportional to
the pressure. It is, however, prudent to calibrate the
gauge each time it is used with an accurately known
quantity of helium, approximately the same as will
ultimately be measured after separation on the column.

The need for calibration demands a system for intro-
ducing known small $(\sim 10^{-7}$ ccs) quantities of helium or
neon into the system (Fig. 22). This is supplied by
introducing a quantity of gas from a reservoir into a
calibrated McLeod gauge, where its volume, pressure and
temperature are measured. This is expanded back into

CALIBRATION SYSTEM

FIG.22

Expansion
volume

Transfer
bulb

Pipette 2 | Pipette 1

He supply
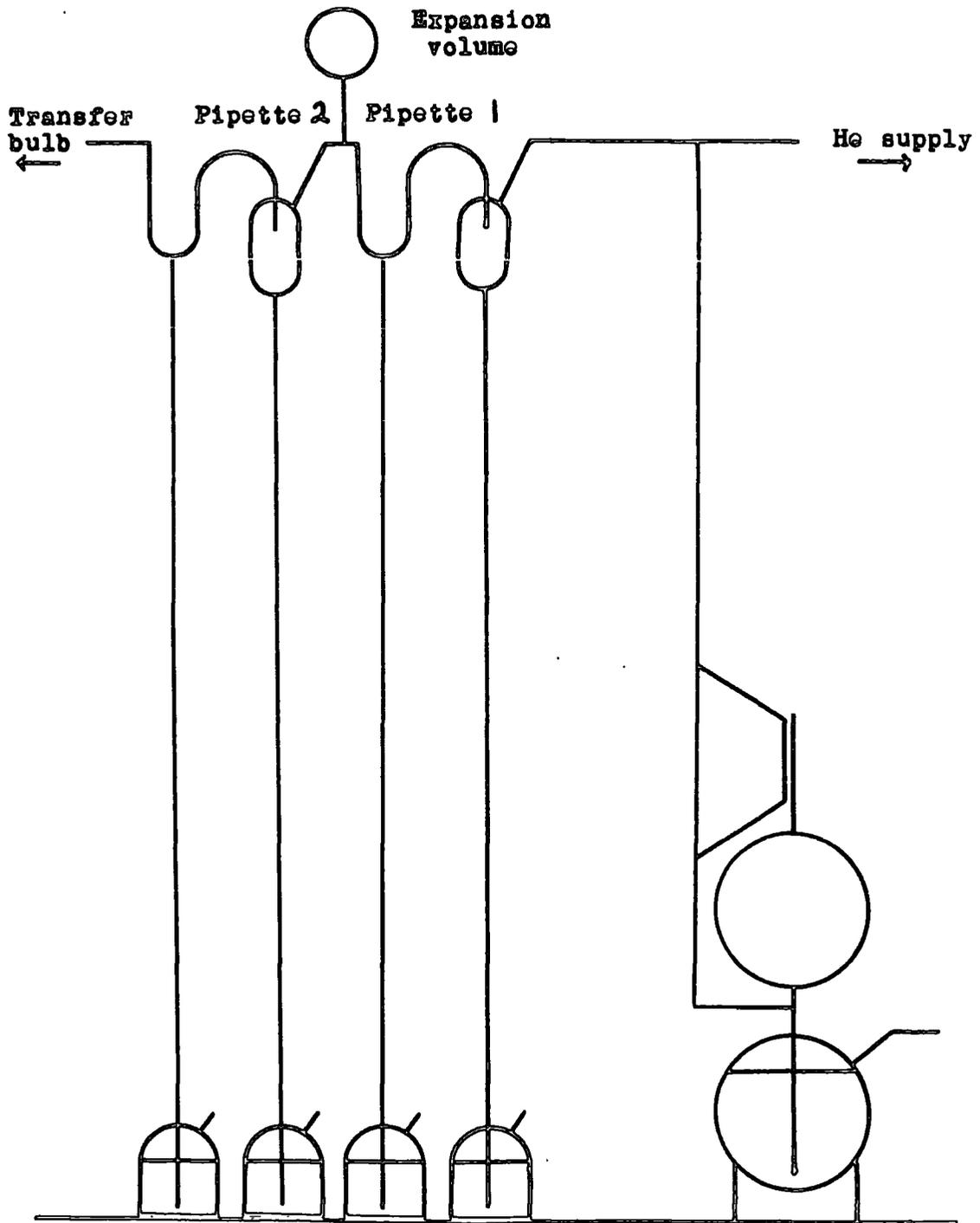
3.1 Contd.

the whole of the McLeod gauge and a small portion is removed in the first gas pipette. The quantity in this pipette is expanded in the next volume and a portion of this removed in the second gas pipette. This portion is transferred via the transfer bulb (Fig. 19) into the Pirani gauge. The overall factor is 8.6565×10^{-7}.

Having measured the helium by compressing the gas into the Pirani gauge, the galvanometer deflection is also observed when the gas is removed by pumping and a mean value taken as the true deflection. The neon is now collected. During the collection of helium, the liquid nitrogen is removed from around the bulbs on the column except bulb 1 to facilitate collection of the neon (i.e. from bulbs 2, 3 and 4 after 25 operations; 5, 6, 7 and 8 after 29; 9, 10, 11 and 12 after 33; 13, 14 and 15 after 36 operations).

The gas is collected until 61 operations of the column have been completed and the measurement is carried out in the same manner as for helium, using neon for calibration of Pirani gauges.

3.2   Stability of Pirani Gauges

3.2.1.   15 – Operations Blank

Although no gas should be collected after 15 – operations, a small quantity is invariably found, due to diffusion through the glass or outgassing even though a thorough degassing procedure is carried out before commencing the separation.

The values of a number of 15 – operations blanks were collected and are seen in Table 11.

TABLE 11

Galvanometer Reading cms	Mean of each pair
0.74 0.40	0.57
0.60 0.22	0.41
0.57 0.51	0.54
0.65 0.25	0.45
0.65 0.70	0.68
0.38 0.42	0.40
0.61 0.53	0.57

Mean = 0.52 cms (i.e. $\sim 5\text{x}10^{-9}$ ccs He)

Standard deviation = $\pm$ 0.10cms (i.e. $\sim 10^{-9}$ ccs He)

3.2.2. Standard Deviation of Pirani Gauge Readings

A volume of helium ($\sim 2 \times 10^{-7}$ ccs) was introduced into the measuring system (Fig. 19) and the mercury in the transfer bulb was alternately raised and lowered. The galvanometer readings were recorded each time and are seen in Table 12.

TABLE 12

Galvanometer Readings cm	Mean of each pair
20.15 19.80	19.98
20.50 19.85	20.18
20.30 20.35	20.33
19.95 20.25	20.10
19.80 19.90	19.85

Mean = 20.09

Standard Deviation = $\pm$ 0.18 cms
(i.e. $\sim 2 \times 10^{-9}$ ccs He).

The standard deviation in measuring the pressure of a sample of helium passed through the column is by normal combination of errors $\pm$ 0.20 cms (i.e. $\sim 2 \times 10^{-9}$ ccs He).

-71-

3.3 Column Calibration

To check the correct operation of the separation column, a quantity of helium was introduced to the apparatus. The distribution of helium collected at the end of the column was measured against the number of column operations. The results are seen in Figure 23 (curve 1).

This experiment was repeated for neon and the results are seen in Figure 23 (curve 2). These results agree with other workers on this separation column (41, 42) and show that the helium collection should be stopped after 36 operations at which time 99.3% of the helium has been collected.

3.4 Efficiency Experiments

A number of portions of helium were taken from the second pipette in the calibration system (Fig. 22). Alternate portions were measured directly in the Pirani gauges and measured after being passed through the separation column. The latter portions were removed quantitatively from the calibration system in bulb D (Fig. 24) in the gas transfer system by means of the Toepler pump and connected on to the gas sample tube in the circulating system (Fig. 17). Due to the length of time required for this experiment, only 3 or 4 portions could be taken in one run and three runs were therefore

COLUMN CALIBRATION

FIG. 23

He
(Curve 1)

Ne
(Curve 2)

Number of operations

Quantity of helium/neon collected per operation

Bulb D

Measuring
System
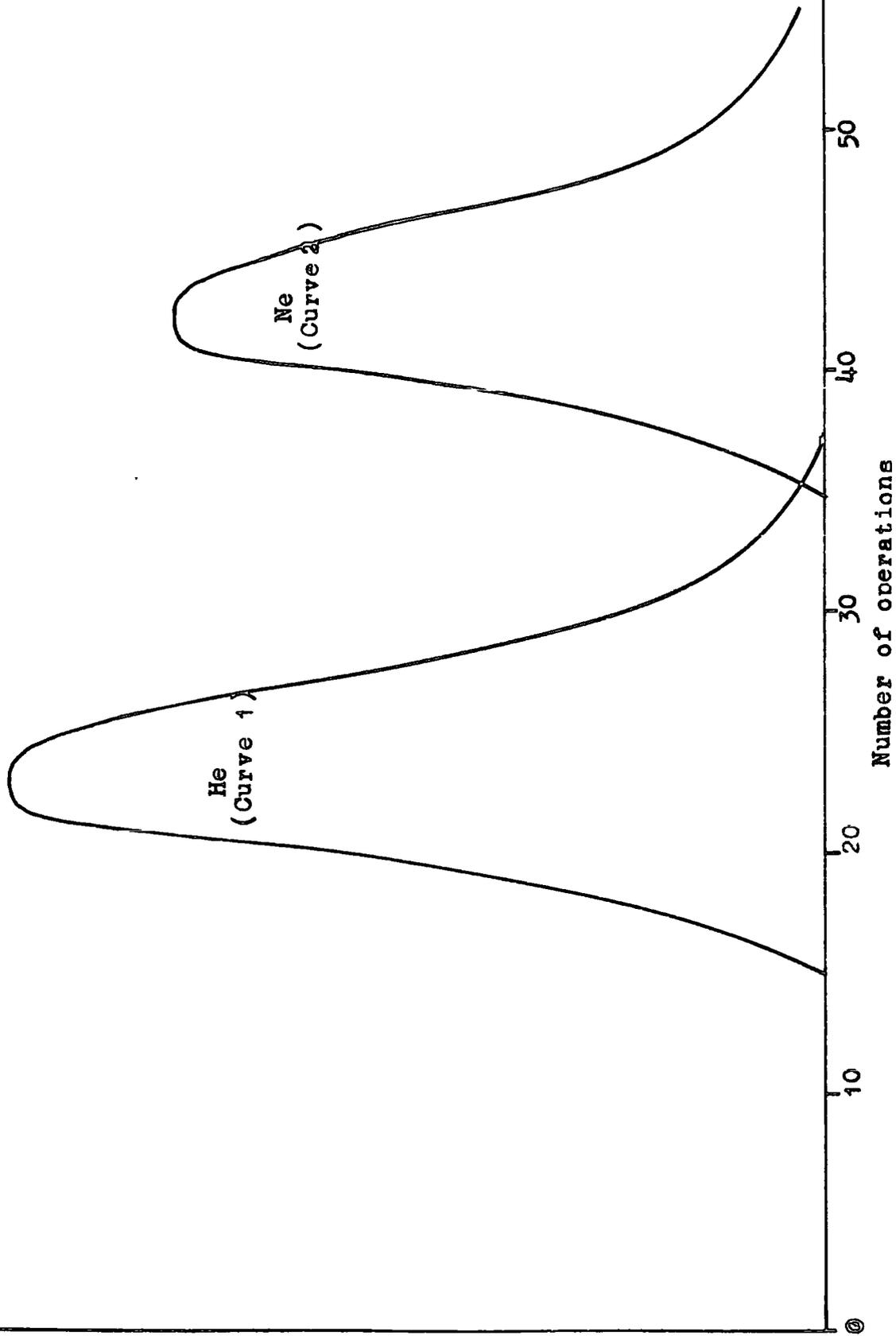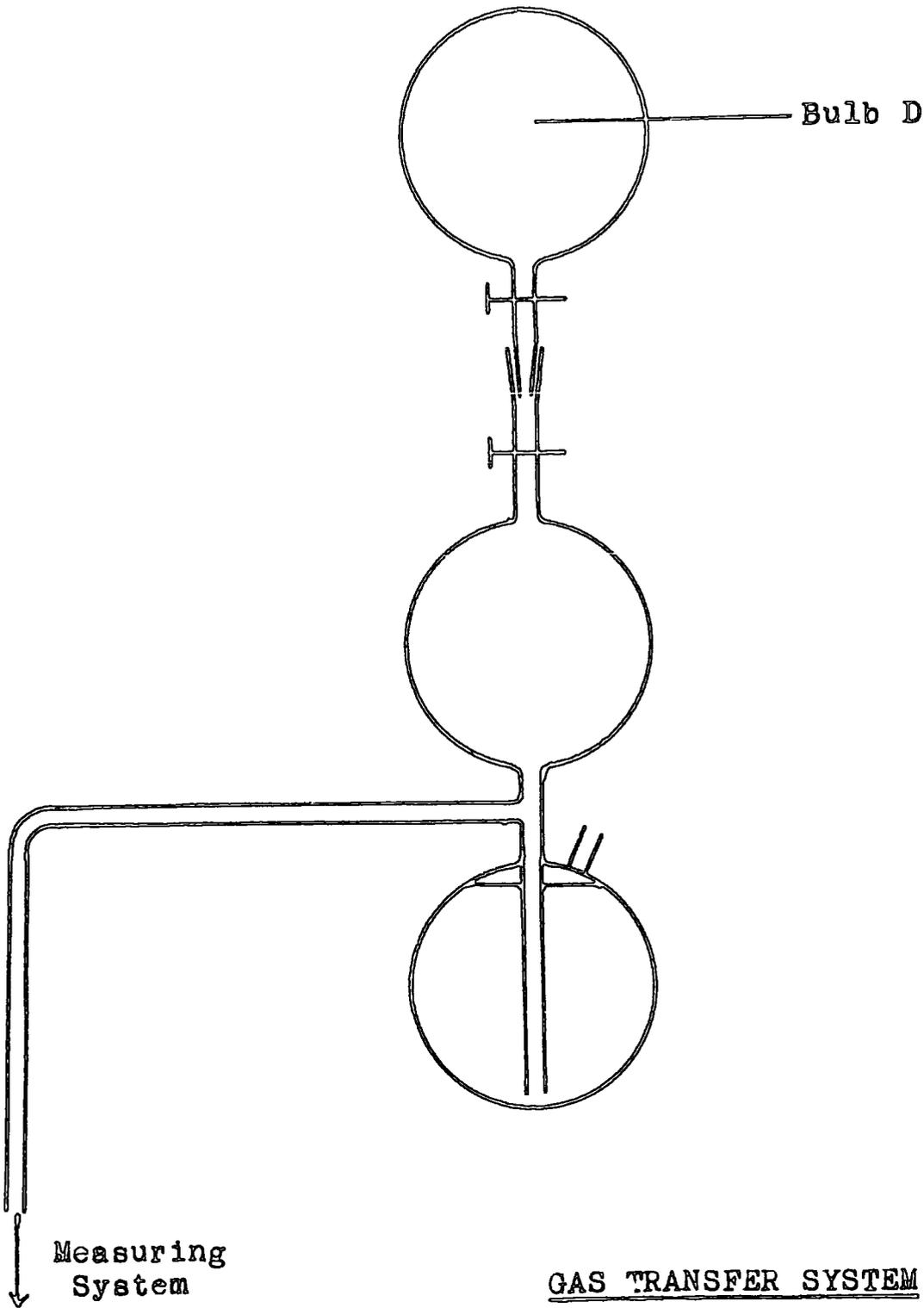
GAS TRANSFER SYSTEM

FIG. 24

3.4 Contd.

carried out (Table 13).

Volume of pipette (2)	=	3.28 ccs.
Volume of bulb etc.	=	166.38 ccs.
Hence Volume minus pipette	=	163.10 ccs.

Hence percentage difference between successive portions

$$= \frac{163.10 \times 100}{166.38}$$

i.e. 98.0%

TABLE 13

Portion Number	Deflection Direct (cms)	Deflection thro' column (cms)	Normalised	Percent Recovery
1	–	34.28	33.59	95.1
2	35.12	–	35.12	–
3	–	32.71	33.38	94.5
4	34.14	–	35.53	–
1	–	27.14	26.60	94.5
2	28.16	–	28.16	–
3	–	26.34	26.88	95.5
1	–	22.39	21.52	95.2
2	–	21.88	21.44	94.8
3	22.61	–	22.61	–

Mean is 94.9%

The efficiency of recovery of helium on passing through the separation column is 94.9 ± 0.16%.

4. DISSOLUTION OF FOILS

4.1 Dissolver

The apparatus for the dissolution of the irradiated aluminium foils (Fig. 25) consists of a 500 ml flask containing an aqueous solution of potassium cupric chloride; this solvent was selected to reduce the quantity of hydrogen produced on dissolution. The aluminium foil is placed in the closed tube inserted into the side – arm of the flask; rotation of the tube allows the foil to fall into the solvent. A dip – tube is used to bubble purified oxygen into the solution to purge out air prior to dissolving and to remove all the helium after dissolving. The helium is flushed through the apparatus into the circulating system (Fig. 17) via a mercury non – return bubbler and the helium is measured as described in section 3.1.

4.2 Purification of oxygen

The quantity of helium expected in the aluminium catcher foil is approximately 10^{-7} ccs and the quantity of oxygen used to sweep the gases out of the dissolver is approximately 300 ccs. The helium impurity content in the oxygen must therefore be considerably less than 3×10^{-4} p.p.m.

ALUMINIUM DISSOLVING APPARATUS

FIG. 25

Oxygen reservoir

Circulating
system

Al
foil

Potassium
cupric
chloride
solution
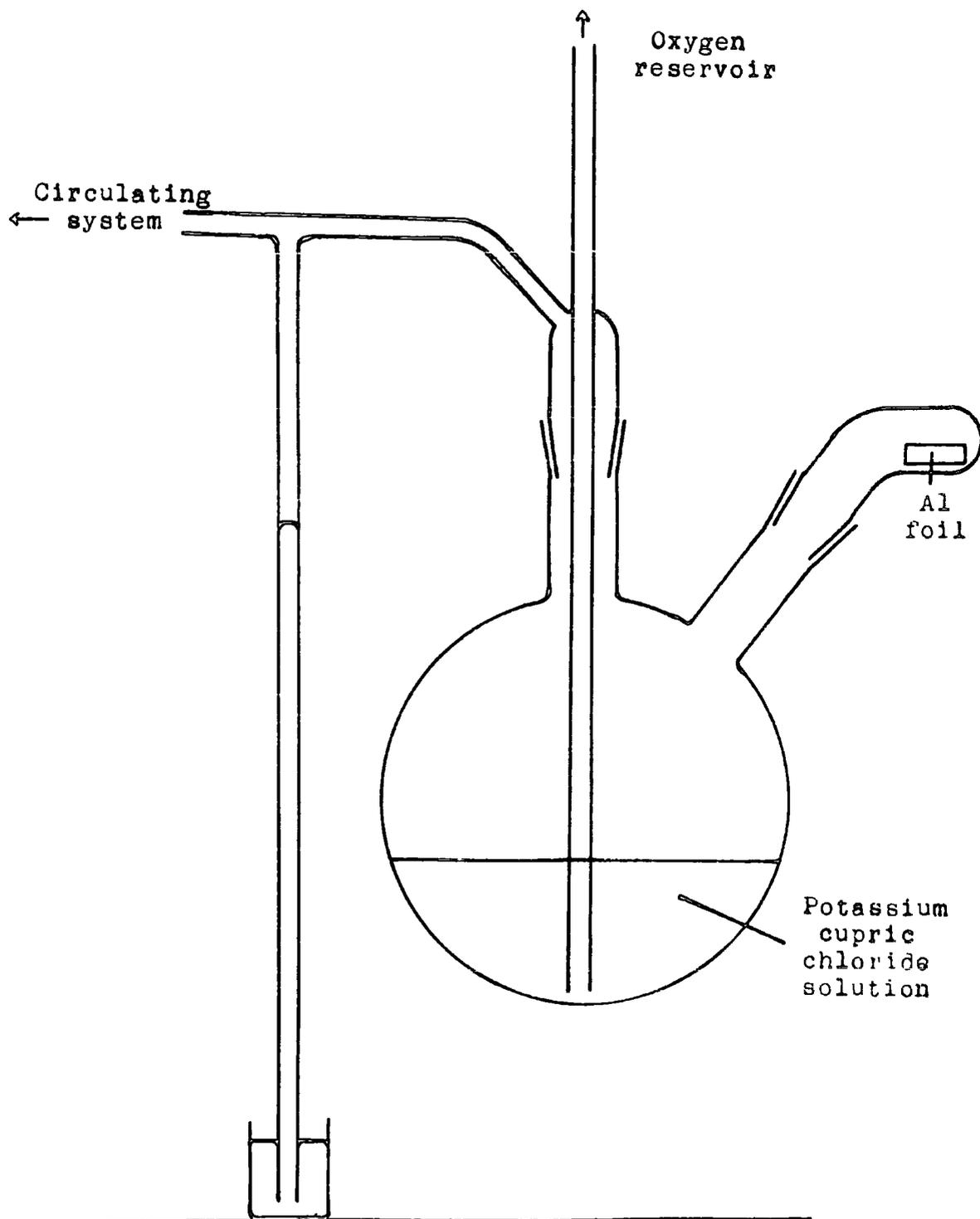
4.2   Contd.

Electrolytic oxygen was selected as the source of gas, since this was considered the type of commercial oxygen most likely to be free from helium. Oxygen from the cylinder was passed via a reducing valve into the oxygen purification system (41) (Fig. 26). The apparatus was pumped down and the still was isolated from the collection bulb and the gas entry point by closing a tap. A Dewar flask of liquid nitrogen was placed round the collection bulb and oxygen gas was bubbled through the mercury in the gas entry point and into the apparatus. The oxygen flow was kept just greater than the rate of condensation so that the excess oxygen bubbled through the mercury to atmosphere and so prevented any possible ingress of air into the apparatus. This was continued until the collection bulb was about three quarters full of liquid oxygen. At this point, the vapour pressure of the liquified gas in the collection bulb was about 45 cms of mercury due to various impurities. An initial purification was performed by pumping out the gas in the free space until the vapour pressure was reduced to approximately 15 cms of mercury (vapour pressure of oxygen at $-195.8^{\circ}C$ is 15.2 cms of mercury).

Vacuum system

Dissolver

Vacuum system

Condenser

Dixon packing

Heater

Oxygen collection bulb

Oxygen

Gas entry point

OXYGEN STORAGE AND PURIFICATION
SYSTEM

FIG.26
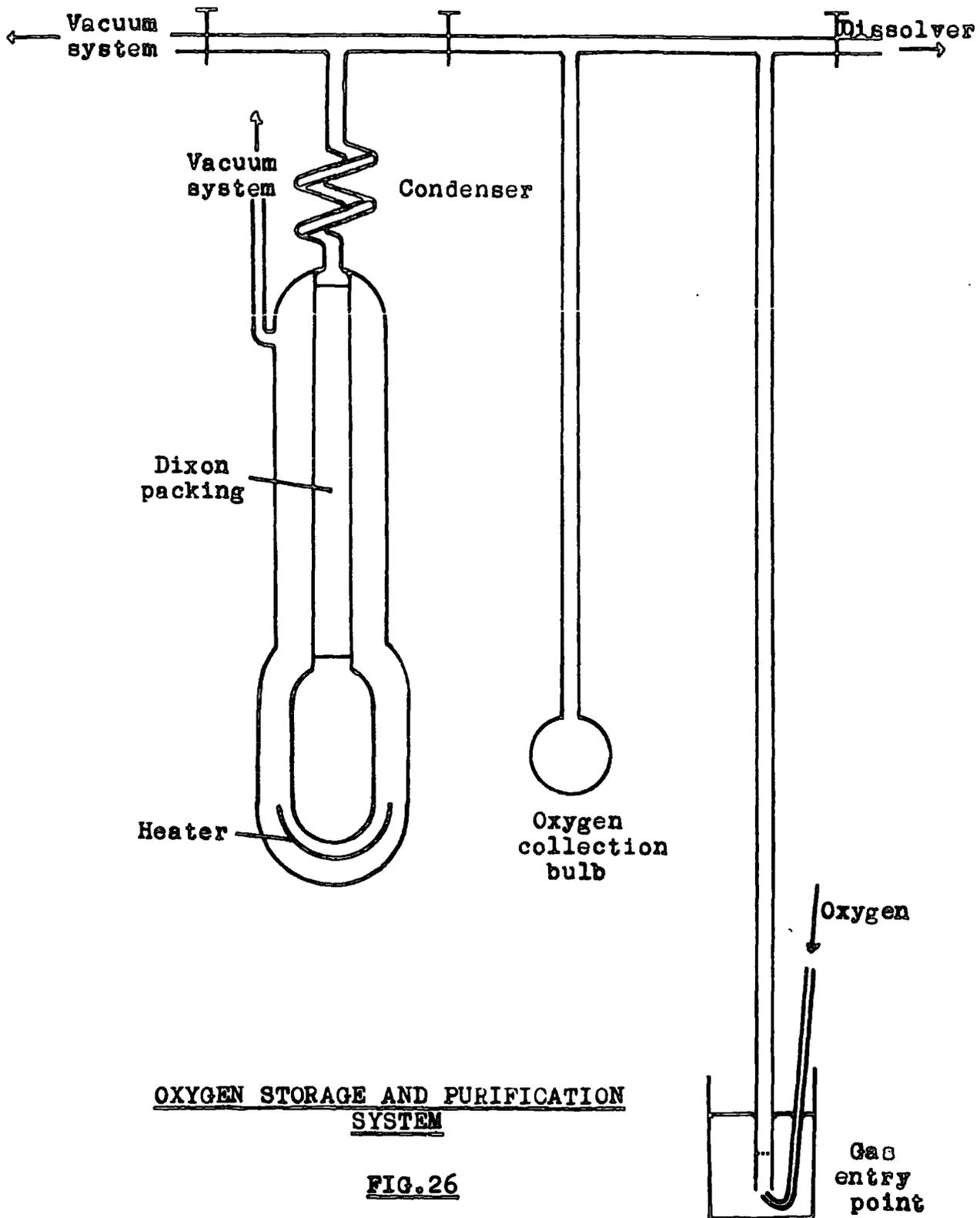
4.2 Contd.

The oxygen was transferred to the distillation apparatus by surrounding it with liquid nitrogen and removing the liquid nitrogen from around the collection bulb. The oxygen condensed in the condenser portion and ran down the Dixon packing fractionation column into the flask, gradually cooling it until all the oxygen had collected in the flask. The heating coil was switched on and fractionation was carried out for approximately 10 hours during which time about one third of the oxygen was lost to the pumping system through the mercury bubbler. The oxygen was returned to the collection bulb and stored under liquid nitrogen.

The helium content of the oxygen was determined in an apparatus designed by Hall (41) for the determination of helium in beryllium metal (Fig. 27). Hydrogen produced by dissolving magnesium metal in dilute sulphuric acid was burned with oxygen from the liquid oxygen supply and after condensation of the water produced, the evolved gases were passed into the helium apparatus for helium content measurement. This value represented a maximum since the helium content of the magnesium was unknown, though it had been previously purified by vacuum sub-limation (the magnesium was supplied by Magnesium Elektron Ltd.).

DISSOLVER

FIG.27

Oxygen

Circulating
system

Hydrogen
burner

Soft iron bar

Platinum
cage

$1.5M\ H_2SO_4$
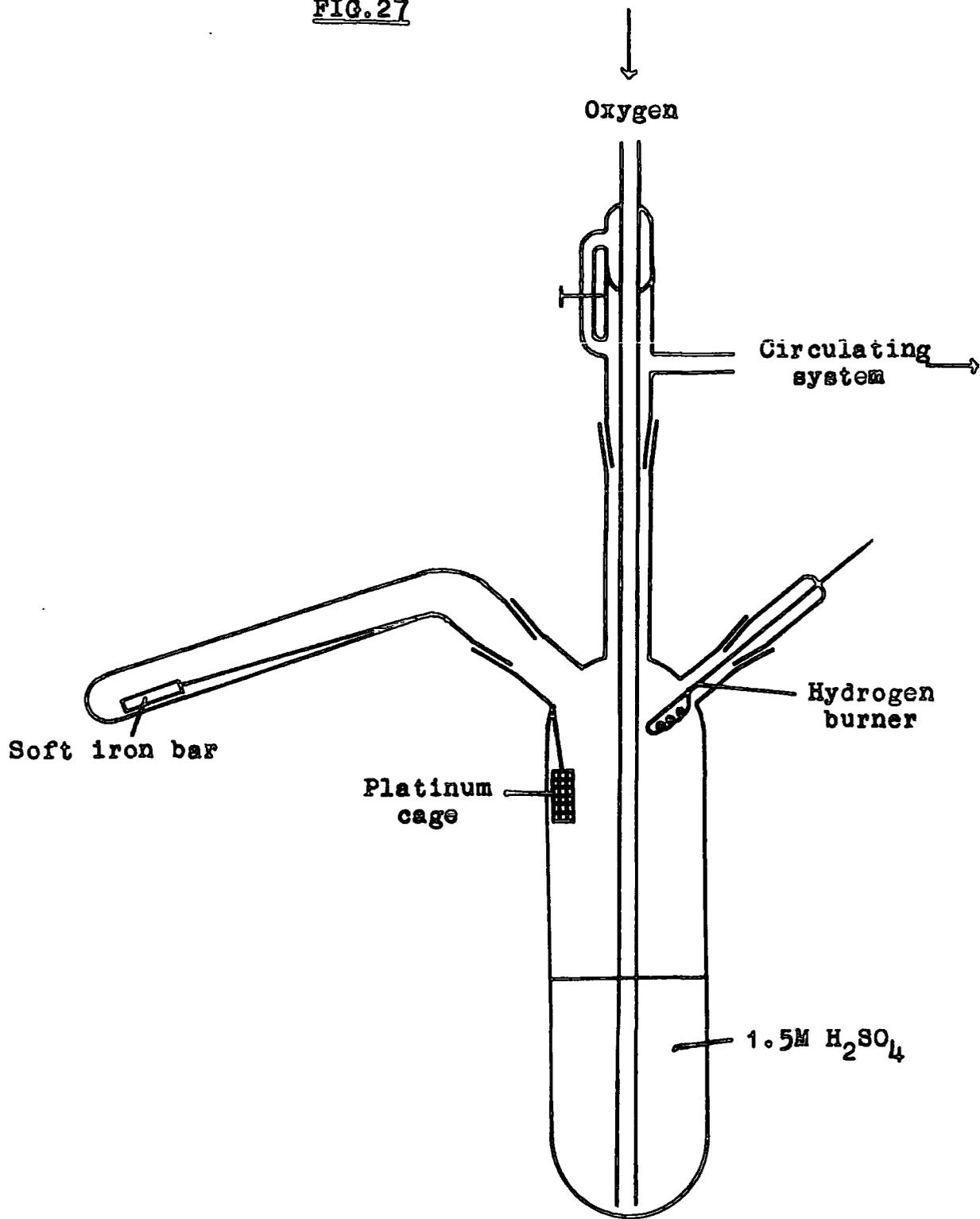
4.2 Contd.

A piece of magnesium (approximately 9g) was degreased in carbon tetrachloride, washed in acetone and water and finally cleaned by immersion in 2M sulphuric acid for a short time followed by washing with water and drying. The magnesium was weighed and fixed into the platinum cage; 1000 mls of 1.5M sulphuric acid were poured into the dissolver. The air was removed from the dissolver and the sulphuric acid solution by flushing with oxygen and pumping. The effectiveness of the flushing was checked by bubbling approximately 100 ccs of oxygen through the solution and measuring the helium content in the helium apparatus. The helium content was found to be less than 10^{-8} ccs.

The dissolver was finally flushed out with oxygen and the oxygen - hydrogen burner was degassed by switching it on for 30 minutes followed by a further flushing out. The cooling vessel was filled with water and ice added. Ice was also added throughout the dissolving to keep the temperature of the solvent well below 60°C, at which temperature the vapour pressure of water approaches that of liquid oxygen at liquid nitrogen temperature and would prevent oxygen entering the dissolver. The burner was switched on and the tap from the oxygen collection bulb opened. The dissolving was commenced by lowering the

4.2   Contd.

magnesium into the sulphuric acid by moving the iron
bar up the long side - arm with a magnet.   The hydrogen
evolved was burned with oxygen.   Care was taken that the
pressure in the dissolver never exceeded the vapour
pressure of liquid oxygen at liquid nitrogen temperature
i.e. there was always an excess of oxygen present.

When dissolving was complete, the evolved gases were
passed into the helium apparatus via a liquid nitrogen
trap.   Three flushings with oxygen were carried out to
ensure the last traces of gas were transferred to the
helium apparatus and the helium content determined.

The experiment was repeated and the results are seen
in Table 14.

TABLE 14

Run Number	1	2
Weight of Magnesium	8.9g	9.4g
Volume of H_2 evolved	8.2 litres	8.8 litres
Volume of O_2 used	4.1 litres	4.4 litres
Volume of He measured	$< 4.6 \times 10^{-8}$ ccs	$< 4.2 \times 10^{-8}$ ccs
He content of O_2	$< 1.1 \times 10^{-5}$ p.p.m.	$< 1.0 \times 10^{-5}$ p.p.m.

This content represents not greater than 3% of the
helium expected in the aluminium foils and was considered
satisfactory.

-78-

4.3 Determination of Helium content of the Foils

The aluminium foil was measured, weighed and placed in the dissolver (section 4.1). Air was removed from the dissolver and the potassium cupric chloride solution by flushing with oxygen and pumping. The effectiveness of the flushing was checked as in section 4.2. The helium content of 100 ccs oxygen flush was found to be less than 10^{-8} ccs.

The tube containing the foil was rotated allowing the foil to fall into the solution and dissolve. The evolved gases were flushed out with oxygen (3 times) into the helium apparatus via a mercury bubbler non − return valve. The hydrogen was removed in the circulating system and the helium content was determined.

Three determinations were carried out on unirradiated foils and two on irradiated foils (the aluminium foil used was from the same source). The results are shown in Table 15.

TABLE 15

Run Number	Blank 1	Blank 2	Blank 3
Volume of Helium (ccs)	3.15×10^{-8}	3.28×10^{-8}	3.58×10^{-8}
Mean Helium Blank		3.34×10^{-8}	$(\pm 0.12 \times 10^{-8})$

Run Number	Irradiation 1	Irradiation 2
Wt. of Foil	96.76 mg	94.71 mg
Volume of Helium (ccs)	6.33×10^{-8}	9.99×10^{-8}
Volume of Helium less blank	2.99×10^{-8}	6.65×10^{-8}
Percentage recovery of Helium	94.9%	94.9%
Net Vol. of Helium (ccs)	3.15×10^{-8}	7.01×10^{-8}

4.4 Na^{24} Counting

This part of the work was carried out by J.H.Davies (43) and is therefore described only briefly.

After allowing about 90 minutes for Mg^{27} ($t_{\frac{1}{2}}$ 9.5 mins) to decay, the aluminium foil was dissolved in 5M hydrochloric acid containing a little sodium carrier. The solution was diluted to 12 mls and 10 mls removed for counting in a liquid counter, which had been calibrated previously for Na^{24} by $4\overline{\Pi}$ counting. Count rates were recorded until sufficient results were available to accurately extrapolate the decay curve back to the time

4.4 <u>Contd.</u>

at the end of the irradiation. The count rate at the
end of the irradiation was corrected for variations in
the neutron yield during the course of the irradiation
(see Part I, Section 1). The number of atoms of Na^{24}
produced during the irradiation was calculated. The
results were 1.87 x 10^{-7} atoms (irradiation 1) and
4.05×10^{7} atoms (irradiation 2).

5. <u>RESULTS AND DISCUSSION</u>

The formula for calculation of cross - section values
was applied to the results of the two irradiations as follows:-

$$\sigma = \frac{\text{Number of } Na^{24} \text{ atoms produced}}{\text{Number of Al atoms/cm}^2 \text{ x Number of He atoms produced}}$$

It was, however, necessary to apply two corrections:-

(i) for the mean neutron path length l through the
activation foil of thickness d.

(ii) for the slight difference between the neutron and
α -particle distributions in the laboratory co-
ordinate system.

The former correction is a function of effective deuteron
energy, which will depend on the target thickness, the distri-
bution of tritium within the target and the extent of build up
of any surface layer. The D + T reaction has a prominant
resonance (48) at about 110 keV deuteron energy and from the

data of Gunnerson and James (44), it was estimated that this
energy would be reached by the deuterons after passing through
about one half of the target thickness. A value for $^1\!/d$ of
1.217 was calculated, assuming this value for the deuteron
energy. The value of $^1\!/d$ is rather insensitive to the deuteron
energy, changing about 0.0001 per keV.

The latter correction was simple since the distribution
of neutrons and α-particles is known to be isotropic about
the centre of mass co-ordinate system at the deuteron energy
employed (45, 46, 47) and a value of Ω_α/Ω_n of 0.8778 was
calculated. This is also energy dependent and changes by
about 0.13% per keV.

The values for the cross - section thus obtained were
114.2 and 113.2 mb.

The greatest error in these experiments was the magnitude
of the helium found in the blank runs. It had been shown
previously that there was a substantial increase in the 15 -
operations blank and that the helium determined did not arise
from the aluminium. The cause of the high blanks was assumed
to be due to a certain permeability produced in the fractionat-
ing column by devitrification of the soda glass, since this
column had been in use for many years. Some confidence was
however, restored by the reproducibility of the helium blanks
(Table 15).

The principal errors in this work were:-

(i) the estimation of the helium blank.

(ii) the determination of helium produced during the irradiation.

(iii) the lack of knowledge of the effective dueteron energy (a variation in deuteron energy of $\pm$ 20 keV represents a variation in the cross - section value of 3.5%).

Other possible sources of error, which were insignificant compared with the above, are however worthy of inclusion:-

(i) the extrapolation of the Na^{24} decay curve.

(ii) back - scatter of α-particles from the target material.

(iii) helium from the Al (n,α) reaction.

(iv) contamination of the catcher foil with He^3 from tritium decay.

The total errors were estimated at $\pm$ 8.9% to give a value for the cross - section of the Al(n,α) reaction for 13.5 MeV neutrons of 113.7 $\pm$ 10.1 mb. Recent experiments on the cross - section for this reaction have been carried out by a number of workers and their results are shown in Table 16.

-83-

TABLE 16

Neutron Energy MeV	Cross – Section mb	Reference
14.8	92 ± 15	49
14.1	116 ± 8	50
13.0	139	51
14.8	114 ± 7	52
13.85	95 ± 19	53
14.76	117.0	54
13.5	130.6 ± 6.5	55
13.8	121 ± 12	56
13.5	118.1 ± 6.0	57

It is seen that there is considerable variation in the reported results and that the value obtained in this work lies in the middle of the range; it agrees very well with more accurate results obtained later by the same method (57). It is, therefore, concluded that this method of determining the cross section for the Al (n, α) reaction enables many of the errors apparent in other methods to be considerably reduced.

REFERENCES

1. Steinberg E.P. and Glendenin L.E. International
    Conference on the Peaceful Uses of Atomic Energy:
    Proceedings, vol. 7, paper 614 (United Nations,
    New York 1956).

2. Keller R.N., Steinberg E.P. and Glendenin L.E.,
    Phys. Rev. $\underline{94}$ 969 (1954).

3. Spence R.W. and Ford G.P. Annual Review of Nuclear
    Science vol. 2, 399 (1953).

4. Glendenin L.E. The Distribution of Nuclear Charge
    in Fission, Massachusetts Institute of Technology,
    Technical Report No. 35.

5. Goeckerman R.H. and Perlman I. Phys. Rev. $\underline{76}$, 628
    (1949).

6. Hahn O. and Strassmann F. Naturwiss $\underline{27}$ 11 (1939).

7. Adams B., Batchelor R. and Green T.S. Reactor
    Science and Technology (J. Nuclear Energy A & B)
    $\underline{14}$ 85 (1961).

8. Coryell C.D. and Sugarman N. Radiochemical Studies:
    The Fission Products vol. 3, p1580 National
    Nuclear Energy Series (McGraw Hill Book Co.
    New York).

9. Ibid p1657.

10. Ibid p1460.

11. Ibid p1538.

12. Vogel A.I. A Text Book of Quantitative Inorganic
    Analysis p441 (Longmans 1955).

13. As for ref. 8 p1549.

14. Ibid p1666.

15. Progress in Nuclear Energy III vol. 1 p147.

References (Contd.)

16. As for ref. 8, p1573.

17. Ibid p1625.

18. Ibid p1451.

19. White C.E. and Rose H.J.   Anal. Chem. $\underline{25}$ 351 (1953).

20. As for ref. 8 p1595.

21. Warf J.C.   J.A.C.S. $\underline{71}$ 3257 (1949).

22. Furnan N.H., Mason W.B. and Pekola J.S.   Anal. Chem. $\underline{21}$ 1325 (1949).

23. Oesper R.E. and Klingenberg J.J.   Anal. Chem. $\underline{21}$ 1509 (1949).

24. Review of Modern Physics $\underline{30}$ Number 2 Part II (1958).

25. Cuninghame J.G. Sizeland M.L. and Willis H.H. A.E.R.E. C/R 2054 (1957).

26. Cuninghame J.G. Sizeland M.L. and Willis H.H. A.E.R.E. C/R 1646 (1955).

27. Curie M., Debierne A., Eve A.S., Geiger H., Hahn O., Lind S.C., Meyer S., Rutherford E., and Schweidler E. Revs. Mod. Physics $\underline{3}$, 427 (1931).

28. Placzek G.   The functions $E_n(x) = \int_1^\infty e^{-xu} u^{-n} du$ NRC - 1547.

29. Silvester D.J. Radiochemical Studies of Nuclear Fission. PhD Thesis Durham 1958.

30. Cuninghame J.G., Journal of Inorganic and Nuclear Chemistry, $\underline{5}$, 1 (1957).

31. Flerov N.N. and Tamanov E.A.   Soviet J. Atomic Energy $\underline{5}$, 1596 (1958).

32. Flerov N.N. and Talyzin V.M. Atomaya Energiya $\underline{5}$ 653 (1958).

References (Contd.)

33. Billand P., Clair C., Gandin M., and Genin R. International Conference on the Peaceful Uses of Atomic Energy; Proceedings Volume 16 paper 1986 (United Nations, New York 1958).

34. Thode H.G. and Graham R.L. Canadian J. Research 25A 1 (1947).

35. Wahl A.C. Phys. Rev. 99 730 (1955).

36. Richter H.G. and Coryell C.D. Phys.Rev. 95 1550 (1954).

37. Paneth F.A., Endeavour 12 5 (1953).

38. Gluckauf E. and Paneth F.A. Proc.Roy.Soc. A185, 89 (1946).

39. Gluckauf E., ibid p98

40. Chackett K.F., Reasbeck. P., and Wilson E.J. Geochim et Cosmochim Acta 3 261 (1953).

41. Hall D., Ph.D. Thesis, Durham 1958.

42. Reasbeck P., Ph.D. Thesis, Durham 1953.

43. Davies J.H., Ph.D. Thesis, Durham.

44. Gunnerson E.M. and G.James. Nucl.Instr. and Methods 8, 173 (1960).

45. Allen D.L. and M.J. Poole, Proc.Roy.Soc. A204 500 (1951).

46. Argo H.V., Taschek R.F., Agnew H.M., Hemmendinger A., and Leland W.T., Phys.Rev. 87 612 (1952).

47. Bame S.J. and Perry J.E., Phys.Rev. 107 1616 (1957).

48. Conner J.P., Bonner T.W. and Smith J.R., Phys.Rev. 88, 468 (1952).

49. Kumabe I., Takekoshi E., Ogata H., Tsumeoka Y. and Oki S., Phys.Rev. 106 155 (1957).

50. Grundl J.A., Henkel R.L. and Perkins B.L. Phys.Rev. 109 425 (1958).

References (Contd.)

51. Kern B. D., Thompson W. E., and Ferguson J. M. Nucl. Phys. $\underline{10}$ 226 (1959).

52. Poularikas A., and Fink R. W., Phys. Rev. $\underline{115}$ 989 (1959).

53. Tewes H. A., Caretto A. A., Miller A. E., and Nethaway D. R., UCRL – 6028 – T.

54. Schmidt H. W. and Halperin J. Phys. Rev. $\underline{109}$ 2031 (1961).

55. Bayhurst B. P., and Prestwood R. J. J. Inorg. Nucl. Chem. $\underline{23}$ 173 (1961).

56. Gaddard F., and Kern B. D., Phys. Rev. $\underline{128}$ 1276 (1962).

57. Hemingway J. D., Martin E. B. M. and Martin G. R., to be published.

58. Coryell C. D. and Sugarman N. Radiochemical Studies: The Fission Products vol. 1 p. 469 National Nuclear Energy Series (McGraw Hill Book Co. New York).

59. Pappas A. C. International Conference on the Peaceful Uses of Atomic Energy: Proceedings vol. 7, paper 881 (United Nations, New York 1956).

60. Wahl A. C. J. Inorg. Nucl. Chem. $\underline{6}$, 263 (1958).

61. Alexander J. M. and Coryell C. D., Phys. Rev. $\underline{108}$, 1274 (1957).

62. Hageoo E., Kjelberg A., Pappas A. C. J. Inorg. Nucl. Chem. $\underline{24}$, 117 (1962).

63. Farrar H. and Tomlinson R. H. Can. J. Phys. $\underline{40}$, 943 (1962).

64. Turkevich A. and Niday J. B. Phys. Rev. $\underline{84}$, 52 (1951).

The decay chains for the fission products expected
to be produced from the 14 MeV neutron fission of
natural uranium (24).

72.   Zn(49hr.) $\longrightarrow$ Ga(14.3hr.) $\longrightarrow$ Ge(s)

73.   Ga(5.0hr.) $\longrightarrow$ Ge(s)

74.   Ga(7.8min.) $\longrightarrow$ Ge(s)

75.   Ga(2min.) $\longrightarrow$ Ge(82min.) $\longrightarrow$ As(s)

76.   Ge(s)

77.   Ge(54sec.)
         $\downarrow$
         Ge(11.3hr.) $\longrightarrow$ As(38.7hr.) $\longrightarrow$ Se(s)

78.   Ge(2.1hr.) $\longrightarrow$ As(91min.) $\longrightarrow$ Se(s)

79.   As(9.0min.) $\longrightarrow$ Se(3.9min.) $\longrightarrow$ Se(6.5×10^4yr.)
                                                         $\downarrow$
                                                         Br(s)

80.   As(15.3sec.) $\longrightarrow$ Se(s)

81.   As(33sec.) $\longrightarrow$ Se(56.8min.) $\longrightarrow$ Se(18.2min.)
                                                            $\downarrow$
                                                            Br(s)

82.   Se(s)

83.   Se(70sec.) $\xrightarrow{>90\%}$ Br(2.3hr.) $\longrightarrow$ Kr(114min.)
         $\downarrow$ <10%
         Se(25min.) $\downarrow$
                                                           Kr(s)

84.   Se(3.3min.) $\longrightarrow$ Br(31.8min.) $\longrightarrow$ Kr(s)

85.   As(0.4sec.) $\longrightarrow$ Se(40sec.) $\longrightarrow$ Br(3.0min.)
                                                            $\downarrow$
         Rb(s) $\longleftarrow$ Kr(10.3yr.) $\xleftarrow{23\%}$ Kr(4.36hr.)
                                     77%

86.   Kr(s)

87.   Se(17sec.) $\longrightarrow$ Br(55.6sec.) $\longrightarrow$ Kr(7.8min.)
                                                            $\downarrow$
                                                            Rb(s)

88. $\quad$ Br(15.5sec.) $\longrightarrow$ Kr(2.77hr.) $\longrightarrow$ Rb(17.8min.)

$\qquad\qquad\qquad\qquad\qquad\qquad\qquad\qquad\qquad\qquad$ Sr(s)

89. $\quad$ Br(4.5sec.) $\longrightarrow$ Kr(3.2min.) $\longrightarrow$ Rb(15.4min.)

$\qquad\qquad\qquad\qquad$ Y(s) $\longleftarrow$ Sr(50.5d)

90. $\quad$ Br(1.4sec.) $\longrightarrow$ Kr(33sec.) $\longrightarrow$ Rb(2.7min.)

$\qquad$ Zr(s) $\longleftarrow$ Y(64.5hr.) $\longleftarrow$ Sr(27.7yr.)

91. $\quad$ Kr(9.8sec.) $\longrightarrow$ Rb(14min.) $\longrightarrow$ Sr(9.7hr.)

$\qquad\qquad\qquad\qquad\qquad$ Rb(100sec.)

$\qquad$ Zr(s) $\longleftarrow$ Y(57d) $\longleftarrow$ Y(50.3min.)

92. $\quad$ Kr(3.0sec.) $\longrightarrow$ Rb(5.3sec.) $\longrightarrow$ Sr(2.7hr.)

$\qquad\qquad\qquad\qquad$ Zr(s) $\longleftarrow$ Y(3.5hr.)

93. $\quad$ Kr(2.0sec.) $\longrightarrow$ Rb(5.6sec.) $\longrightarrow$ Sr(7.5min.)

$\qquad$ Nb(s) $\longleftarrow$ Zr(1.1×10^{6}yr.) $\longleftarrow$ Y(10.0hr.)

94. $\quad$ Kr(1.4sec.) $\longrightarrow$ Rb(2.9sec.) $\longrightarrow$ Sr(1.3min.)

$\qquad\qquad\qquad\qquad$ Zr(s) $\longleftarrow$ Y(16.5min.)

95. $\quad$ Kr(short) $\longrightarrow$ Rb(2.5sec.) $\longrightarrow$ Sr(40sec.)

$\qquad$ Nb(90hr.) $\longleftarrow$ Zr(65d) $\longleftarrow$ Y(10.5min.)

$\qquad$ Nb(35d)

$\qquad$ Mo(s)

96. $\quad$ Zr(s)

97. $\quad$ Kr(1sec.) $\longrightarrow$ Rb(short) $\longrightarrow$ Sr(short)

$\qquad$ Nb(60sec.) $\longleftarrow$ Zr(17.0hr.) $\longleftarrow$ Y(short)

$\qquad$ Nb(72min.)

$\qquad$ Mo(s)

98. $\quad$ Zr(1min.) $\longrightarrow$ Nb(51.5min.) $\longrightarrow$ Mo(s)

99. $\quad$ Zr(30sec.) $\longrightarrow$ Nb(2.4min.) $\longrightarrow$ Mo(67.0hr.)

$\quad\quad\quad$ Ru(s) $\longleftarrow$ Tc(2×10^5yr.) $\longleftarrow$ Tc(6.0hr.)

100. $\quad$ Nb(3.0min.) $\longrightarrow$ Mo(s)

101. $\quad$ Nb(1.0min.) $\longrightarrow$ Mo(14.6min.) $\longrightarrow$ Tc(14.0min.)

$\quad\quad\quad\quad\quad\quad\quad\quad\quad\quad\quad\quad\quad\quad\quad\quad\quad$ Ru(s)

102. $\quad$ Mo(11.5min.) $\longrightarrow$ Tc(4.1min.) $\longrightarrow$ Ru(s)

$\quad\quad\quad\quad\quad\quad\quad\quad\quad\quad\longrightarrow$ Tc(5sec.)

103. $\quad$ Tc(1.2min.) $\longrightarrow$ Ru(40d) $\quad\longrightarrow$ Rh(57min.)

$\quad\quad\quad\quad\quad\quad\quad\quad\quad\quad\quad\quad\quad\quad\quad\quad$ Rh(s)

104. $\quad$ Tc(18min.) $\longrightarrow$ Ru(s)

105. $\quad$ Mo(<2min.) $\longrightarrow$ Tc(10min.) $\longrightarrow$ Ru(4.5hr.)

$\quad\quad\quad$ Pd(s) $\longleftarrow$ Rh(36.5hr.) $\longleftarrow$ Rh(45sec.)

106. $\quad$ Ru(1.0yr.) $\longrightarrow$ Rh(2.2hr.) $\longrightarrow$ Pd(s)

$\quad\quad\quad\quad\quad\quad\quad\quad\quad\quad\longrightarrow$ Rh(30sec.)

107. $\quad$ Tc(<1.5min.) $\longrightarrow$ Ru(4.8min.) $\longrightarrow$ Rh(24min.)

$\quad\quad\quad$ Ag(s) $\longleftarrow$ Ag(44.3sec.) $\longleftarrow$ Pd(7×10^6yr.)

108. $\quad$ Ru(~4min.) $\longrightarrow$ Rh(18sec.) $\longrightarrow$ Pd(s)

109. $\quad$ Rh(30sec.) $\longrightarrow$ Pd(4.7min.) $\longrightarrow$ Pd(13.5hr.)

$\quad\quad\quad\quad\quad\quad\quad\quad$ Ag(s) $\longleftarrow$ Ag(44.3sec.)

110. $\quad$ Rh(~3sec.) $\longrightarrow$ Pd(s)

111. $\quad\quad\quad\quad\quad\quad\quad\quad$ Pd(22min.) $\longrightarrow$ Ag(74sec.)

$\quad\quad\quad$ Cd(s) $\longleftarrow$ Cd(48.6min.) $\longleftarrow$ Ag(7.5d)

112. $\quad$ Pd(21hr.) $\longrightarrow$ Ag(3.4hr.) $\longrightarrow$ Cd(s)

113. $Pd(1.4min.) \longrightarrow Ag(1.2min.) \longrightarrow Ag(5.3hr.)$

$Cd(s) \longleftarrow Cd(5.1yr.)$
      mainly
$In(s) \longleftarrow In(104min.)$

114. $Pd(2.4min.) \longrightarrow Ag(5sec.) \longrightarrow Cd(s)$

115. $Pd(45sec.) \longrightarrow Ag(21.1min.)$

$\downarrow 91\%$ 9%

$Cd(53hr.)$ $Cd(43d)$

2% $\downarrow 98\%$

$In(4.5hr.)$ 95% $In(6 \times 10^{14}yr.)$

$\downarrow 5\%$

$Sn(s)$

116. $Ag(2.5min.) \Longrightarrow Cd(s)$

117. $Ag(1.1min.) \longrightarrow Cd(3.0hr.)$

$Cd(50min.)$

$In(1.1hr.) \longleftarrow 22\% \; In(1.9hr.)$

23% 55%

$Sn(14.0d)$

$Sn(s)$

118. $Cd(50min.) \longrightarrow In(5.5sec.) \longrightarrow Sn(s)$

119. $Cd(10min.) \longrightarrow In(17.5min.) \longrightarrow Sn(s)$

$Cd(2.9min.)$

120. $In(55sec.) \longrightarrow Sn(s)$

121. $Sn(27.5hr.) \longrightarrow Sb(s)$

$Sn(>5 \; yr.)$

122. $Sn(s)$

123. $Sn(41min.) \longrightarrow Sb(s)$

$Sn(125d)$

-92-

124. Sn(s)

125. Sn(9.5min.) $\longrightarrow$ Sb(2.6yr.) $\longrightarrow$ Te(58d)

      Sn(9.4d) $\nearrow$ $\downarrow$
                                                Te(s)

126. $Sn(10^5 yr.)$ $\longrightarrow$ Sb(18.8min.) $\longrightarrow$ Te(s)

                     $\searrow$ Sb(11d) $\nearrow$

127. Sn(2.6hr.) $\longrightarrow$ Sb(88hr.) $\xrightarrow{84\%}$ Te(9.4hr.)

                       16% $\downarrow$ 98% $\nearrow$ $\downarrow$

                     Te(105d)   2% $\searrow$

                                                  I(s)

---

128. Sn(57min.) $\longrightarrow$ Sb(9.6hr.) $\longrightarrow$ Te(s)

                     $\searrow$ Sb(19.7min.) $\nearrow$

129. Sb(4.6hr.) $\xrightarrow{64\%}$ Te(72min.) $\longrightarrow$ $I(1.6 \times 10^7 yr.)$

                 36% $\searrow$ $\uparrow$ $\downarrow$

                        Te(33d)   Xe(s)

130. Sn(2.6min.) $\longrightarrow$ Sb(7.1min.) $\longrightarrow$ Te(s)

131. Sn(3.4min.) $\longrightarrow$ Sb(23.1min.) $\longrightarrow$ Te(24.8min.)

                          $\downarrow$ 22% $\nearrow$

                        Te(30hr.) $\downarrow$

                               78% $\searrow$ I(8.1d)

                       Xe(12d) $\leftarrow$ 1%   99% $\downarrow$

                                $\searrow$ Xe(s)

132. Sn(2.2min.) $\longrightarrow$ Sb(2.1min.) $\longrightarrow$ Te(77.7hr.)

                                              $\downarrow$

                     Xe(s) $\longleftarrow$ I(2.26hr.)

133. $Sb(4.4min.) \longrightarrow Te(63min.) \xrightarrow{87\%} I(20.8hr.)$

$\qquad\qquad\qquad\qquad \downarrow 13\%$

$\qquad\qquad\qquad\qquad Te(2min.)$

$\qquad\qquad\qquad\qquad\qquad\qquad\qquad\qquad\qquad\qquad 2.4\%$

$\qquad\qquad\qquad\qquad\qquad\qquad 97.6\%$

$Cs(s) \longleftarrow Xe(5.3d) \longleftarrow Xe(2.3d)$

134. $Sb(0.8min.) \longrightarrow Te(44min.) \longrightarrow I(52.5min.)$

$\qquad\qquad\qquad\qquad\qquad\qquad\qquad\qquad\qquad\qquad \downarrow$

$\qquad\qquad\qquad\qquad\qquad\qquad\qquad\qquad\qquad\qquad Xe(s)$

135. $Te(<2min.) \longrightarrow I(6.7hr.) \xrightarrow{30\%} Xe(15.6min.)$

$\qquad\qquad\qquad\qquad\qquad\quad \downarrow 70\%$

$\qquad\qquad\qquad\qquad\qquad\quad Xe(9.13hr.)$

$\qquad\qquad\qquad\qquad\qquad\qquad \downarrow$

$\qquad\qquad\qquad\qquad\qquad\quad Cs(2.0\times10^6 yr.) \longrightarrow Ba(s)$

136. $I(83sec.) \longrightarrow Xe(s)$

137. $I(22sec.) \longrightarrow Xe(3.9min.) \longrightarrow Cs(30yr.)$

$\qquad\qquad\qquad\qquad\qquad\qquad\qquad\quad Ba(s) \longleftarrow Ba(2.6min.)$

138. $I(6sec.) \longrightarrow Xe(17min.) \longrightarrow Cs(32.2min.)$

$\qquad\qquad\qquad\qquad\qquad\qquad\qquad\qquad\qquad\quad \downarrow$

$\qquad\qquad\qquad\qquad\qquad\qquad\qquad\qquad\qquad\quad Ba(s)$

139. $I(2.7sec.) \longrightarrow Xe(41sec.) \longrightarrow Cs(9.5min.)$

$\qquad\qquad\qquad\qquad\qquad\qquad\qquad La(s) \longleftarrow Ba(85min.)$

140. $Xe(16sec.) \longrightarrow Cs(66sec.) \longrightarrow Ba(12.8d)$

$\qquad\qquad\qquad\qquad\qquad\qquad Ce(s) \longleftarrow La(40.2hr.)$

141. $Xe(1.7sec.) \longrightarrow Cs(short) \longrightarrow Ba(18min.)$

$\qquad Pr(s) \longleftarrow Ce(32.5d) \longleftarrow La(3.9hr.)$

142. $Cs(\sim1min.) \longrightarrow Ba(11min.) \longrightarrow La(92min.)$

$\qquad\qquad\qquad\qquad\qquad\qquad\qquad\qquad\qquad\quad \downarrow$

$\qquad\qquad\qquad\qquad\qquad\qquad\qquad\qquad\qquad\quad Ce(s)$
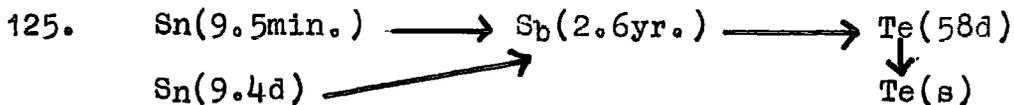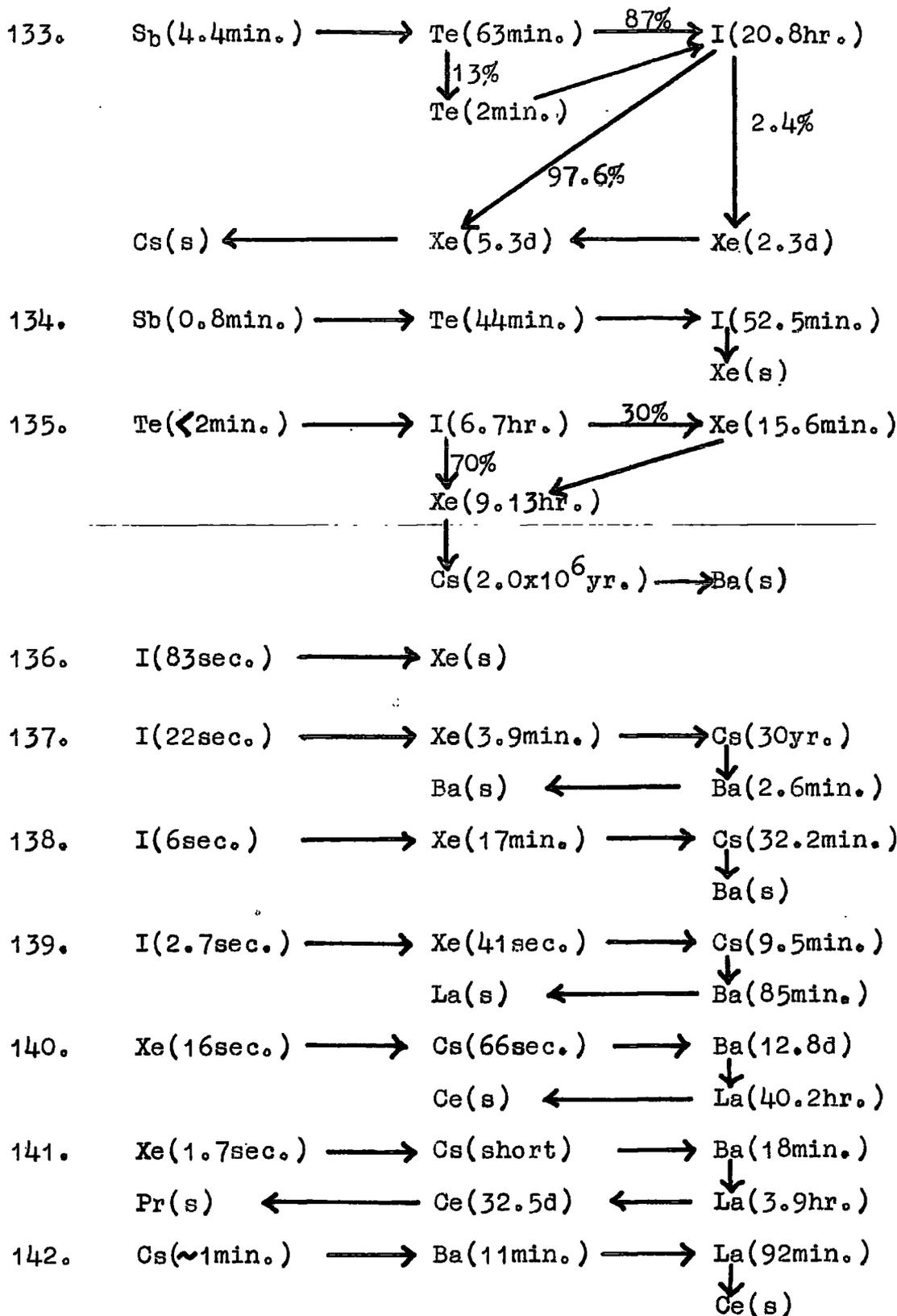
143. $Xe(1.0sec.) \longrightarrow Cs(short) \longrightarrow Ba(13sec.)$

$Pr(13.8d) \longleftarrow Ce(33hr.) \longleftarrow La(14min.)$ ↓

$Nd(s)$

144. $Xe(1sec.) \longrightarrow Cs(short) \longrightarrow Ba(short)$

$Pr(17.3min.) \longleftarrow Ce(284d) \longleftarrow La(short)$ ↓

$Nd(s)$

145. $Ce(3.0min.) \longrightarrow Pr(5.9hr.) \longrightarrow Nd(s)$

146. $Ce(13.9min.) \longrightarrow Pr(24.4min.) \longrightarrow Nd(s)$

147. $Ce(1.2min.) \longrightarrow Pr(12min.) \longrightarrow Nd(11.1d)$

$Sm(s) \longleftarrow Pm(2.64yr.)$

---

148. $Pr(2min.) \longrightarrow Nd(s)$

149. $Nd(1.8hr.) \longrightarrow Pm(53hr.) \longrightarrow S_m(s)$

150. $Nd(s)$

151. $Nd(12min.) \longrightarrow Pm(28.4hr.) \longrightarrow S_m(93yr.)$ ↓

$E_u(s)$

152. $Pr(6min.) \longrightarrow S_m(s)$

153. $S_m(47.1hr.) \longrightarrow E_u(s)$

154. $Pr(2.5min.) \longrightarrow S_m(s)$

155. $S_m(23.5min.) \longrightarrow Eu(1.7yr.) \longrightarrow Gd(s)$

156. $S_m(9.1hr.) \longrightarrow Eu(15.4d) \longrightarrow Gd(s)$

157. $Sm(30sec.) \longrightarrow Eu(15.4hr.) \longrightarrow Gd(s)$

158. $Eu(60min.) \longrightarrow Gd(s)$

159. $E_u(20min.) \longrightarrow Gd(18.5hr.) \longrightarrow Tb(s)$

160. $Gd(s)$

161. $Gd(3.6min.) \longrightarrow Tb(7.2d) \longrightarrow Dy(s)$

-95-

The radiochemical separations carried out by the author are described in further detail.

Silver (8)

The irradiated uranyl nitrate solution is warmed on a water - bath and 5 mls of 2M hydrochloric acid are added. The solution is centrifuged and the supernate collected for barium and strontium determinations. The precipitate is washed twice with water and dissolved in 1 ml. of con-centrated ammonia solution. The solution is diluted to 5mls. with water and two ferric hydroxide scavenges are carried out. Hydrogen sulphide gas is passed through the solution and the silver sulphide is centrifuged down and washed twice with water. The precipitate is dissolved in 2 mls of concentrated nitric acid and boiled to remove any sulphur, which may have been precipitated with the sulphide. The solution is diluted to 10 mls. with water, 5 mls. of 2M hydrochloric acid added and the solution warmed on a water - bath. The silver chloride is filtered onto a tared filter - paper, washed with 0.5M hydrochloric acid, water, alcohol and ether, dried in a vacuum desiccator and weighed.

The carrier solution is prepared by dissolving an accurately weighed amount of silver nitrate (1.520g) in 0.1M nitric acid and diluting to 100 mls. The concentration

of the carrier solution is 9.65 mg Ag/ml.

Strontium (10)

The supernate from the barium separation (section 3.2) is almost 11M in hydrochloric acid and of large volume (30 mls.). This solution is evaporated to small bulk with nitric acid to remove the hydrochloric acid. The solution is cooled and transferred to an ice-bath. 25 mls. of fuming nitric acid are added and the solution allowed to stand for $\frac{1}{2}$ hour. The precipitated strontium nitrate is centrifuged down, dissolved in water and the solution made alkaline by the addition of a few drops of concentrated ammonia solution. Two ferric hydroxide scavenges are carried out and the solution again reduced to small bulk, cooled in an ice – bath and 25 mls of fuming nitric acid added. The solution is allowed to stand for $\frac{1}{2}$ hour and the precipitated strontium nitrate centrifuged down. The precipitate is dissolved in the minimum quantity of water, made just alkaline with ammonia solution and 5 mls of saturated oxalic acid solution added. The strontium oxalate is filtered onto a tared filter – paper, washed with water, alcohol and ether, dried in a vacuum desiccator and weighed.

The strontium carrier solution is an aqueous solution of strontium nitrate standardised by oxalate precipitation

and ignition to oxide. The concentration of the strontium carrier solution is 9.55 mg/ml.

Molybdenum (11)

The solution of irradiated uranyl nitrate is treated with 1 ml of saturated oxalic acid solution and 5 mls of α-benzoin oxime solution (2% in ethyl alcohol). The solution is allowed to stand for 2 minutes, the precipitate centrifuged down and washed twice with water. The precipitate is boiled with 2 mls of concentrated nitric acid and 1 ml of concentrated perchloric acid to destroy the α-benzoin oxime, the solution is allowed to cool and made alkaline by the addition of ammonia solution. Two ferric hydroxide scavenges are carried out and the α-benzoin oxime complex is again precipitated by acidifying the solution to approximately 1M in nitric acid and adding 5 mls of α-benzoin oxime solution. The precipitate is centrifuged down, washed twice with water and dissolved by boiling with 2 mls of concentrated nitric acid and 1 ml of concentrated perchloric acid. The solution is made neutral by the addition of ammonium hydroxide and then acidified with a few drops of 2N sulphuric acid. 5 mls of 2M ammonium acetate solution are added, the solution heated to boiling and 5 mls of oxime solution (5% in 10% acetic acid) added. The precipitate is filtered onto a tared filter paper, washed with hot water, alcohol and ether and sucked dry. The precipitate is

allowed to dry in a vacuum desiccator and weighed as $MoO_2(C_6H_6ON)_2$.

The molybdenum carrier solution (concentration 24.3 mg Mo/ml) is an accurate solution of molybdenum trioxide in 6M ammonium hydroxide, diluted to 100 mls with water.

Ruthenium (13)

The solution of irradiated uranyl nitrate is added to the distillation flask together with 1g sodium bismuthate, 1ml of phosphoric acid, and 10 mls of concentrated perchloric acid. The flask is heated and after distillation of the excess water, ruthenium tetroxide distills over and is collected in the receiver, which contains 10 mls of 6M sodium hydroxide solution. The ruthenate solution is transferred to a centrifuge tube, 3 mls of ethyl alcohol added and the solution heated on a water bath. Ruthenium oxide is precipitated, centrifuged down and washed twice with 2M sodium hydroxide solution. The oxide is dissolved in 2 mls of 6M hydrochloric acid and diluted to 10 mls with water. Excess (0.2g) of aluminium powder is added to the solution to precipitate ruthenium metal and 5 mls of 2M hydrochloric acid is added to dissolve any residual aluminium powder. The ruthenium metal is filtered onto a tared filter - paper, washed with 2M hydrochloric acid, water, alcohol and ether, dried in a vacuum desiccator and weighed. The ruthenium metal contains a small, but constant, amount of oxide and is 94.3% ruthenium.

The ruthenium carrier solution is prepared by dissolving an accurately weighed amount of ruthenium chloride (2.049g) in 0.1M hydrochloric acid and diluting the solution to 100 mls with water. The concentration of the carrier solution is 10.01 mg Ru/ml.

Palladium (16)

1 ml of 2M hydrochloric acid and 5 mls of dimethyl glyoxime solution (1% in alcohol) are added to the solution of irradiated uranyl nitrate. The solution is allowed to stand for 5 minutes and centrifuged; the precipitate is washed twice with water and dissolved by boiling with 1 ml of concentrated nitric acid. The solution is made alkaline with ammonia solution and two ferric hydroxide and two silver iodide scavenges are carried out. The solution is made 0.4M with respect to hydrochloric acid and the excess silver separated off as silver chloride by centrifuging. The supernate is treated with 5 mls of dimethyl glyoxime solution. The precipitate is filtered onto a tared filter - paper, washed with water, alcohol and ether, dried in a vacuum desiccator and weighed.

The palladium carrier solution is prepared by dissolving palladium chloride (approximately 1.3g) in 0.1M hydrochloric acid and diluting to 100 mls. The solution is standardised by dimethyl glyoxime precipitation; the concentration is 8.08 mg Pd/ml.

Cerium (21)

The solution of irradiated uranyl nitrate is boiled in a beaker with 5 mls of concentrated nitric acid and 2g sodium nitrate; 0.5g sodium bismuthate are added gradually. The solution is cooled and cerium extracted in 10 mls of tributyl phosphate. The solvent layer is separated and treated with a mixture of 5 mls of 2M nitric acid and 5 mls of hydroxyl-amine hydrochloride solution (6% in water). The cerium is precipitated as hydroxide with ammonia solution, washed twice with water, dissolved in 1 ml of 2M hydrochloric acid and finally precipitated by addition of 15 mls of saturated oxalic acid solution. The precipitate is filtered onto a tared filter - paper, washed with a minimum of water, and acetone, dried in vacuum desiccator and weighed.

The cerium carrier solution is an aqueous solution of cerium nitrate, standardised by oxalate precipitation and ignition to oxide. The concentration of the carrier solution is 4.92 mg/ml.

APPENDIX III

Discussion of sources of error in fission yield measurements and their significance.

The errors quoted in Table 10 (page 54) are the standard deviations of the determinations for any particular fission yield and therefore give no indication of the overall errors. Since most of the errors arising in this work are likely to be associated with the estimation of the fission yield from A_O, it is pertinent to discuss the effect of these errors. The probable sources of error are:-

(i) lack of interchange between carrier and tracer. This is unlikely in cases where the chemistry is unambiguous and when it can possibly occur, oxidation - reduction reactions have been carried out to ensure complete interchange (e.g. in the bromine and iodine separations).

(ii) absorption of water onto, or incomplete removal of water from, the separated precipitates. Although precautions were taken to avoid this, it could cause an overestimate in the chemical yield giving a low fission yield result. It would be expected to affect the standard deviation as well as the overall error, since the water

(ii) Contd.

content would almost certainly be variable, and
the relatively small standard deviations suggest
that this is not a large effect.

(iii) lack of accurate knowledge of the half - lives.
This affects all three factors in the fission
yield calculation. (See page 8). The error in
the extrapolation of the decay curve will depend
on the extent of the extrapolation, but an
increase of 10% in the half - life results in a
similar decrease in the A_0 value for an extra-
polation over one half - life, so that the
difference in $A_0 \times t_{\frac{1}{2}}$ is very small. The error
in the calculation of the summation $\sum$ for a
10% error in half - life is less than one or two
percent, hence, provided the extrapolation is
over about one half - life, errors of 10% in the
value of the half - life can be accommodated
without much effect on the fission yield calcul-
ation. In fact, uncertainties of as much as 10%
in the half - lives concerned are extremely
inprobable.

(iv)   rather poor agreement between theory and experiment of the Sellotape absorption factor (see Section 4.5.2). The possible error in the absorption factor will become greater, the more the factor deviates from unity and is thus greatest for those isotopes with the lowest energy. It is estimated that for those isotopes with an absorption factor of less than 1.3, the error is unlikely to be more than ±5%.

(v)   lack of accurate knowledge of the energetics of the radioactive decays. This is linked with the previous possible source of error in that the exact decay schemes and the energies of the β - particles are less accurately known for these short - lived fission products. Generally, the shorter - lived products have the highest energies, and the correction factor (and its lack of precision) are correspondingly small. The possible presence of conversion electrons is one complication, but since most of these are of low energy and will be absorbed in the Sellotape covering, they may be ignored. In the case of

(v)   Contd.

Ba^{140} - La^{140}, where the energy of the conversion
electrons is higher, the correction factor has
been determined in a separate experiment (page 40).

(vi)   errors in ignoring the independent yields of
later members of the decay chain.   An examination
of the problem using Glendenin and Coryell's
theory of equal charge distribution (58) shows
that the most likely sources of error are Zr^{97}
and Sb^{129} and these will be examined in greater
detail.

The equation for the most probable charge (Zp) is

$$Zp = Z_A - \frac{Z_A + Z_A' - Z_f}{2}$$

where Z_A and Z_A' are the most stable charges
of the fission fragments and Z_f is the charge of
the fissioning isotope.

Using Glendenin and Coryell's continuous Z_A values,
which do not take into account the closed shell
effects, cumulative yields of greater than 99.0%

are found for Sb^{129} and for Zr^{97}, assuming a ν
of 4 (the value used in plotting the mirror points
in Fig. 14). A ν of 3 will increase the
cumulative yields and a ν of 5 gives 99.5% and
98.0% for the cumulative yields of Sb^{129} and Zr^{97}.
Using the Z_A values of Pappas (59) who takes
account of the closed shell effect, cumulative
yields of greater than 99.0% for Sb^{129} and Zr^{97}
are obtained.

Wahl's empirical results (60) of Zp from thermal
neutron fission of U^{235} for masses in the region
of 105 and 130 show a deviation from the values
obtained in the above calculations. For example
Zp (A = 129) is 49.9 by calculation (Glendenin and
Coryell), but is 50.3 from Wahl's results. This
results in a decrease from 99.0% to 93.3% in the
cumulative yield for Sb^{129}. Wahl in his work on
14 MeV neutron fission of U^{235} (35) showed that
the Z - Zp correlation could be taken as the same
as that for low energy fission by assuming a ν
of about 5 (which is not unreasonable), but he

considered that there was insufficient evidence
that the nuclear charge distribution pattern
remained the same. Alexander and Coryell (61)
found reasonable agreement with the equal charge
distribution postulate in their work on U^{238} and
Th^{232} irradiated by 13.6 MeV deuterons and fast
neutrons, but poor agreement with the unchanged
charge distribution theory. The latter, which
postulates that the most probable charge to mass
ratio in a fission fragment is the same as in the
fissioning nucleus results in cumulative yields of
greater than 99.9% for Zr^{97} (for ν = 3, 4 or 5)
and 93.3%, 89.7% and 84.6% (for ν = 3,4, and 5)
for Sb^{129}. Thus, whatever basis of interpretation
is taken, it appears that Sb^{129} is the only nuclide
likely to be affected, and the error even in that
case is likely to be less than 10%, and possibly
completely negligible.

Most of the points on the mass/yield plot (Fig. 14)
lie within 10% of the smooth curve and this gives confidence
in the curve as drawn, even though a number of standard

deviations of individual yields are greater than $\pm$ 10%.
Five points (masses 84, 91, 105, 111 and 129) lie greater
than 10% from the curve and it is necessary to consider
these in detail with respect to the possible sources of
error listed above.

In the case of Br^{84}, any possible errors arising from
the chemical separation can be ignored, since they would
apply equally to Br^{83}. The Sellotape absorption factor is
low (1.14) and is likely to be one of the more accurate
values. The most likely source of error probably involves
the resolution of the Br^{83}/Br^{84} decay curve. The latter
has a half - life of 31.8 minutes and the extrapolation
after resolution was normally over at least two half - lives.
Any error here would be expected to show up as a high
standard deviation; this was not the case, however. ($\sigma \pm$ 3%).

In the case of Sr^{91}, the half - life is well established
and the Sellotape absorption factor was determined experi-
mentally. No possible deviation from stoichiometry in the
oxalate monohydrate precipitate could explain the observed
discrepancy between the yield (4.5%) and the value taken
from the smooth curve (3.0%).

The low Ru^{106} yield (2.0 compared with 3.5 from the curve) is very difficult to explain. For example, even if the final precipitate was all RuO_2 (and this is very unlikely), the chemical yields would have been overestimated by about 25%. Similarly, the absorption factor would need to be increased to an absurd extent to account for the difference. It may be noted that the mass/yield curve is very steep at this point, and a relatively small displacement along the mass axis would produce a very marked error in the yield value.

Mass 111 relies on results from a short - lived isotope and a long - lived isotope, both of which have their disadvantages. The former (Pd^{111}) has a large possible error from a resolution and an extrapolation over about 3 half - lives, while the latter (Ag^{111}) had very low count rates. With the neutron intensities available, a more precise result could not be obtained.

Sb^{129} has already been considered in relation to the cumulative fission yield. Hageoo et al. (62) has shown the presence of a long - lived precursor of Sb^{129}, namely Sn^{129} (half - life 1.0 hr). He estimates, however, that the ratio of the short - lived Sn^{129} (8.8 minutes) to the

long - lived Sn^{129} in thermal fission of U^{235} is about 10:1. However, calculations show that the difference in fission yield in assuming that all the Sb^{129} is derived from the 1 hour half - life precursor is only about 10%. The calculation is based on a 4 hour irradiation followed by a 2 hour period before beginning the antimony separation. The remark relating to Ru^{106} applies with equal force in this case.

The choice of the exact position of the curve in the trough region is very difficult in view of the fact that masses 106 (mirror point of 129), 109 and 111 all have approximately the same yield and are all, to some degree, more prone to error than most of the other points. There were only two determinations of the Sb^{129} yield, the Pd^{109} results include the mathematical resolution of the Pd^{109}/Pd^{112} decay curve and Ag^{111}/Pd^{111} has been discussed above. Redrawing the curve to pass through the Sb^{129} point would also include the Ru^{106} point in whose accuracy there is more confidence than the points for masses 129, 109 and 111.

In drawing the mass/yield curve assumptions have to be made about the number of secondary neutrons, and it is

conventional to assume that the mean value ($\bar{\nu}$) can be applied over the whole range of mass ratios. Farrar and Tomlinson (63) have, in fact, shown that in thermal neutron induced fission, the total number of secondary neutrons is sensibly independent of the mass ratio of the fragments, although the distribution between light and heavy fragments showed a strong dependence upon the mass ratio. Their experiments would not have shown up any detailed fine - structure in the secondary neutron yield pattern, and it is not at all beyond the bounds of possibility that some of the anomalies apparent in the present curve (as in those found in previous work) arise from local variations in the secondary neutron/fragment mass relationship. If the "two - mode" concept of fission introduced by Turkevich and Niday (64) is accepted, then it must be remarked that the results of Farrar and Tomlinson apply to thermal neutron induced fission, where only the asymmetric mode is assumed to be effective, whereas the present discrepancies lie in the trough region, where, at 14 MeV, the alternative, essentially symmetrical, mode is dominant, and for which the secondary neutron distribution pattern may well not show the "saw tooth" shape found by Farrar and Tomlinson.

In the present work it has not been possible, with the neutron intensities available, to measure independently the yields of isometric pairs of products. Such information would be of considerable interest in relation to the possible interpretations of the "two mode" hypothesis, but from the present evidence no further clear conclusions on this subject can be drawn.

ACKNOWLEDGEMENTS

My most sincere thanks are due to:-

Professor G. R. Martin, under whose supervision this work was carried out, for his encouragement and advice on all aspects of radiochemistry.

Dr. D. J. Silvester, in collaboration with whom the experimental work in Part 1 was carried out, for permission to use his results in this thesis, for many useful discussions and for his cheerful companionship.

Mrs. E. B. M. Martin for her advice and assistance in the operation of the neutron generator.

Dr. D. Hall for many useful discussions and advice on the operation of the helium measuring apparatus and associated equipment.

The Council of the Durham Colleges for successive appointments as Research Assistant and as Research Fellow in Radiochemistry, during the tenure of which this work was carried out.

Part I of the thesis describes work carried out in connection with an Extra - Mural Research contract between the Council of the Durham Colleges and the Atomic Energy Research Establishment, Harwell; and thanks are due to the Director A. E. R. E. for permission to publish.